A continental reconstruction of hydroclimatic variability in South America during the past 2000 years

Mathurin A. Choblet[1,2,3], Janica C. Bühler[3], Valdir F. Novello[3], Nathan J. Steiger[4,5], and Kira Rehfeld[3]

[1]Department of Astrophysics, Geophysics and Oceanography, University of Liège, Liège, Belgium
[2]Institute of Environmental Physics, Heidelberg University, Heidelberg, Germany
[3]Department of Geosciences, University of Tübingen, Tübingen, Germany
[4]Hebrew University of Jerusalem, Jerusalem, Israel
[5]Lamont-Doherty Earth Observatory, Columbia University, Palisades, NY, USA

Correspondence: Mathurin A. Choblet (mathurin@choblet.com)

Abstract. Paleoclimatological field reconstructions are valuable for understanding ~~hydroclimatic variability. While being similarly~~ past hydroclimatic variability, which is crucial for assessing potential future hydroclimate changes. Despite being as impactful on societies as temperature variability, hydroclimatic variability ~~has still remained less in focus~~—particularly beyond the instrumental record—has received less attention. However, reconstructing globally complete fields of climate variables lacks adequate proxy data from tropical regions like South America, limiting our understanding of past hydroclimatic changes in these areas. This study addresses this gap using low resolution climate archives, including speleothems, previously omitted from reconstructions. Speleothems record climate variations on decadal to centennial time scales and provide a rich dataset for the otherwise proxy data scarce region of tropical South America. By employing a multi-time scale Paleoclimate Data Assimilation approach, we synthesize climate proxy records and climate model simulations, capable of simulating water isotopologues in the atmosphere, to reconstruct 2000 years of South American climate. This includes surface air temperature, precipitation amount, drought index, isotopic composition of precipitation amount, and the intensity of the South American Summer Monsoon. The reconstruction reveals anomalous climate periods: a wetter and colder phase during the Little Ice Age (∼1500 - 1850 CE) and a drier, warmer period corresponding to the early Medieval Climate Anomaly (∼600 - 900 CE). However, these patterns are not uniform across the continent, with ~~exceptions~~ climate trends in northeastern Brazil and the Southern Cone not following the patterns of the rest of the continent, indicating regional variability. The anomalies are more pronounced than in previous reconstructions, but ~~align with~~ match trends found in local proxy record studies, thus highlighting the importance of including speleothem proxies. The multi-timescale approach is essential for reconstructing multi-decadal and centennial climate variability. Despite methodological uncertainties regarding climate model biases and proxy record interpretations, this study marks a crucial first step in incorporating low resolution proxy records as speleothems into climate field reconstructions ~~, potentially enhancing~~ using a multi-timescale approach. Adequately extracting and using the information from speleothems potentially enhances insights into past hydroclimatic variability and hydroclimate projections.

1 Introduction

The climate of the Common Era (CE), which spans the last two millennia, is considered the most thoroughly studied prein-
dustrial paleoclimatic period owing to the abundance of records from various paleoclimate archives (PAGES 2k Consortium, 2019) and climate observations. It provides rather stable, close to present-day boundary conditions prior to the onset of industrialization with relatively constant ~~external forcing and close to present-day boundary conditions and thus also~~ greenhouse gas concentration and sea level, and climate variability due to natural, solar and volcanic forcings. Thus, it represents a well-studied benchmark for climate models (e.g. Jungclaus et al., 2017). Over the last two millennia, the global climate presents itself as an interplay and superposition of various major atmospheric and oceanic modes of variability. As such, different regions of South America are influenced by the El Niño-Southern Oscillation (ENSO), the Pacific Decadal Oscillation (PDO), the Atlantic Multidecadal Oscillation (AMO), the Southern Annular Mode (SAM) and variations in the position of the Intertropical Convergence Zone (ITCZ) (Garreaud et al., 2009). The spatial and temporal variability of the South American Summer Monsoon (SASM) (Zhou and Lau, 1998; Marengo et al., 2010) and its sub-component, the South Atlantic Convergence Zone (SACZ) (Carvalho et al., 2004), create a wide range of climate zones across the continent. This makes the South American continent an intriguing testbed for climatological research of the interplay of different phenomena before the onset of the current warming period.

The challenges posed by anthropogenic climate change are particularly pronounced in South America. The implications for water resources are significant, given that South America comprises two of the world's most crucial river basins: the Amazon Basin in the center-north and the Parana/La Plata Basin in the center-southeast. However, the broader effects of anthropogenic climate change on the entire hydrological cycle and its variability, including changes in precipitation extremes and the occurrence of droughts, remain ~~widely unknown~~ less studied than for temperature. Improving the understanding of the full range of climate variability in South America is imperative, given the high vulnerability of human livelihoods in tropical and subtropical regions to the impacts of climate change. This vulnerability is especially evident in extreme events like droughts and floods, due to both geographic and socioeconomic factors (Pörtner et al., 2022), as seen for example in the current megadrought in central Chile (Garreaud et al., 2019).

The climate of the past beyond the instrumental period is studied to enhance our understanding of hydroclimate and contextualize recent changes. For instance, extreme events and their socioeconomic consequences have been recorded in historical documents (Prieto and García Herrera, 2009), such as a sequence of drought in northeastern Brazil (Aceituno et al., 2008; Utida et al., 2023), droughts in Bolivia (Gioda and Prieto, 1999), and extreme floodings of the Parana River (Prieto, 2007).

Climate archives are increasingly used to reconstruct and interpret changes in climate beyond the instrumental era. These reconstructions offer statistically robust estimates of the climate, particularly for the CE, the period of interest in our study. In principle, existing global climate field reconstructions of the CE already provide estimates for both surface temperature and hydroclimate variables, including for South America (e.g., Hakim et al., 2016; Franke et al., 2017; Steiger et al., 2018; Tardif et al., 2019; Neukom et al., 2019). However, global CE reconstructions predominantly rely on proxy records from the mid-to-high latitudes, particularly tree rings from the Northern Hemisphere. Climate proxy record density for the CE in tropical and

subtropical regions is much lower, in particular for terrestrial locations (Neukom and Gergis, 2012). Terrestrial proxy records are, however, crucial, when it comes to reconstructing hydroclimatic variability. Although climate field reconstruction can make use of teleconnections to alleviate data scarcity, the lack of local data limits the viability of global reconstruction in (sub-)tropical regions (Anchukaitis and Smerdon, 2022).

For South America, climate field reconstructions are constrained by the scarcity of climate proxy records for all regions except for the central and southern Andes, where tree rings serve as an abundant climate archive. Regional climate field reconstructions have thus primarily focused on Southern South America ~~(Neukom et al., 2010, 2011; Luterbacher et al., 2011; Morales et al., 202~~ (Neukom et al., 2010, 2011; Boucher et al., 2011; Luterbacher et al., 2011; Morales et al., 2020). However, in recent years speleothems have emerged as a promising climate archive with the potential to alleviate data scarcity in tropical South America (Vuille et al., 2012). Speleothems are geological cave formations created by accumulating layers of calcium carbonates transported by seepage water. Among the many climate proxies archived in speleothems, the ratio between heavy and light oxygen isotopes (δ^{18}O) as saved in accumulating layers of calcium carbonate reflects the isotopic composition of the precipitation above a cave and, thus, records hydroclimatic changes (Bradley, 2015). The δ^{18}O signatures of precipitation are sensitive to air temperature, precipitation amount changes, and the geographical location in terms of altitude, latitude, and distance from the coast (Dansgaard, 1964).

For South America, particularly in the South American Summer Monsoon (SASM) influenced region, the primary driver of $\delta^{18}O$ signatures in precipitation is the amount of rainfall during the monsoon season, rather than temperature (Vuille et al., 2003; Moquet et. Additionally, the $\delta^{18}O$ signatures are influenced by the location of the moisture source, notably the moisture contribution from the ITCZ region, and the degree of upstream rainout, which captures the precipitation history of the air mass along its trajectory as demonstrated by cave monitoring studies (Ampuero et al., 2020; Jiménez-Iñiguez et al., 2022; Moquet et al., 2016) and modeling studies (Vuille et al., 2003; Vuille and Werner, 2005; Vuille et al., 2012) working with station data from the Global Network of Isotopes in Precipitation (GNIP) (IAEA/WMO, 2020). $\delta^{18}O$ in speleothems in tropical South America is thus closely linked to changes in both regional and large-scale atmospheric circulation patterns.

Tropical South America is an archetypical region for speleothem research with a growing number of published records in recent years. For instance, single records have been used to demonstrate changes in the intensity of the SASM on millennial to centennial time scales in response to changes in orbital and solar forcing (Novello et al., 2016; Bernal et al., 2016). For the hydroclimate of the last millennium, pronounced anomalies found in speleothem δ^{18}O values have been associated to the Medieval Climate Anomaly (MCA) and the Little Ice Age (LIA) (Novello et al., 2018; Apaéstegui et al., 2018; Azevedo et al., 2019). Moreover, through the analysis of several South American speleothem records using dimensionality-reduction techniques, Orrison et al. (2022) demonstrated that climate model simulations of the last millennium consistently underestimate centennial climate changes over the South American continent, reinforcing findings of Rojas et al. (2016), who investigated SASM variability in climate model simulations.

~~Nevertheless,~~ It is not clear, if existing climate field reconstructions include these insights into South American Hydroclimate variability during the CE ~~may be excluded from existing climate field reconstructions~~ due to the limited integration of speleothem records~~into these reconstructions~~. Their incorporation proves difficult for two main reasons. First, reconstructions

of the CE are usually attempted at seasonal or annual resolution and, thus, only include proxy records of at least annual resolution. Speleothems are seldom dated annually with dating uncertainties often on the scale of several years. Even so, karst processes above the caves work as smoothing filters of the isotopic variations in precipitation. Thus, speleothem δ^{18}O time series reflect the mixing of rainfall from different seasons and the transit time through the epikarst to the water dripping point in the cave (for speleothems in Brazil see Moquet et al., 2016). Second, climate field reconstructions usually require a calibration of the proxy records against instrumental data. This calibration is hampered by the low temporal resolution of speleothem records and short data overlap with regional instrumental observations. Similar restrictions also apply to many lake and marine sediments, precluding their use in current climate field reconstructions. In this study, we aim to overcome these limitations to explore the information gain associated with including previously excluded climate archives of annual to decadal resolution.

Here, we present the first climate field reconstruction of the hydroclimate of the South American continent for the entire CE, employing speleothems besides more commonly-used climate archives such as tree rings, lake sediments, ice cores, corals, sclerosponges, and marine sediments marine sediments and historical documents. We combine proxy records from a multitude of proxy record databases (Emile-Geay et al., 2017; Comas-Bru et al., 2020; Konecky et al., 2020; Morales et al., 2020) (Emile-Geay et al., 2017; Comas-Bru et al., 2020; Konecky et al., 2020; Morales et al., 2020; Neukom et al., 2009) and individual records provided by original authors. This yields a total of 295 307 proxy records (See Figure 1). Our selection represents the at present spatially most complete collection of publicly available proxy record data for the region.

As a climate field reconstruction technique, we choose Paleoclimate Data Assimilation (PaleoDA) (Bhend et al., 2012; Steiger et al., 2014). Based on the principles of DA, which has been successfully applied in weather and ocean forecasting for three decades (Evensen et al., 2022), PaleoDA fuses information from climate model simulations and climate observations to provide a best state estimate. In contrast to other regression-based techniques (e.g Principal Component Regression as in Luterbacher et al., 2002; Neukom et al., 2014), PaleoDA does not directly rely on gridded instrumental datasets. The climate simulations provide time series long enough to also include proxy records of relatively low resolution, such as speleothems, which cannot be calibrated to instrumental data. We use five state-of-the-art isotope-enabled climate simulations, which simulate the isotopic composition of precipitation and which were made publicly available recently (Bühler et al., 2022). This leads to Employing these previously unused simulations in PaleoDA provides a twofold information gain: first, it enables the inclusion of speleothem records in the PaleoDA without the uncertainties associated with instrumental calibration, and second, it facilitates the comparison of multiple simulations of rainfall δ^{18}O values from different models, thereby mitigating biases stemming from individual proxies and models. In this study, we will focus on surface temperature, precipitation amount, the drought index SPEI (Standardized Precipitation Evapotranspiration Index, Vicente-Serrano et al. (2010); Beguería et al. (2014)), and the isotopic composition of precipitation. While in theory, PaleoDA allows reconstructing climate fields for all simulated climate variables, the chosen variables are most closely related to the climate signal recorded by the selected climate archives and, thus, hold the highest potential for reliable reconstructions. To overcome the difficulties posed by proxy records of annual to decadal resolution such as speleothems, we adapt the PaleoDA algorithm to a multi-timescale method enhancing the concept proposed by Steiger and Hakim (2016).

The structure of this study is as follows: We introduce the proxy record and climate model simulation data on which we base our reconstruction. We then provide a complete description of the multi-timescale PaleoDA methodology, its assumptions and key parameters. We present our obtained reconstruction (for both annual and austral summer means) and validate it by means of comparison to instrumental data, other reconstructions, and non-assimilated proxy record data. As one of several climatological applications of the reconstruction dataset, we study the main centennial hydroclimatological changes in South America during the MCA and the LIA and ~~compare our reconstruction to~~ assess if our reconstruction aligns with insights from other studies. In addition, we investigate the reconstructed intensity and variability of the SASM using a precipitation-based monsoon index, which has not been studied in climate field reconstructions before.

2 Data

2.1 Paleoclimate Proxy Data
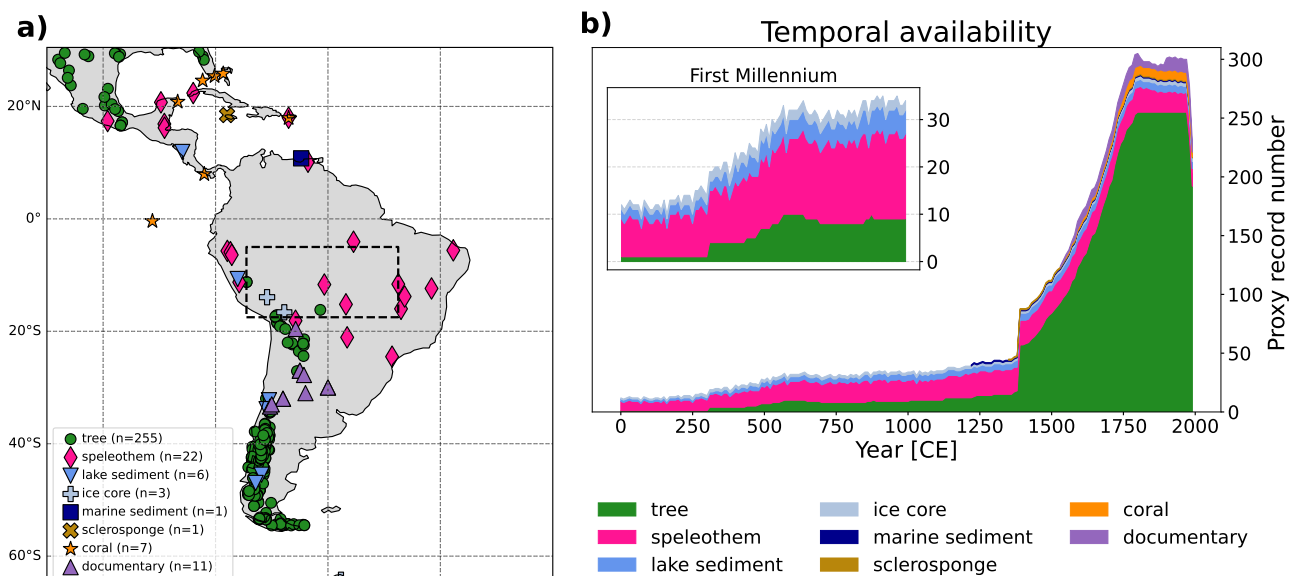
Figure 1. Spatiotemporal availability of the employed proxy records. a) Spatial distribution of all employed proxy records. Archive types are encoded by shape and color. The represented spatial domain (65°S-35°N, 20°W-110°W) is the spatial domain reconstructed in this study. In addition, the black box demarcates the core region of the South American Summer Monsoon (SASM) following the definition by Vuille et al. (2012), which we use to reconstruct the SASM index. b) Temporal availability of proxy archive types, with a zoom on the first millennium.

The continental climate field reconstruction provided in this study is based on a selection of different climate archive types. While focusing on climate archives that store information about the hydroclimate, we also include other types of archives for

better covering the range of variables. The archives include trees, speleothems, ice cores, lake sediments, corals, sclerosponges and marine sediments. To ensure the best possible spatio-temporal coverage of the region, we have chosen and combined proxy records from three published paleoclimate proxy databases: PAGES2k (Emile-Geay et al., 2017) , Iso2k (Konecky et al., 2020), the third version of the database from then Speleothem Isotopes Synthesis and AnaLysis group SISALv3 (Atsawawaranunt et al., 2018; Comas-Bru et al., 2020; Kaushal et al., 2023), and tree rings used for the South American Drought Atlas (Morales et al., 2020) and historical documentary indices presented by Neukom et al. (2009). We additionally included single proxy records which are currently not part of published proxy record databases (individual references in Appendix Supplement S1.2). In contrast to the other proxy record databases, the SISALv3 speleothem database has not been employed in climate field reconstruction previously.

The SISALv3 database provides different sets of chronologies for the different speleothems. For this analysis, we use the authors' original chronology only. Further, age uncertainties, which are only provided for SISALv3, are not explicitly considered as these are mostly smaller than the timesteps in the multi-time scale PaleoDA algorithm (see Section 3.2). A description table for each climate archive type that we included, including metadata for the individual proxy records, the proxy variable, median resolution and methodological choices (Proxy System Model, assumed noise, seasonality, time scale) is provided in the Appendix Supplement Tables S1.1 to S1.6 S1.7.

We define four selection criteria for choosing proxy records from the respective databases:

1. The sites where the climate archives where obtained are located in the region 65°S-35°N, 20°W-110°W (See Figure 1). Proxy records from Central America are explicitly included as they can provide information for the northern part of South America, where few proxy records for the past two millennia exist.

2. The proxy variable is approximately linearly related to one of the climate variables provided by the climate model simulations (see Section 2.2 and 3.3). We follow the recommendations given by the authors in the original publications to decide if such a relationship holds. Note, that speleothem and ice core δ^{18}O values can also be included in our proxy record collection because the climate model data also includes simulated isotopic-composition of rainfall.

3. The proxy records span at least 200 years and have at least one sample value in the period from 1750 to 1850 CE. This period is used as the reference period for computing anomalies of the proxy records relative to a shared time period. It has the advantage of including crucial records as speleothems, that lack data points during the more commonly chosen reference period of the 20th century. At the same time, this excludes many shorter records which would lead to high reconstruction skill during the instrumental era, but would not contribute to the reconstruction of centennial scale hydroclimate changes, and are, thus, acceptable to omit.

4. The resolution of the proxy records is better than 10 years (median), as we set 10 years as the largest reconstruction time scale in the multi-time scale PaleoData Assimilation approach (described in the Section 3.2). While decadal to multi-decadal and lower resolution is technically possible, the proxy records falling into that category are too coarsely resolved to contribute to the skill of the reconstruction of the past two millennia on multi decadal and centennial time scales, which is the focus of this study.

Our selection of proxy records for the South American reconstruction consists of ~~295~~ 307 records covering southern and central America (Figure 1). Due to our selection criteria, the maximum number of proxy records is available in the reference period 1750 - 1850 CE and the least in the first century (13 records). Despite the decreasing number of available proxy records back in time during the CE, the spatial coverage remains fairly similar throughout time, as older proxy records are evenly distributed. This is particularly evident for tree rings, which are clustered in the Andes (see also SF 1.1 for the spatiotemporal availability of proxy records for each reconstructed century). The temporal availability of proxy records shows a sharp decline in tree ring data in the year 1400 CE, coinciding with the start of the SADA tree ring database. Throughout the reconstruction, we remain attentive to potential artifacts resulting from this decline. Despite this concern, we anticipate only a small impact, given that the tree rings are situated in regions where there are already existing proxy records. Non-speleothem archives mostly cover the central and southern Andes and coastal regions, while speleothems significantly contribute to the coverage of tropical inner-continental regions over the entire two millennia. Regions lacking archive sites for proxy records can be found in the northern part of South America, namely Colombia, the Guianas and the north western states of Brazil. Additionally, the western part of the Southern Cone, the cone-shaped area of South America south of the Tropic of Capricorn (∼23.4°S), lacks proxy records. However, the South American Drought Atlas has demonstrated that tree ring records from the central and southern Andes can be skillfully used to reconstruct the hydroclimate of that region. The northern part of the Southern Cone is covered by documentary data from the 16th century on.

2.2 Isotope-enabled climate model simulations

We use five state-of-the-art isotope-enabled climate model simulations of the last millennium (Bühler et al. (2022) and Table 1). Additional information about boundary conditions and forcing parameters can be found in Bühler et al. (2022). Isotope-enabled climate models are essential for our study as they allow us to bypass the uncertain calibration of speleothem δ^{18}O records to temperature or precipitation. The isotopic composition of precipitation (δ^{18}O values) is an important hydrological marker that conveys additional information not captured by precipitation or temperature alone. From the simulations, we use the variables surface temperature, total precipitation amount, and the isotopic precipitation. The drought index SPEI (Standardized Precipitation Evapotranspiration Index Vicente-Serrano et al. (2010)) is computed from simulated precipitation and temperature using the code based on the Thornthwaite's method for estimating potential evapotranspiration from the climate-indices package (Adams, 2017). The time scale is set to 12 months. We choose Thornthwaite's method over the more precise Penman-Monteith formula, because the available climate model simulation data does not include all variables required for the latter. In parts of the analysis, we use a Multi-Model Ensemble (MME) by conducting separate reconstructions for each model prior and then computing the mean of the five reconstructions. In PaleoDA, MMEs are being used to provide more reliable reconstructions than provided by single model priors (Parsons et al., 2021; Annan et al., 2022; King et al., 2021, 2023). As we will use the climate model data only as anomalies, the purpose of the MME in this study is not to alleviate the effect of mean value biases in the models, but to provide a more diverse covariance structure, which constitutes the backbone of the PaleoDA reconstruction algorithm (see Section 3.1). This covariance structure across models is particularly relevant in our study, as the covariance relationships between δ^{18}O and other climate variables as temperature and precipitation vary considerably in

Model	Resolution	Reference
ECHAM5/MPI-OM	$3.75° \times 3.75°$	Sjolte et al. (2020) Werner et al. (2016)
GISS ModelE2-R	$2.5° \times 2°$	Lewis and LeGrande (2015) Colose et al. (2016a) Colose et al. (2016b)
iCESM1	$2.5° \times 1.875°$	Brady et al. (2019) Stevenson et al. (2019)
isoGSM	$1.875° \times 1.875°$	Yoshimura et al. (2008)
iHadCM3	$3.75° \times 2.5°$	Bühler et al. (2021) Tindall et al. (2009)

Table 1. Spatial resolutions and references of the isotope-enabled last millennium simulations used in this study. The listed references also include the model descriptions. For a detailed description of boundary conditions and forcing parameters see Bühler et al. (2022).

the different climate models. An MME requires regridding of all climate model simulations to the same grid. We choose to interpolate all climate model simulations to the highest resolution provided by one of our input models, isoGSM ($1.875°$ x $1.875°$). This allows for keeping the spatial information of the higher resolving models. Computing the correlation fields for the regridded climate fields, we found that the regredding produces smoothed correlation fields without introducing artefacts (not shown). Note, that it is also conceivable to construct an MME by concatenating the model priors before applying the Ensemble Kalman Filter equations, but this method is not used here.

3 Methods

3.1 Data Assimilation with the Ensemble Kalman Filter as a Climate Field Reconstruction technique

Data assimilation (DA), which has been developed mainly for improving numerical weather and ocean fore- and hindcasts, combines two sets of information: a statistical prior state estimate that is provided by an ensemble of estimates from a numerical model, and information from observations (e.g. climate proxy records). The prior estimate is updated conditional on the observations (Evensen et al., 2022). The obtained posterior state is then propagated through time by the numerical model until new observations are available. PaleoDA often simplifies some aspects of DA compared to operational weather and ocean forecasting systems, particularly by omitting the model ensemble restart step due to the limited predictability and the computational cost of General Circulation Models (GCMs) on paleoclimatic timescales (Dirren and Hakim, 2005; Huntley and Hakim, 2010). SF 2.1 illustrates the main steps of the PaleoDA algorithm.

Here, the updating operation is performed by the Ensemble Kalman Filter (EnKF) (Evensen, 1994), which assumes that the prior and the observations are sampled from the same true, but unknown Gaussian distribution. The errors with respect to the true distribution are assumed to be unbiased and normally distributed. The EnKF further assumes that the observations are linearly related to the true distribution. Despite the normality assumptions, it has proven to be also a good es-

timator in non-linear cases where the assumptions do not strictly hold, which explains its wide use in real-word applications (Evensen et al., 2022). In the last decade, the EnKF has been introduced into the field of climate field reconstructions (Bhend et al., 2012; Steiger et al., 2014) and been used to reconstruct the climate of the last two millennia (e.g Hakim et al., 2016; Steiger e and older periods such as the Last Glacial Maximum (Tierney et al., 2020; Annan et al., 2022), the last deglaciation (Osman et al., 2021; Er
230 , and the Paleocene–Eocene Thermal Maximum (Tierney et al., 2022).

The EnKF assimilation equation states

$$\mathbf{X} = \hat{\mathbf{X}} + \mathbf{K}(\mathbf{Y} - \mathcal{H}\hat{\mathbf{X}}), \tag{1}$$

where $\hat{\mathbf{X}}$ is the prior state (e.g. a surface temperature field over all simulated time steps, which creates an ensemble) and $\mathbf{X}$ the posterior state matrix. $\mathbf{Y}$ is the observation vector containing the proxy record values at a specific time step and $\mathcal{H}$ is the
235 observation operator mapping the prior values to the observations (further explained in Section 3.3), thus creating $\mathcal{H}\hat{\mathbf{X}}$, the observation estimates for the simulated values. $\mathbf{K}$ is the Kalman gain matrix, a weighting matrix, which blends the prior state estimate and observations according to covariances in the prior ensemble and the proxy record uncertainty. It is computed as

$$\mathbf{K} = \text{cov}(\mathbf{X}, \mathcal{H}(\mathbf{X}))(\text{cov}(\mathcal{H}(\mathbf{X}), \mathcal{H}(\mathbf{X})) + \mathbf{R})^{-1}. \tag{2}$$

$\mathbf{R}$ is the observation error covariance matrix which contains the error associated with the proxy records (see Section 3.4).
240 We assume, that the observation error of different proxy records is uncorrelated, hence $\mathbf{R}$ is a diagonal matrix. The EnKF assimilation equation can be effectively described as an interpolation process, where the model prior provides covariance estimates between observation locations and all simulated locations to perform the interpolation. Equation 2 follows from minimizing the posterior error covariance matrix, which is given by

$$\text{cov}(\mathbf{X}, \mathbf{X}) = (\mathbf{I} - \mathbf{K}\mathcal{H})\text{cov}(\hat{\mathbf{X}}, \hat{\mathbf{X}}). \tag{3}$$

245 The uncertainty of the reconstructed variables at each time step can be computed as the standard deviations of the diagonal entries of the posterior error covariance matrix (Equation 3). The posterior covariance matrix is by construction less than or equal to the prior covariance. To solve the equations 1, 2 and 3 efficiently, we utilize the Ensemble Transform Kalman Filter (Bishop et al., 2001) as formulated in Vetra-Carvalho et al. (2018). The prior covariance matrix $\hat{\mathbf{X}}$ is used from already computed simulations instead of restarting the model ensemble and thus represents the climatological covariance. To compute it,
250 we use an ensemble of 100 randomly selected simulation years (see Section 3.5). This approach has been named stationary offline PaleoDA (Okazaki et al., 2021) and assumes a stationary covariance between climate variables at the grid cells. Each year is reconstructed separately, with the temporal pacing determined by the climate proxy records and the spatial information provided by the covariances from the climate model simulations. Note, that by using an MME (Section 2.2), we effectively use the mean Kalman gain from the five model priors. The offline PaleoDa concept is similar to computationally efficient Opti-
255 mal/Statistical Interpolation methods (Evensen, 2003; Oke et al., 2005), although these still forward a single model simulation in time according to the results of the assimilation.

We reconstruct both annual (April-March, according to the vegetation cycle) and austral summer (DJF) means separately, due to the selected proxy records likely representing either annual or summer means (in particular speleothems from the SASM region).

In our reconstruction, the prior ensemble mean for each grid cell and climate variable is always enforced to be zero to limit model mean value biases. We consider this a valid approach, as the CE is a relatively stable climatic period. Not performing such debiasing would introduce steplike, unphysical shifts in the reconstructed time series depending on the availability of specific proxy record with a strong difference towards the prior (as also noted in Franke et al. (2017) for example).

In the last decade, the EnKF has been introduced into the field of climate field reconstructions (Bhend et al., 2012; Steiger et al., 2014) and been used to reconstruct the climate of the last two millennia (e.g Hakim et al., 2016; Steiger et al., 2018; Tardif et al., 2019) and older periods such as the Last Glacial Maximum (Tierney et al., 2020; Annan et al., 2022), the last deglaciation (Osman et al., 2021; Erb, and the Paleocene–Eocene Thermal Maximum (Tierney et al., 2022).

3.2 Multi-time scale Paleoclimate Data Assimilation

The PaleoDA algorithm described in the Section 3.1 is usually employed for the assimilation of proxy records at a single time scale, e.g. annual or seasonal for the CE. However, the speleothem records that are the backbone of our regional reconstruction have median temporal resolutions of 1 to 8 years and actually represent smoothed climate signals due to mixing effects of the karst system on the cave drip water (Moquet et al., 2016). Therefore, we developed a new multi-time scale adaptation of the EnKF-PaleoDA algorithm, building on the concept proposed by Steiger and Hakim (2016), which allows us to use low- and high-resolution proxy records simultaneously in a computationally efficient manner.

The key idea is to add an additional time dimension for consecutive years in the prior state matrix $\mathbf{X}$, enabling the use of multi-year means and covariances in the PaleoDA algorithm (see SF 2.2). The number of years added in the prior state matrix is determined by the largest time scale imposed by the proxy records, which we determine as decadal for the employed speleothems. Instead of reconstructing the target time period (1-2000 CE) year by year, we divide it into decadal blocks, as we will use the speleothem values on a decadal time scale only. Additionally, we reconstruct annual and quinquennial time scales as sub-blocks of the decadal block (see S2.1). The decadal prior block is the same during the entire reconstruction period. For each decadal block, the algorithm computes the assimilation equations for all proxy records that represent the largest time scale, using decadal means in the prior state matrix. The resulting decadal mean value is then exchanged in the prior state matrix. The algorithm continues with the smaller time scales using the corresponding proxy records. Each proxy record is used on a single time scale. This procedure requires resampling the records to the target resolution of the desired timescale prior to the Data Assimilation. We first bin all the non-annual proxy records to the respective resolution using a simple equidistancing resampling routine, which consists of upsampling the time series values to annual resolution, filtering the time series with a low-pass filter and finally resampling to the targeted resolution (similar to the `MakeEquidistant` function of the Paleospec R package (Laepple et al., 2023a)). We ensure the resampling does not add spurious datapoints by choosing target resolutions that are larger than the largest proxy record sampling interval and mask longer gaps in the proxy records. The multi-time scale algorithm involves more calculation steps than the single-time scale algorithm due to the

repeated calculation of multi-year means and anomalies in the prior state matrix. As such, the algorithm also requires the repeated application of the observation operator $\mathcal{H}$ in the Kalman Filter equations. However, this is avoided by appending the observation estimates to the prior state matrix, such that the algorithm also updates the observation estimates. A multi-time scale paleoclimate data assimilation approach is not only advantageous to allow for the assimilation of irregular proxy-records, it should also improve the reconstruction of multi-decadal to centennial climate variability according to pseudoproxy experiments (Steiger and Hakim, 2016; Choblet et al., 2023). Note, that this multi-time scale PaleoDA algorithm differs from the one used in the Holocene temperature reconstruction by Erb et al. (2022), where the multi-time scale prior ensemble is constructed as a moving prior ensemble from transient climate simulations.

3.3 Proxy system models

In PaleoDA, Proxy System Models (PSM) (Evans et al., 2013; Dee et al., 2015) are employed for the observation operator $\mathcal{H}$ in equation 1 and 2. They have been developed to enhance model-data comparison by encapsulating the physical, geological, biological and biogeochemical processes into mathematical formulas to translate the external climatic conditions into a proxy record signal. These processes are usually divided into three different stages, the sensor, archive and observation stage. In this study, we use PSMs in a one-stage manner, which is commonly chosen in PaleoDA studies targeting the CE climate (e.g. Hakim et al., 2016; Steiger et al., 2018; Tardif et al., 2019). Within this PaleoDA study, the PSMs translate the signal of simulated climate to proxy record units (the proxy record variance), accounting for seasonality. We employ three types of PSMs depending on the nature of the proxy records:

A) For records already calibrated to temperature, such as some lake and marine sediments and sclerosponges, the PSM takes the temperature of the model grid box closest to the proxy record location as the simulated temperature value. Seasonal means or annual means (April to March) are used depending on the indications in the original publication of the record. This way, seasonal biases in the reconstruction are constrained.

B) For proxy records that reflect changes in δ^{18}O of precipitation, such as speleothems, ice cores, and some lake sediments, the PSM uses the simulated δ^{18}O of precipitation values from the closest locations to the proxy records. Annual means of precipitation-weighted δ^{18}O values are computed to account for varying precipitation intensity over the year. The values of the two ice core records given in deuterium are divided by 8 to represent the variability in δ^{18}O according to the Global Meteoric Water Line (Craig, 1961). Although the δ^{18}O values in these different archives is stored in different materials (e.g ice, carbonates, trees) and, thus, have different mean values, this is not relevant for our reconstruction, because we use proxy record anomalies respective to a reference period. We assume that temperature dependent fractionation effects are small compared to the variation in the δ^{18}O of precipitation values.

C) For proxy records that can be calibrated to instrumental data, such as corals~~and tree rings~~, tree rings and documentary indices, we employ a linear ~~regression-based PSM (e.g. Hakim et al., 2016; Steiger et al., 2018; Tardif et al., 2019)~~regression-based PSM as usually employed in PaleoDA (e.g. (Hakim et al., 2016; Steiger et al., 2018; Tardif et al., 2019; King et al., 2021; San̦ . While more specific PSMs for corals and tree rings exist, the linear-regression based PSMs also yield similar reconstruction

results in PaleoDA (Dee et al., 2016). More complex PSMs for corals and tree rings also require environmental variables for sea water and air moisture, which are not available for all employed climate model simulations. Furthermore, we consider it preferable to use this type of univariate linear PSMs in PaleoDA, as the covariance relationship between observations and reconstructed climate field remains more tractable. Linear regression equations are estimated between the proxy time series and instrumental time series over a calibration period. The regression parameters are then applied to the model data in the data assimilation. Different predictor variables, such as surface temperature, precipitation, or the SPEI drought index, are used based on the lowest p-value for each proxy record. For coral records, we only use surface temperature as a predictor variable. As instrumental calibration datasets, we use the Berkeley Earth dataset for surface temperature (Rohde and Hausfather, 2020), precipitation from CRUTS 4 (Harris et al., 2020b) and an SPEI drought index computed from the temperature and precipitation in CRUTS 4. The temperature calibration is performed over the period 1920 - 2000 CE. For precipitation and SPEI, we use the period 1950 - 2000 CE due to limited local station data in South America before 1950 CE (Garreaud et al., 2009). These spatially highly resolved instrumental datasets have been regridded to the spatial resolution used in the climate field reconstruction to account for the lower spatial resolution of the climate model simulation data. We compute these regressions both for the annual and seasonal instrumental means and choose the best predictor variable separately (as in Steiger et al., 2018). For the annual reconstruction, 110 tree-ring records were predicted with temperature, 94 with SPEI and 51 with precipitation. One historical documentary records was predicted with temperature, four with SPEI and nine with precipitation. For the austral summer reconstruction, 102 tree-ring records were predicted with temperature, 92 with SPEI and 61 with precipitation, whereas two historical documentary records were predicted with temperature, six with SPEI and three with precipitation.

3.4 The proxy record error

The proxy record error in Data Assimilation represents the non-climatic noise recorded by proxy records and is challenging to quantify. Measurement noise is considered negligible. For the tree and coral, coral and documentary archives, where calibration could be performed with instrumental data, the proxy error follows directly from the linear regression in the PSM (See Section 3.3). The mean of the squared linear regression residuals is the proxy error variance. For all other records in the non-instrumental era, we express the proxy record error in terms of the signal-to-noise ratio (SNR), assuming Gaussian and timescale-independent noise (Smerdon, 2012). We assume an SNR of 0.5 for all proxy records which we have not calibrated to instrumental variables, following exploratory studies by Wang et al. (2014) and Orrison et al. (2022). The SNR can then be converted into the entries of the observation error matrix $\mathbf{R}$ in Equation 2 by taking into account the variance of the proxy records, var($\mathbf{Y}$), (see Appendix Supplement S2.2 for the derivation):

$$\mathbf{R} = \text{var}(\mathbf{Y})/(1 + \text{SNR}^2) \tag{4}$$

$\mathbf{R}$ is computed for each proxy record that can not be calibrated using its resampled time series (see Section 3.2). Given that some proxy records, particularly speleothems, exhibit significant shifts in local climate or environment, we observed that the variance and thus $\mathbf{R}$ would be larger compared to those not indicating such local changes. Consequently, the former records

exerted less influence during the reconstruction. To address this issue, we used the mean of the variance in a running 200-year window for computing $\text{var}(\mathbf{Y})$ to reduce the influence of shifts on the variance and to ensure comparable noise levels for all proxy records. We thus assume, that for a 200 year window, the statistical assumptions of Gaussian and timescale-independent noise leading to equation 4 hold. We ~~assume an SNR of 0.5 for all proxy records which we have not calibrated to instrumental variables, following exploratory studies by Wang et al. (2014) and Orrison et al. (2022). We~~ emphasize that the proxy record error should not be considered separately from the variance in the prior ensemble matrix, which represents the model error (see Equation 1). The relationship between proxy error and prior variance is crucial in PaleoDA. While in regular Data Assimilation via the optimal interpolation method, the static prior variance is usually considered to be too large and thus reduced by a factor (e.g. Oke et al., 2005), climate simulations have been allegedly underestimating climate variability, for instance in surface temperature (Laepple and Huybers, 2014; Laepple et al., 2023b) or isotopic variability in precipitation (Bühler et al., 2022), which could be used as an argument in favor of inflating the variances in the prior. Instead of adjusting the variance in the prior, we also performed alternative reconstructions in which the proxy error variance for non-calibratable records was set equal to the variance in the prior observation estimates. This approach gives equal weight to the proxy observations and the model prior.

3.5 Further reconstruction refinements

We use a Monte Carlo technique of repeating the reconstructions 50 times with different ensembles of 100 randomly selected simulation years and using 80% of all proxy records in each repetition similar to Hakim et al. (2016) and Tardif et al. (2019). Doing so improves the representation of the reconstruction uncertainty~~and~~, attenuates the effect of outliers in the proxy record selection and the prior ensemble provided by the climate model simulations as suggested by Pseudoproxy Experiments. The withheld proxy records will be used for internal validation of the reconstruction. Covariance localization, which is used to suppress spurious long range covariances is not employed in this study, because the prior ensemble size is considered large. Furthermore, PaleoDA studies that use covariance localisation usually do so with very large decorrelation lengths larger than 12000 km (e.g. Tardif et al., 2019; Tierney et al., 2020; Osman et al., 2021), exceeding the targeted area in our reconstruction.

4 Validation

We validate our reconstruction using gridded instrumental data sets from the 20th century, independent reconstructions and proxy records withheld from the reconstruction. The focus here is put on the internal validation using withheld proxy records as performed in previous PaleoDA studies (e.g. Tardif et al., 2019; King et al., 2021; Tierney et al., 2020; Osman et al., 2021). The reason for doing so is that although instrumental validations are commonly used in PaleoDA and most easy to interpret, we do not consider them representative in our case due to the shortness of the instrumental record compared to our decadal and quinquennial climate archives. The instrumental temperature and precipitation time series are too short for validating a decadal-scale reconstruction. The 20th century validation mainly reflects the reconstruction capability of tree rings, which are the most abundant climate archive in the instrumental period but only provide limited spatial and temporal coverage during the entire CE. The inclusion of speleothems in this study mainly relies on the assumption that their $\delta^{18}O$ signatures capture

390 An extensive validation using gridded instrumental temperature and precipitation data for evaluating the reconstruction regionally and for the SASM precipitation amount is presented in ~~Appendix~~ Supplement S3.1 and S3.2. A validation of the reconstructed drought index for the Southern Cone, for which independent reconstructions exist is presented in ~~Appendix~~ Supplement S3.3.
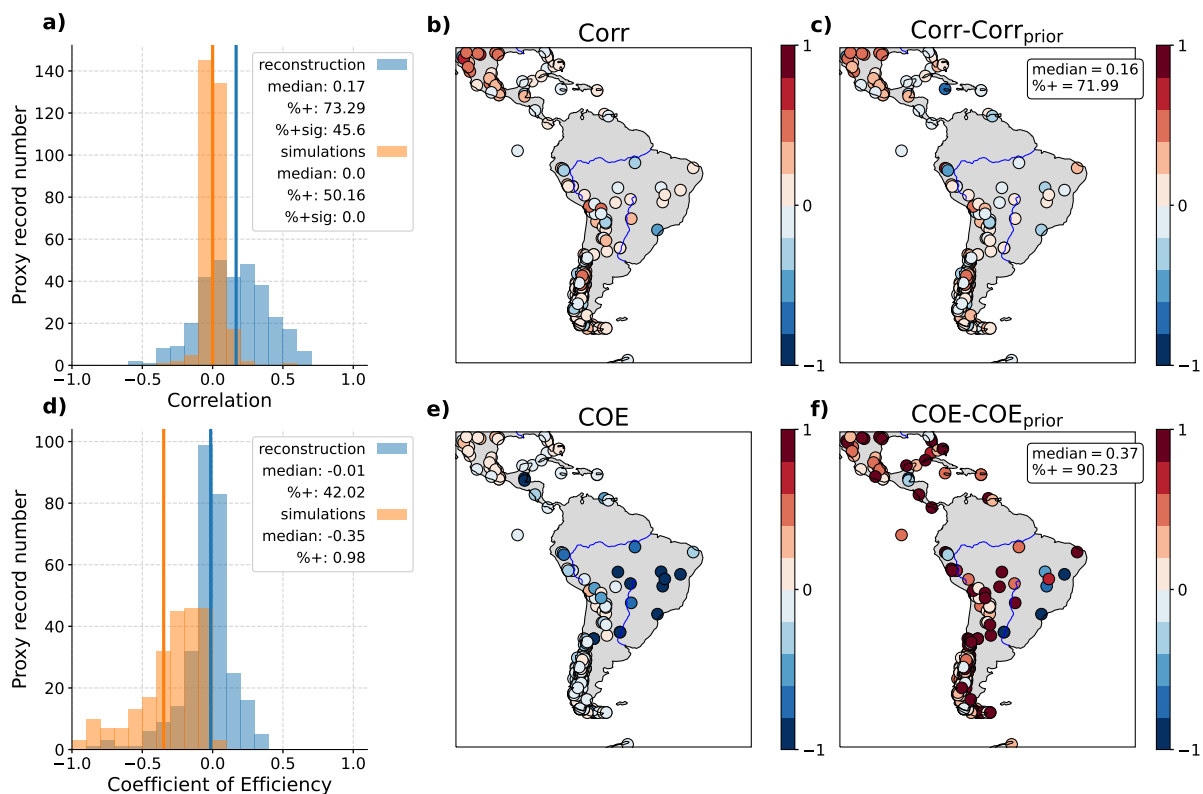
Figure 2. Internal validation. We compute the correlation (a,b,c) and Coefficient of Efficiency (COE) (d,e,f) of reconstructed proxy record time series to true proxy record timeseries when the proxy records are not used as input data in the reconstruction (withheld proxy records). Panel a) and d) show the histogram of the skill scores. The box in the upper right corner displays the median value, the percentage of positive values (%+) and the percentage of positive and significant correlations (%+sig, p-value < 0.05) for the distributions. Panels b) and e) display the skill scores for each location. We additionally computed the skill scores for the model simulations (mean of the five models for each proxy record), which are also included in the histograms and used for a comparison between reconstruction skill scores and the model simulations (c,f). Note, that the COE can also take values smaller than -1. In effect, ~~24~~25% of the COE values for the simulations fall outside of the histogram. While all colorbars have been limited to the range (-1,1) for clarity, values in e) and f) can be more negative than -1, and the difference between reconstruction and simulations in f) also larger than 1.

395   Withholding proxy records in each repetition of the repeated Monte Carlo reconstructions allows us to perform an internal validation of the reconstruction (see Section 3.5). The proxy record estimates from the simulation data (e.g. the simulated isotopic composition of precipitation of the grid cell in which a cave is located) are still part of the prior state matrix, also when a proxy is not used as input data and, therefore, updated in the PaleoDA algorithm. We calculate the correlation and Coefficient of Efficiency (COE) (Nash and Sutcliffe, 1970) of the withheld proxy record time series to their reconstructed

400   counterparts. While the correlation rewards a correct timing of the reconstructed values, the COE is also sensitive to bias and errors in the amplitude by taking into account the variance of the true signal. The COE can take values in the range $[-\infty, 1]$, with positive values indicating skill. However, as pointed out by Cook et al. (1999) and Hakim et al. (2016), the coefficient of efficiency (COE) can misleadingly yield negative skill scores due to proxy records and reconstructions having different mean values and thus the comparison to the prior can be more meaningful than the raw skill scores. We therefore also compute

405   these scores for the prior model simulations and compare the obtained values to those of our reconstruction. To enable a fair comparison between model priors and reconstructions, the skill scores are computed for the period 850-1850CE, which is the period covered by the model simulations. The correlation and COE are computed as the mean correlation for all Monte Carlo repetitions in which a proxy record is not used, by ~~averaging~~ resampling the reconstructed time series to the respective temporal resolution of each proxy record. As we performed 50 Monte Carlo reconstructions with 20% of withheld proxy records, there

410   are on average 10 reconstructions for each proxy record for which it has not been used as input data. ~~We also compute these scores for the prior model simulations and compare the obtained values to those of our reconstruction.~~ This allows us to assess if the reconstruction is in accordance with independent proxy record data and indirectly identify regions in which proxy data share a common climate signal and are similarly reconstructed. The results are displayed in the form of histograms and on maps in Figure 2.

415   We obtain predominantly positive correlations (~~82.03~~73.29%), with a median value of ~~0.21. Most~~ 0.17. Almost half of the correlations are positive and significant (~~60.34~~45.60%). As the correlations of the model simulations to the proxy records are negligible, the reconstruction does lead to a clear improvement in correlation with a median increase of ~~0.22 and 81.02~~0.16 and 71.99% of the records with an improvement. However, a few records stand out with negative correlations in the reconstruction, particularly in geographically isolated areas, while higher correlations are generally obtained in regions with numerous proxy

420   records. For the COE, the obtained median value is -0.01. Yet, ~~43.05~~42.02% of the values result in a positive COE. In comparison to the model priors, there is a notable median increase of ~~0.34, with 89.83~~0.37, with 90.23% of records demonstrating an improved COE value ~~.~~ and thus skill of the reconstruction.

The COE score results underscore the high dissimilarity of proxy records in northern and eastern Brazil, possibly linked to the climate dipole between northeastern Brazil and the core SASM region (Novello et al., 2018; Campos et al., 2019; Wong

425   et al., 2021), where speleothem records exhibit opposing $\delta^{18}O$ trends. This spatial homogeneity in the reconstruction may potentially mask this crucial feature of South American climate. Such homogeneity is expected due to the coarse model grid resolution ~~, which also dictates the reconstructed resolution.~~

~~While the~~ and the spatial smoothing of the EnKF based reconstruction method, in contrast to the high spatial variability of the proxy records. While the raw skill values appear low, they are comparable to those obtained in the global multi-proxy

430 reconstruction by Hakim et al. (2016); Tardif et al. (2019); King et al. (2021). ~~Furthermore, the comparison to~~ The comparison to the skill scores of the ~~raw simulation data underlines~~ prior model simulations emphasizes that the assimilated product represents the climate signal of the proxy records better.

5 Results

5.1 Centennial climate changes

435 Having examined the potential and limitations of our algorithm we now examine the climatic features displayed by the reconstruction. As a first application, we analyze the newly reconstructed climate anomalies during the MCA and the LIA. The definition of these anomalous climate periods is equivocal, as they have not occurred synchronously globally (Neukom et al., 2019). Therefore, we decide to examine finer intervals, namely the period preceding the MCA (Pre MCA, 700 - 925 CE), the Early and Late MCA (925 - 1150 CE, 1150 - 1350 CE) as in Azevedo et al. (2019), a transition period (Trans, 1350 - 1500

440 CE), the LIA (1500 - 1850 CE), and also the current warm period (CWP) (1900 - 2000 CE) to put the anomalies into context. Figure 3 shows the anomalies for the annual reconstruction with respect to the mean of the last millennium (LM, 850 - 1850 CE). The same figure for austral summer (DJF), which overlaps with the monsoon period is displayed in SF 4.1 and for the alternative proxy error definition in SF 4.2. ~~The centennial~~ For the precise temporal evolution of the ~~mean states for the entire CE is shown in ?? to ??.~~ reconstructed variables, the reader is referred to video supplement 1. The reconstructed patterns are

445 mostly homogeneous over the continent and show a trend towards colder and wetter conditions during the LIA, especially for the central and northern part of the continent. The Southern Cone, however, experienced warmer and drier conditions during the LIA. Warmer and drier conditions are predominant during the transition period, in particular preceding the MCA, except for the Southern Cone and the Nordeste (North Eastern Brazil). In the reconstruction using the equal variance proxy error definition (SF 4.2), trends with similar pacing are observed, yet exhibiting greater strength. Remarkably, the important changes

450 of the hydroclimate state before the CWP are mostly conveyed by the speleothem proxy record information, as reconstructions relying only on speleothem data and without speleothem data reveals (SF 4.3 and SF 4.4).

We observe in-phase trends for all reconstructed climate variables and studied periods, generally indicating a simultaneous occurrence of warmer with drier conditions and colder with wetter periods, except during the CWP. Compared to the last millennium mean, the reconstructed CWP anomalies show a more spatially diverse precipitation anomaly field with increased

455 precipitation for the center of the continent. Less precipitation is reconstructed for coastal locations in the north, east, and southern margins of the continent. Temperature and SPEI, in contrast, show warmer and drier conditions for the entire continent, except parts of the La Plata basin and parts of the Southern Cone. The austral summer reconstruction (SF 4.1), however, shows the largest positive temperature anomaly for ~~these regions~~ the Southern Cone. For both annual and austral summer reconstructions, the 20th century is warmer and drier than all preceding phases. In terms of spatial homogeneity, the temperature and

460 SPEI anomalies are more extensive compared to the precipitation reconstruction, which has more diverse spatial features. The reconstructed $\delta^{18}O$ of precipitation values for the studied periods change most in the center of the continent, with a trend towards most depleted precipitation during the LIA. The center of the largest changes in the isotopic composition of precipitation
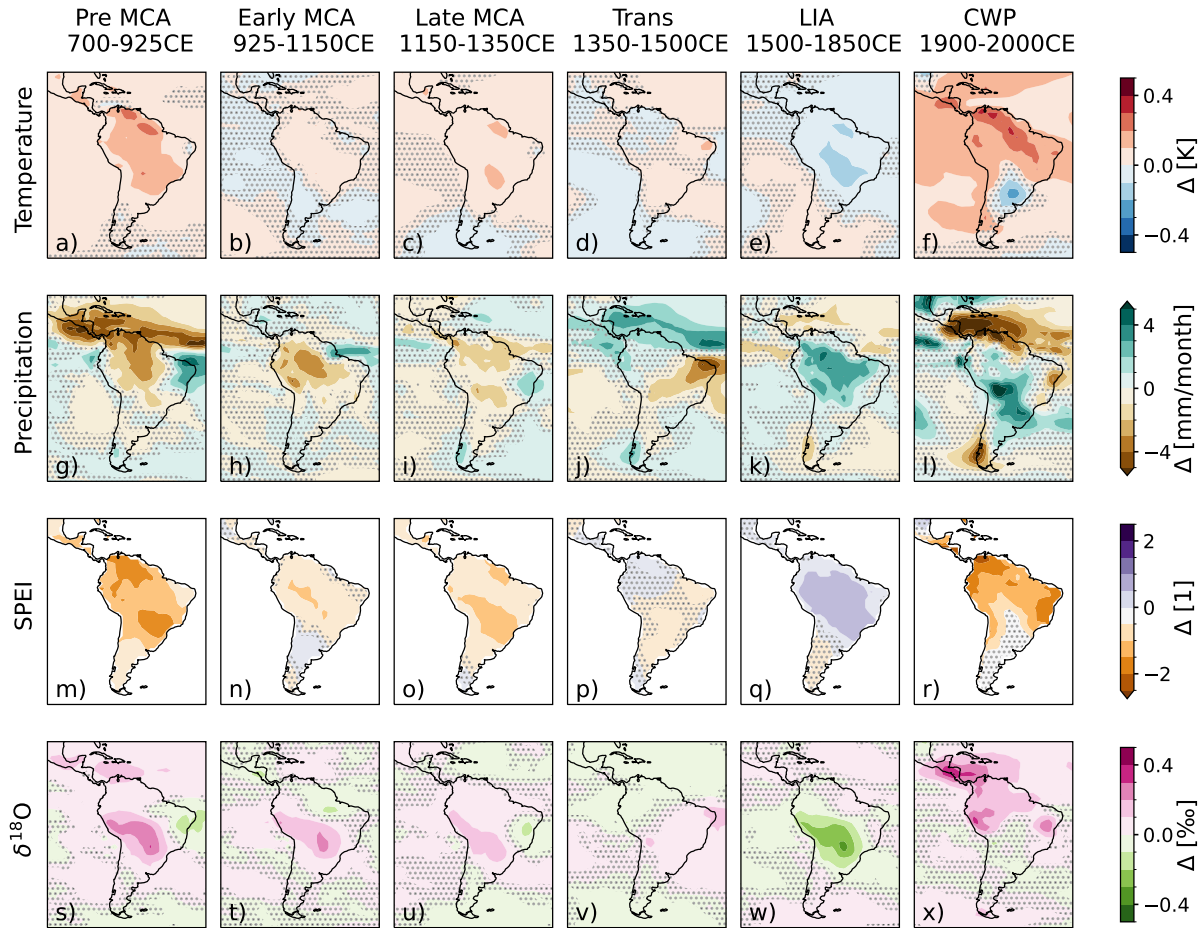
Figure 3. Reconstructed mean anomaly fields for temperature (a-f), precipitation (g-l), SPEI (m-r) and δ^{18}O (s-x) during five periods with respect to the Last Millennium mean (LM, 850 - 1850 CE). The studied periods are the years preceding the Medieval Climate Anomaly (Pre MCA, 700-925 CE, first column), the early MCA (925-1150 CE, second column), the late MCA (1150-1350 CE, third column), the transition period (Trans, 1350 - 1500 CE, fourth column), the LIA (1500 - 1850 CE, fifth column) and the current warm period (CWP) (1900-2000 CE, sixth column). The SPEI values have been standardized using the variance of the period 850 - 1850 CE. Stippling indicates grid cells where the difference to the Last Millennium values is not significant according to a Welch's t-test ($\alpha > 0.01$).

is located further to the south than the region of the largest precipitation changes. The δ^{18}O values of precipitation display a dipole pattern over the Nordeste and central South America, except during the more homogeneous MCA-LIA transition period and CWP, where a pronounced δ^{18}O enrichment is seen for the northern and western part of the continent.

5.2 South American Summer Monsoon variability

Spectra of reconstructed monsoon precipitation index. On the left (a), the Multitaper method (MTM) - power spectral densities (PSD) of the annual reconstructions involving different subsets of the proxy record database. The time series have not been standardized and detrended, but resampled to 10 year averages to achieve comparability between reconstructions involving different time scales. On the right (b), the continuous wavelet spectrum for the reconstructed time series involving all proxy records is shown. The dotted black line indicates the cone of influence and the white lines indicate the 95% significance level for an AR1 process. All spectra have been computed using the Pyleoclim package in Python (Khider et al., 2022).

To assess changes in the SASM strength throughout the past two millennia, we analyze the mean precipitation anomaly in the core monsoon region as a simplified monsoon index. We use the definition by Vuille et al. (2012), who proposed computing the mean precipitation in the core monsoon region (5° S–17.5° S/72.5° W–47.5° W, see black rectangle in Figure 1) as an indicator of monsoon strength. Additionally, we further investigate δ^{18}O, temperature and SPEI changes in the core monsoon region. Figure 4 shows the anomalies from the annual reconstructions in comparison to the reconstructions LMRv2.1 (Tardif et al., 2019) and PHYDA (Steiger et al., 2018). We also performed the reconstruction with subsets of the complete proxy record database, only relying on speleothems or tree data, or excluding the speleothems from the complete proxy record database to investigate the effect of using different climate archives.

Overall, the reconstructed monsoon index in Figure 4 shows and the video supplements 2 and 3 show a colder and wetter LIA, particularly after 1500 CE with anomalies of up to 4 mm/month in the lowpass-filtered curve. Least precipitation is reconstructed for the period from 750 - 1100 CE, while the SPEI values reach a local minimum earlier in the period 600 - 900 CE, and thus seem to more strongly follow the temperature curve, which reaches a local maximum during the same period. Reconstructed temperatures are highest and SPEI - SASM indices lowest during the 20th century. This hints at the effects of anthropogenic warming being evident in the core monsoon region on a centennial time scale. Figure 4 shows that the tree-only reconstruction does not reflect the pronounced centennial hydroclimate variability, although the tree ring data represents the dominant climate archive in our proxy record database in terms of numbers. Comparing the reconstruction that exclusively uses speleothem records to the one that excludes speleothems reveals reconstructed hydroclimate changes in the core monsoon region to be largely driven by the speleothem signal. However, wetter LIA conditions are also captured by other archives. The same figure for the austral summer reconstruction and the *all proxies* estimates of the single model priors can be found in SF 4.5and SF 4.7. We note that the presented results draw on mean values of the MME reconstruction . As visible in SF 4.7, the magnitude of reconstructed changes can vary considerably between the single model reconstructions, in particular for precipitation, exhibiting similar trends but larger magnitudes. Furthermore, the smaller reconstruction uncertainty for reconstructions involving speleothems is noticeable, especially compared to the tree ring only reconstruction prior to 1400CE (SF 4.6), although the overall uncertainty remains large due to the large spread in the prior ensemble.
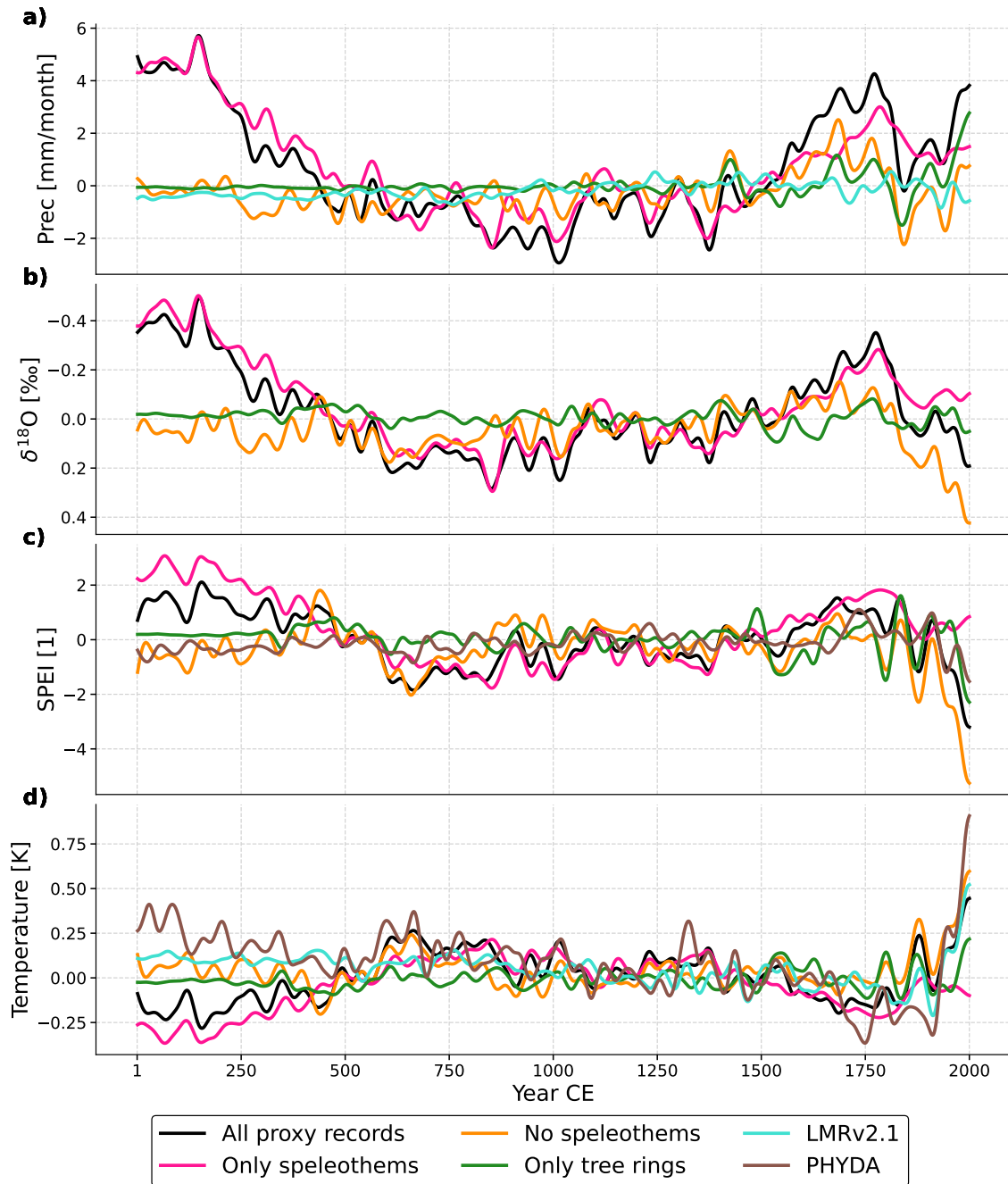
Figure 4. Mean anomalies of precipitation, δ^{18}O , SPEI, and temperature in the core monsoon region $(5° − 17.5° \text{ S } / 72.5° − 47.5°$ W). Comparison of reconstructed mean annual precipitation (panel a), δ^{18}O (panel b), SPEI (panel c) and temperature (panel d) anomalies in the core monsoon region from reconstructions using all proxy records, excluding the speleothems, using only speleothems and only trees and the reconstruction products PHYDA (Steiger et al., 2018) and LMRv2.1 (Tardif et al., 2019). All time series have been smoothed with a 50-year-lowpass-filter. The anomalies are displayed with respect to the 850 - 1850 CE mean. Note the inverted y-axis for δ^{18}O in order to match the precipitation trend. PHYDA and LMRv2.1 do not include all variables studied here, and are thus partially missing in panel a), b) and c). The SPEI values have been standardized using the variance of the 850 - 1850 CE period. For means of comparability between different reconstructions, we have chosen to display the annual mean reconstruction.

Figure 4a additionally displays the LMRv2.1 precipitation reconstruction, which shows lower centennial-scale variations, including no significant changes during MCA, LIA or CWP. Precipitation is not included in the PHYDA reconstruction; however, the comparison of reconstructed SPEI also presents less hydroclimate variability during the LIA and the pre and early

500   MCA phase. The temperature reconstruction in Figure 4c shows the largest range of values for the PHYDA reconstruction, followed by the reconstructions of this study, and lastly the LMR reconstruction, which shows the least temperature variability. PHYDA shows a constant temperature decline during the CE with a steep reversal during the 20th century, resulting in the expected hockey stick-like curve, which is also found in our reconstruction, except before 400 CE. The period before 400 CE is peculiar for our reconstruction in all four variables. It shows very wet and cold conditions for the first two centuries of the

505   CE and a subsequent transition to more neutral conditions. The reconstructed extremes even exceed the LIA in magnitude.
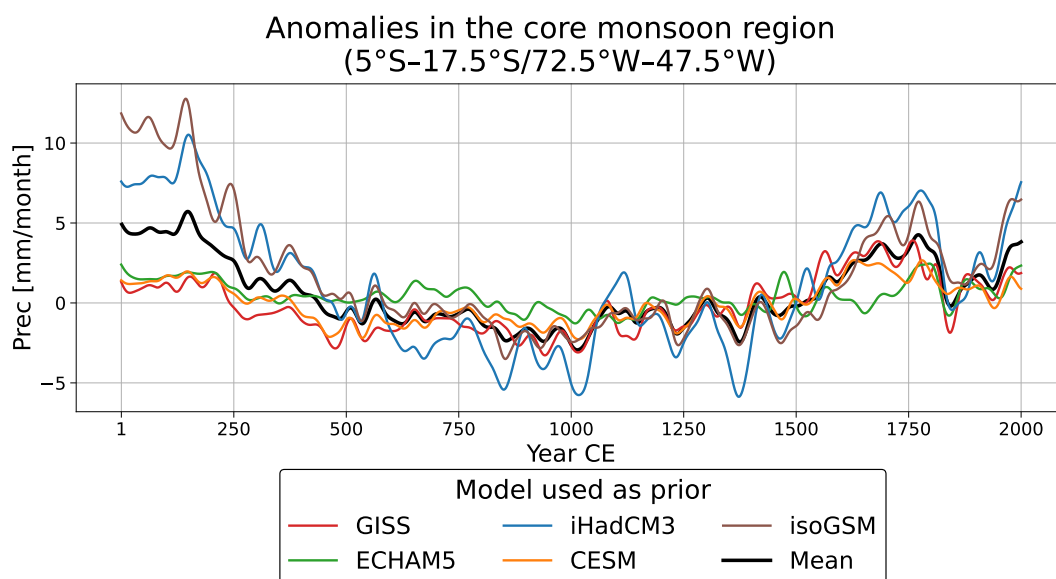
Figure 5. Single model reconstructions of the monsoon precipitation index using all proxy records, highlighting the prior dependency of the precipitation reconstruction. The black denotes the the multi-model mean, which is used in the multi-model ensemble analysis.

We note that the presented results draw on mean values of the MME reconstruction. As visible in Figure 5 for the precipitation and SF 4.7 for all reconstructed variables, the magnitude of reconstructed changes can vary considerably between the single model reconstruction. It is noticeable, that the prior to 400CE wet phase is particularly pronounced in the isoGSM and ECHAM5 model, and is only wetter than the LIA in these two models. For the austral summer SASM index reconstruc-

510   tion (SF 4.7SF 4.5), the range of values for the precipitation anomalies is almost twice as large as for the annual reconstruction, although the overall trends are very similar. Comparing the all proxy record reconstruction to the raw prior model simulation without PaleoDA shows that while the model simulations do exhibit more important fluctuations, they do not exhibit clear trends, for instance of a cooler and wetter hydroclimate during the LIA (SF 4.8).
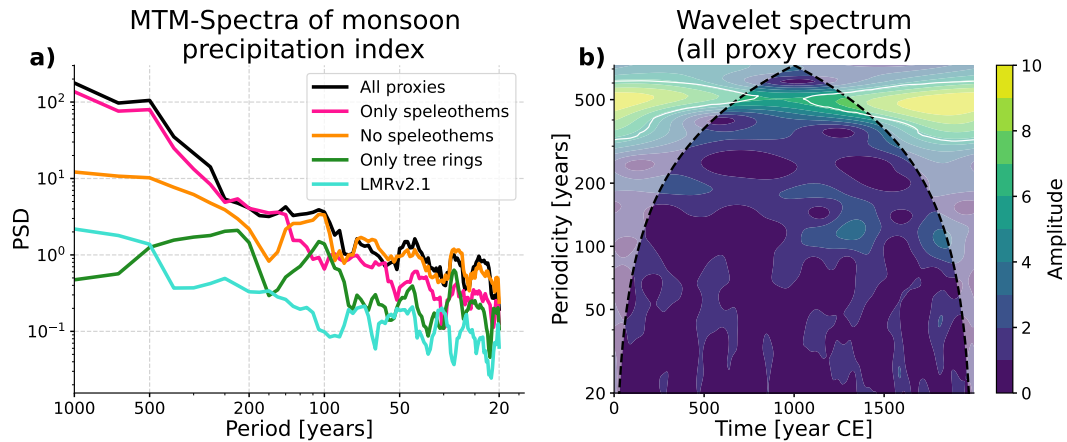
Figure 6. **Spectra of reconstructed monsoon precipitation index**. On the left (a), the Multitaper method (MTM) - power spectral densities (PSD) of the annual reconstructions involving different subsets of the proxy record database. The time series have not been standardized and detrended, but resampled to 10 year averages to achieve comparability between reconstructions involving different time scales. On the right (b), the continuous wavelet spectrum for the reconstructed time series involving all proxy records is shown. The dotted black line indicates the cone of influence and the white lines indicate the 95% significance level for an AR1 process. All spectra have been computed using the Pyleoclim package in Python (Khider et al., 2022).

To further study and quantify climate variability in the core monsoon region we calculated the power spectral distributions of the precipitation anomaly curves (Fig. 6a). In addition, the continuous wavelet spectrum of the SASM precipitation reconstruction involving all proxy records was computed to investigate the power variation in time over the common era. The same spectral analysis for the reconstructed $\delta^{18}O$ signal in the core monsoon region can be found in SF 4.9. The precipitation spectra have typical *red noise* characteristics, with the power decreasing exponentially towards higher frequencies, except for the reconstruction only based on tree data, which has a flat power spectrum. The reconstructions including the speleothems show the highest redness with a decline in power over three orders of magnitudes, as also indicated by the pronounced multi-centennial variability in Figure 4. Without the speleothems, the power distribution extends over two orders of magnitude. The power spectrum of the SASM precipitation anomaly in the LMRv2.1 reconstruction, remains flat and similar to the spectrum of the tree-ring only reconstruction. The wavelet spectrum of the all proxy precipitation reconstruction also exhibits multi-centennial variability of the SASM (Fig. 6b), although it is not above the signifance threshold. The spectra for the $\delta^{18}O$-SASM index, which might be represented more directly by the available proxy records show similar *red noise* characteristics (SF 4.9). For further comparison, we compared the spectrum of the SASM precipitation index to the spectra of the index in the prior model simulations. To do so, we took into account that the model simulations span a shorter time period than the entire reconstruction period and that they have a higher variance than the reconstruction. The spectra of all five model simulations have a flat shape and thus a smaller variability scaling than the reconstruction (SF 4.10).

6   Discussion

6.1   Reconstructed hydroclimate changes

Our climate field reconstruction of the South American Hydroclimate during the CE represents a comprehensive synthesis of an encompassing diverse collection of proxy record data and isotope-enabled climate simulations. The reconstructed centennial climate changes in tropical South America, transitioning from a drier MCA to a wetter LIA, align well with individual proxy record assessments from the region (Bird et al., 2011a; Vuille et al., 2012; Deininger et al., 2019) and proxy record syntheses (Campos et al., 2019; Orrison et al., 2022). ~~This consistency~~ The consistency with the conclusions of these studies is expected, given that we used the same (and more) proxy records and the temporal pacing of the reconstruction relies on the information provided by the proxy records within the offline PaleoDA algorithm. We did not perform direct quantitative comparisons between our climate field reconstruction and individual proxy records from single or multi-proxy studies. This is because speleothem δ^{18}O values, being a proxy for large-scale regional atmospheric behavior, is not expected to agree precisely with local hydrology. Our reconstruction aims to capture broader regional patterns rather than exact local conditions.

The PaleoDA climate field reconstruction offers the advantage of extrapolating proxy record information to more climate variables, such as temperature from speleothem δ^{18}O for instance, which in this region is mainly only interpreted in terms of precipitation amount changes. The magnitude of reconstructed precipitation amount and SPEI surpass the estimates from the PHYDA and LMRv2.1 reconstructions, while the changes in temperature show similar magnitudes. It is worth noting that the highest temperature anomalies are reconstructed for the period preceding the MCA reference period 950 - 1250 CE (Fig. 6~~and ??~~). This pattern is also observed in the PHYDA and LMR reconstructions (SF 4.11 and SF 4.12), which rely on fewer local proxy record data points from South America for that period. In line with Neukom et al. (2019), South America does not show coherent warming during the MCA compared to other regions globally, which contrasts with the qualitative study by Lüning et al. (2019). Although our reconstruction includes anomalous conditions, their timing might differ from the Northern Hemisphere anomalies. Thus, this reference time period should be used with caution in global comparisons.

Another similarity between our reconstruction and PHYDA and LMRv2.1 is the presence of anomalies of opposite signs in the Southern Cone region compared to the Northern and Central part of the continent. The influence of the Southern Annular Mode in this region may, for instance, cause this distinct opposite climate system. Our reconstruction also reveals a spatial feature over northeastern Brazil, where opposite anomalies in precipitation, drought index and δ^{18}O are observed compared to the rest of tropical South America. This dipole pattern, previously identified in regional speleothem studies, has been linked to meridional changes in the Hadley cells (Cruz et al., 2009; Novello et al., 2012, 2018) and interhemispheric temperature gradients (Campos et al., 2022). The presence of this dipole pattern in our reconstruction was not necessarily expected, considering the limited number of speleothems from the Nordeste and the relatively coarse spatial resolution of the climate models. In addition, looking into the spatial correlations of the mean δ^{18}O of precipitation values for that region in the model simulations ~~does not reveal a clear dipole in all~~ only shows a dipole in two out of the five climate model simulations (SF 4.13)~~and thus reveals~~, thus revealing the benefit of combining proxy and model data with PaleoDA. However, more research for quantifying

the extent and possible spatio-temporal variations of the South American δ^{18}O and precipitation dipole is required, also by incorporating additional proxy records from NEB as we currently only employ two.

565   A consistent pattern in our hydroclimate reconstruction are the synchronous trends for all variables during most of the CE, except for the 20th century. However, it is essential to acknowledge that the reconstruction technique may also influence this in-phase relationship. Offline PaleoDA with the EnKF, being inherently linear, employs the same static covariance patterns from the simulations at each time step. The in-phase relationship represents the default state of the reconstruction. The increased strength of the SASM during the LIA has been explained by cooler temperatures on the Northern Hemisphere, resulting in a

570   southward shift of the ITCZ (Deininger et al., 2019; Vuille et al., 2012). Integrating our employed proxy records into a global climate field reconstruction, and possibly including more atmospheric variables, could provide a more in-depth understanding and allow for testing this hypothesis.

An unexpected finding in our reconstruction is the evidence of wetter and colder conditions prior to 400 CE. Primarily, the speleothem data support these changes. Upon closer examination of the individual anomalies of the available records in SF

575   4.14, only three records exhibit particularly negative δ^{18}O anomalies for that period. ~~Also~~Furthermore, during that time, proxy records from the margin and outside the core monsoon region are the only available sources. Still, the spatial correlations in the model simulations for the precipitation in the core SASM region prove to be extensive, such that the signal from proxy records outside of the region can influence the reconstructed SASM precipitation (SF 4.15). The increased SASM strength stays consistent even after excluding possibly diverging single records that were suspected to cause the anomalies in the

580   reconstruction.

While the magnitude of the wet conditions also proved to be model prior dependent, the source of model differences in the reconstruction cannot be directly deduced from the simulated SASM indices and the correlations in the model, requiring further analysis of the topic. In addition to the correlation analysis that we did for the core monsoon region and NEB, an optimal sensor placement analysis as performed by Comboul et al. (2015) and King et al. (2023) could give insights into how different proxy

585   records influence the reconstruction depending on the model prior.

6.2   ~~Comparison~~ Examining reconstructed trends in relation to ~~reconstructions from~~ single proxy records

Putting attention to particularly anomalous proxy records reveals further insights into the nature of our reconstruction. For instance, the record with the strongest negative anomaly from Paraiso Cave (SISAL-ID 424) in the eastern Amazon basin (Ward et al., 2019; Azevedo et al., 2019) exhibits a distinctive increase in δ^{18}O values after 900 CE, resulting in negative δ^{18}O

590   anomalies during the early Common Era compared to the reference period (1750-1850 CE). This increase may be caused by non-climatic influences, which potentially introduces artifacts in our anomaly reconstruction. The record also stands out in the internal validation procedure (Figure 2). Nonetheless, this record has been cross-validated with archaeological evidence from the region, which also suggests a shift from wetter conditions in the first millennium to drier conditions in the second millennium (de Souza et al., 2019). In contrast to other speleothem locations in tropical South America, the Paraiso Cave

595   record is additionally influenced by the rainfall of the two distinct systems, SASM and ITCZ. Our PaleoDA approach may not be able to resolve this complex local climate. Different to the drier conditions recorded in Paraiso Cave (Ward et al., 2019),

the reconstruction does not show drier conditions during the LIA for the eastern Amazon basin, but wetter conditions as for entire tropical South America. While this record has an important influence in the first centuries of the reconstruction, it is outweighed by the multitude of other records during the LIA.

The contrast between reconstructed wetter and colder climate anomaly fields during the LIA to the information provided by single records highlights the spatial smoothing caused by the PaleoDA method, which we consider the central limitation of our study. The EnKF employs spatial covariances between grid cells and variables in the climate model simulations, which tend to be spatially extensive when computed over the last millennium. As a result, the reconstruction for the eastern Amazon basin displays wetter conditions, because this is the condition recorded by the majority of the proxy records. While the PaleoDA methodology aims to compute the best climate field estimate from all observations, this example demonstrates that the reconstruction may not always align well with individual observations. This spatial smoothing effect due to the model covariances has been noted in PaleoDA literature before, e.g., Sanchez et al. (2021), who focused on ENSO reconstructed from coral records during the 19th century, or Erb et al. (2022) who reconstructed the entire Holocene (see the outstanding proxy record anomalies in their Figure 10). In statistical terms, PaleoDA with the EnKF may cause a loss of spatial degrees of freedom in the reconstruction, which can be expressed in terms of the explained variance of the leading modes obtained via a Principal Component Analysis (Bretherton et al., 1999). We are not aware of studies investigating climate field reconstructions under the aspect of spatial degrees of freedom, and doing so would be out of scope for this study. However, we note that when investigating spatial temperature correlations of CE reconstructions, Bakker et al. (2022) found larger inter-continental correlations for a PaleoDA reconstruction product compared to other methods (see their Figure 5). Although our reconstruction product is provided at a spatial resolution of 1.875° x 1.875°, it is more likely to reliably represent spatially extensive regions rather than single grid cells. This aspect is further emphasized by the fact that the climate model simulation data was up-sampled to the resolution of the model with the highest spatial resolution.

Despite using five different isotope-enabled climate model simulations to mitigate the effect of single model biases, an ensemble of five models still represents a small ensemble of opportunity. Further, water isotopes have not been included in climate model intercomparison projects, and the number of publicly available simulations is limited to the five models we have employed. The reconstruction would importantly benefit from more isotope-enabled simulations with a variety of models and more up-to-date forcing, such as volcanic forcing (e.g Sigl et al., 2015). Future PaleoDA reconstructions will also profit from explicitly studying the differences in spatial covariances simulated by the models to potentially discard overly or undersensitive models (e.g., in the covariance relationship of $\delta^{18}O$ values and precipitation changes). Multi-model reconstructions should further account for similarities between models in the form of weighted ensembles (Eyring et al., 2019). Alternatively, perturbed physics ensembles of isotope-enabled simulations for a single model would allow for larger ensembles and a transient offline PaleoDA approach as used by Franke et al. (2017) and Valler et al. (2020). The high computational cost of including water isotopes in the simulations currently restrains this type of experiment.

PaleoDA reconstructions going back deeper in time have also employed prior ensembles that are moving with time to account for changing boundary conditions and, thus, the non-stationarity of simulated covariances (Osman et al., 2021; Erb

et al., 2022). However, the time scales on which covariance patterns of specific hydroclimate variables in the climate system change have not been studied formally yet.

6.3 Multi-decadal hydroclimate variability in the reconstruction

We also studied the reconstructed hydroclimate variability to assess the impact of different proxy archives, particularly speleothems.
635 The power spectral distributions of the reconstructed SASM precipitation strength underscore that the use of different climate archives yields distinct hydroclimate variability patterns. Remarkably, the inclusion of speleothems lead to substantial variability increase on multi-decadal to centennial time scales, contributing to a potentially more realistic reconstruction of the South American hydroclimate.

The signficant multi-centennial variability of the SASM (Fig. 6) is comparable, albeit less pronounced and persistent, to
640 findings in individual speleothem records (Novello et al., 2012; Apaéstegui et al., 2014; Novello et al., 2016; Deininger et al., 2019), where this variability was attributed to solar cycles of 83 and 208 years. However, it is essential to consider that the reconstructed 2000-year time series is probably too short to definitively establish causal relationships for multi-centennial variability. Previous research found only small attributions of solar forcing over the last millennium (Schurer et al., 2013). Future PaleoDA reconstructions using speleothem data may focus on longer reconstruction periods to more thoroughly investigate
645 links to solar forcing.

The resemblance between the reconstructed hydroclimate variability in our study and the estimates from single proxy record studies is expected, given that we use data from these studies as input. However, PaleoDA enables us to underscore the connection between the isotopic composition of precipitation and precipitation amount. Moreover, spectral analyses derived from proxy record compilations generally yield more reliable estimates of hydroclimate variability.

650 Our study did not explicitly aim to compare hydroclimate variability in the reconstruction with that of climate model simulations. However, initial analyses reveal a more pronounced multi-decadal to centennial hydroclimate variability in the reconstruction, corroborating previous model-data comparisons for speleothems and isotope-enabled climate models. For tropical South America, (Orrison et al., 2022) demonstrated that the GISS and iCESM last millennium simulations underestimate centennial monsoon intensity changes in the isotopic composition of precipitation. On a global scale, (Bühler et al., 2020) found
655 an underestimation of multi-decadal to centennial variability, using climate simulations also included in our study. A similar underestimation of multi-decadal to centennial variability was previously found for precipitation in the CMIP5 Last Millennium ensemble both for tropical South America (Parsons et al., 2018) and globally (Ault et al., 2012; Parsons et al., 2017), where the spectra were shown to resemble that of white noise. Additionally, for temperature, it is now established that while climate models generally capture the climate variability of global mean temperature, they underestimate regional temperature
660 variability (Laepple et al., 2023b). Our PaleoDA reconstruction, thus, represents a compromise between climate models and climate proxy records, potentially providing a more realistic representation of hydroclimate variability scaling than models alone. We emphasize that the reconstruction of multi-decadal to centennial variability would not have been feasible without the multi-timescale PaleoDA approach, enabling the inclusion of speleothems primarily for technical reasons. It remains to be determined if the use of multi-year covariances, instead of annual ones, in the PaleoDA algorithm also contributed to this, a

665 matter beyond the scope of this publication but suggested by pseudo-proxy experiments (Steiger and Hakim, 2016; Choblet et al., 2023).

In principle, our reconstruction could be employed to investigate interannual variations in SASM strength, for which ENSO is considered a driver (Garreaud et al., 2009). However, we only employed the key archive for SASM variability, the speleothems, at a decadal resolution, even though many of the records technically have a finer resolution. The conservative approach of using

670 decadal time scales for speleothems was adopted to avoid additional complexity arising from dating uncertainty, sampling from age-model ensembles during the reconstruction and taking into account the transit time of cave seepage water. Developing a scheme that considers all these factors would enable to study the influence of ENSO on SASM variability. Employing speleothems at higher resolutions might also improve validation results against 20th-century instrumental precipitation in the region.

675 ## 6.4 Future developments

To enhance the PaleoDA reconstruction, exploring more elaborate PSMs could be beneficial to perform absolute value reconstructions instead of anomaly reconstructions. In previous work leading up to this study, the speleothem PSM proposed by Dee et al. (2015) was tested, but did not reduce offsets between models proxy records. This can result from either model-biases, from PSMs that do not incorporate processes known to a local cave expert, or from lack of physical understanding of the

680 records. Therefore, we compared simulation and proxy record anomalies by taking known seasonality into account or via a linear regression for tree and coral time series. For speleothems, including information from local cave monitoring studies (e.g. Moquet et al., 2016; Sekhon et al., 2021; Jiménez-Iñiguez et al., 2022), could provide a better understanding of the proxy record and help recognize model biases in simulated $\delta^{18}O$ of precipitation values as well as improve PSMs. However, this usually requires more metadata of individual cave systems, which is not always available and may reduce the selection of usable proxy

685 records.

When employing more elaborate PSMs in PaleoDA, it is essential to test their effect on the covariance patterns as nonlinear mathematical operations can impact covariances unexpectedly. Applying PSMs of higher complexity to instrumental data could also improve the assessment of proxy error and SNR. Although we consider the employed SNR of 0.5 ratio reasonable, it remains a broad assumption due to the lack of sufficiently long instrumental data at the cave locations. Previous PaleoDA

690 reconstructions without clear proxy record error have used a post-hoc adjustment of the error variance (Tierney et al., 2020; Osman et al., 2021). However, we refrain from doing so here, as the tuned errors might be confounded by model biases in the covariances and the proxy record error should represent a real physical and statistical property rather than a tunable hyperparameter. An alternative reconstruction setting proxy record variance equal to the prior record variance yielded similar climate fields with more pronounced magnitudes in hydroclimatic changes (SF 4.2). Due to the similarity, we have not investigated

695 these reconstructions further, but emphasize, that in the light of the unclear SNR of speleothems and other proxy records, an equal prior/proxy weighting approach would be equally legitimate.

7 Conclusion

This study presents the first South American climate field reconstruction for the entire CE and the entire continent. By incorporating speleothems and other non-annually resolved climate archives through a multi-timescale Data Assimilation approach, we have improved spatial proxy record coverage for South America compared to previous global reconstructions and eliminated the need for uncertain calibration of low-resolution isotopic records to temperature and precipitation. Our primary focus was centered on centennial climate changes, with particular attention to the intensity of the SASM. The reconstruction reveals compelling evidence of a strengthened monsoon during the LIA, contrasting with a weaker SASM before, in particular during the early phase of the MCA. We also found a strengthening during the first centuries of the CE, which remains more elusive due to the more limited number of proxy records. In our reconstruction, speleothems played a vital role in capturing centennial variability.

While this study showcases the potential of the multi-timescale PaleoDA reconstruction approach including speleothems, we acknowledge certain limitations that warrant further investigation. ~~The reconstruction's validation, uncertainties~~ Uncertainties in proxy record errors, spatial smoothing of the reconstruction, and the necessity for a larger ensemble of isotope-enabled climate model simulations with diverse models are important areas for future research. Particular emphasis must be placed on improving the validation of multi-time scale PaleoDA reconstructions based on low-resolution proxy records such as speleothems, as this proves to be particularly challenging due to lack of instrumental data. Our work relies on the assumption that speleothem δ^{18}O values indicate large-scale precipitation changes. This assumption will benefit from further validation, particularly through analysis of speleothem records that reliably capture SASM fluctuations at sub-decadal timescales. The establishment of validation protocols will further help in better assessing the reconstruction skill of multi-time scale PaleoDA reconstructions. Additionally, exploring differences in simulated covariance patterns, fundamental to the PaleoDA EnKF reconstruction algorithm, holds promise for refining and enhancing this methodological approach. We make our reconstructed datasets publicly available, providing a foundation for future climatological data analysis including comparisons to proxy records, other reconstructions, and climate simulations. Furthermore, by publishing the code for the multi-timescale PaleoDA algorithm alongside this study, we encourage and enable the application of the multi-timescale PaleoDA method to proxy records of different temporal resolutions. This concept has great potential for global climate field reconstructions, particularly for the CE and older time periods, where speleothems and other non-annually and irregularly resolved proxy records serve as essential indicators of past hydroclimate changes.

Code and data availability. Code to reproduce reconstructions, figures and data preprocessing are available on GitHub https://github.com/mchoblet/paleoda_sa. The reconstructed climate fields are available via a Zenodo repository https://zenodo.org/records/10622264. We recommend using the multi-model ensemble mean of the reconstructions. The input data for running the reconstruction is accessible via a second Zenodo repository https://zenodo.org/records/10370000. We use the model data originally available at https://zenodo.org/records/7516327 (Bühler et al., 2022).

The SISAL (Speleothem Isotopes Synthesis and AnaLysis Working Group) version 3 database (SISALv3) is publicly available at https://doi.org/10.5287/ora-mzy8pozvk (Kaushal et al., 2023). The PAGES2k Database (Emile-Geay et al., 2017) is available at https://lipdverse.org/project/pages2k/. The Iso2K Database (Konecky et al., 2020) is available at https://lipdverse.org/project/iso2k/. The South American Drought Atlas Database is available at https://www.cr2.cl/datos-dendro-sada/. References for the individual records are listed in Supplement S1.2.

The PaleoDA code and the figures were created using the Python programming language (Van Rossum and De Boer, 1991), version 3.10 and with a collection of open-source packages, notably Xarray (Hoyer and Hamman, 2017), Numpy (Harris et al., 2020a), Matplotlib (Hunter, 2007), Cartopy (Met Office, 2010 - 2015), Pyleoclim (Khider et al., 2022), Scipy (Virtanen et al., 2020), Pandas (Wes McKinney, 2010) and Numba (Lam et al., 2015).

Video supplement. The reconstructed climate fields are also provided for the *all proxy records* reconstruction in animated form for

1. Temperature, Precipitation, SPEI and δ^{18}O climate fields: https://av.tib.eu/media/66877 (DOI: 10.5446/66877).

2. Precipitation reconstruction and monsoon curve side by side, comparison to the reconstruction by Neukom et al. (2019) https://av.tib.eu/media/66879 (DOI: 10.5446/66879).

3. Precipitation reconstruction and monsoon curve side by side, overlaying of the speleothem δ^{18}O anomalies, comparison to the reconstruction by Neukom et al. (2019) https://av.tib.eu/media/66880 (DOI: 10.5446/66880).

Author contributions. MC, JB, VN, NS and KR designed this study. MC developed the PaleoDA code and produced the reconstructions. MC and JB wrote the paper and MC created the figures. VN, NS and KR contributed with data interpretations and to the revisions of the manuscript. All authors approved of the final version of the paper.

Competing interests. The authors declare that they have no conflict of interest.

Acknowledgements. We thank Raphael Neukom and one anonymous referee for insightful comments and helpful suggestions, which helped in improving the quality of our reconstructions and the manuscript. As this study includes data complied by SISAL (Speleothem Isotopes Synthesis and Analysis), we thank the Pages2k and the Iso2k network, working groups of the Past Global Changes (PAGES) project. We thank all initial authors that provided model simulation data, proxy record data and those researchers who compiled the proxy record databases. We thank Mariano Morales from CONICET, Argentina for sharing tree ring data from the South American Drought Atlas and further tree ring collections and Michael Erb and Matt Osman for fruitful discussions about PaleoDA. Nils Weitzel, Beatrice Ellerhoff and Markus Maisch are acknowledged for helpful advice and comments during the elaboration of this project.

We acknowledge support from the Open Access Publication Fund of the University of Tübingen.

Financial support. This research has been supported by the Deutsche Forschungsgemeinschaft (grant nos. 316076679, 395588486, and 442926051) and the Bundesministerium für Bildung und Forschung through the PalMod project (grant no. 01LP1926C). NS is supported by the Israel Science Foundation (grant no. 2654/20). We acknowledge support from the Open Access Publication Fund of the University of Tübingen.

References

Abram, N. J., Mulvaney, R., Wolff, E. W., Triest, J., Kipfstuhl, S., Trusel, L. D., Vimeux, F., Fleet, L., and Arrowsmith, C.: Acceleration of snow melt in an Antarctic Peninsula ice core during the twentieth century, Nature Geoscience, 6, 404–411, https://doi.org/10.1038/ngeo1787, 2013.

Aceituno, P., del Rosario Prieto, M., Solari, M. E., Martínez, A., Poveda, G., and Falvey, M.: The 1877–1878 El Niño episode: associated impacts in South America, Climatic Change, 92, 389–416, https://doi.org/10.1007/s10584-008-9470-5, 2008.

Adams, J.: climate indices, an open source Python library providing reference implementations of commonly used climate indices, https://github.com/monocongo/climate_indices, 2017.

Akers, P. D., Brook, G. A., Railsback, L. B., Liang, F., Iannone, G., Webster, J. W., Reeder, P. P., Cheng, H., and Edwards, R. L.: An extended and higher-resolution record of climate and land use from stalagmite MC01 from Macal Chasm, Belize, revealing connections between major dry events, overall climate variability, and Maya sociopolitical changes, Palaeogeography, Palaeoclimatology, Palaeoecology, 459, 268–288, https://doi.org/10.1016/j.palaeo.2016.07.007, 2016.

Ampuero, A., Stríkis, N. M., Apaéstegui, J., Vuille, M., Novello, V. F., Espinoza, J. C., Cruz, F. W., Vonhof, H., Mayta, V. C., Martins, V. T. S., Cordeiro, R. C., Azevedo, V., and Sifeddine, A.: The Forest Effects on the Isotopic Composition of Rainfall in the Northwestern Amazon Basin, Journal of Geophysical Research: Atmospheres, 125, https://doi.org/10.1029/2019jd031445, 2020.

Anchukaitis, K. J. and Smerdon, J. E.: Progress and Uncertainties in Global and Hemispheric Temperature Reconstructions of the Common Era, Quaternary Science Reviews, 286, 107 537, https://doi.org/10.1016/j.quascirev.2022.107537, 2022.

Annan, J. D., Hargreaves, J. C., and Mauritsen, T.: A New Global Surface Temperature Reconstruction for the Last Glacial Maximum, Climate of the Past, 18, 1883–1896, https://doi.org/10.5194/cp-18-1883-2022, 2022.

Apaéstegui, J., Cruz, F. W., Sifeddine, A., Vuille, M., Espinoza, J. C., Guyot, J. L., Khodri, M., Strikis, N., Santos, R. V., Cheng, H., Edwards, L., Carvalho, E., and Santini, W.: Hydroclimate Variability of the Northwestern Amazon Basin near the Andean Foothills of Peru Related to the South American Monsoon System during the Last 1600 Years, Climate of the Past, 10, 1967–1981, https://doi.org/10.5194/cp-10-1967-2014, 2014.

Apaéstegui, J., Cruz, F. W., Vuille, M., Fohlmeister, J., Espinoza, J. C., Sifeddine, A., Strikis, N., Guyot, J. L., Ventura, R., Cheng, H., and Edwards, R. L.: Precipitation Changes over the Eastern Bolivian Andes Inferred from Speleothem (δ18O) Records for the Last 1400 Years, Earth and Planetary Science Letters, 494, 124–134, https://doi.org/10.1016/j.epsl.2018.04.048, 2018.

Atsawawaranunt, K., Comas-Bru, L., Amirnezhad Mozhdehi, S., Deininger, M., Harrison, S. P., Baker, A., Boyd, M., Kaushal, N., Ahmad, S. M., Ait Brahim, Y., Arienzo, M., Bajo, P., Braun, K., Burstyn, Y., Chawchai, S., Duan, W., Hatvani, I. G., Hu, J., Kern, Z., Labuhn, I., Lachniet, M., Lechleitner, F. A., Lorrey, A., Pérez-Mejías, C., Pickering, R., Scroxton, N., and SISAL Working Group Members: The SISAL Database: A Global Resource to Document Oxygen and Carbon Isotope Records from Speleothems, Earth System Science Data, 10, 1687–1713, https://doi.org/10.5194/essd-10-1687-2018, 2018.

Ault, T. R., Cole, J. E., and St. George, S.: The amplitude of decadal to multidecadal variability in precipitation simulated by state-of-the-art climate models, Geophysical Research Letters, 39, https://doi.org/10.1029/2012gl053424, 2012.

Azevedo, V., Stríkis, N. M., Santos, R. A., de Souza, J. G., Ampuero, A., Cruz, F. W., de Oliveira, P., Iriarte, J., Stumpf, C. F., Vuille, M., Mendes, V. R., Cheng, H., and Edwards, R. L.: Medieval Climate Variability in the Eastern Amazon-Cerrado Regions and Its Archeological Implications, Scientific Reports, 9, 20 306, https://doi.org/10.1038/s41598-019-56852-7, 2019.

Bakker, P., Goosse, H., and Roche, D. M.: Internal climate variability and spatial temperature correlations during the past 2000 years, Climate of the Past, 18, 2523–2544, 2022.

Beguería, S., Vicente-Serrano, S. M., Reig, F., and Latorre, B.: Standardized Precipitation Evapotranspiration Index (SPEI) Revisited: Parameter Fitting, Evapotranspiration Models, Tools, Datasets and Drought Monitoring, International Journal of Climatology, 34, 3001–3023, https://doi.org/10.1002/joc.3887, 2014.

Bernal, J., Cruz, F. W., Stríkis, N. M., Wang, X., Deininger, M., Catunda, M. C. A., Ortega-Obregón, C., Cheng, H., Edwards, R. L., and Auler, A. S.: High-resolution Holocene South American monsoon history recorded by a speleothem from Botuverá Cave, Brazil, Earth and Planetary Science Letters, 450, 186–196, https://doi.org/10.1016/j.epsl.2016.06.008, 2016.

Bhend, J., Franke, J., Folini, D., Wild, M., and Brönnimann, S.: An Ensemble-Based Approach to Climate Reconstructions, Climate of the Past, 8, 963–976, https://doi.org/10.5194/cp-8-963-2012, 2012.

Bird, B. W., Abbott, M. B., Rodbell, D. T., and Vuille, M.: Holocene Tropical South American Hydroclimate Revealed from a Decadally Resolved Lake Sediment δ18O Record, Earth and Planetary Science Letters, 310, 192–202, https://doi.org/10.1016/j.epsl.2011.08.040, 2011a.

Bird, B. W., Abbott, M. B., Vuille, M., Rodbell, D. T., Stansell, N. D., and Rosenmeier, M. F.: A 2,300-Year-Long Annually Resolved Record of the South American Summer Monsoon from the Peruvian Andes, Proceedings of the National Academy of Sciences, 108, 8583–8588, https://doi.org/10.1073/pnas.1003719108, 2011b.

Bishop, C. H., Etherton, B. J., and Majumdar, S. J.: Adaptive Sampling with the Ensemble Transform Kalman Filter. Part I: Theoretical Aspects, Monthly Weather Review, 129, 420–436, https://doi.org/10.1175/1520-0493(2001)129<0420:ASWTET>2.0.CO;2, 2001.

Black, D. E., Abahazi, M. A., Thunell, R. C., Kaplan, A., Tappa, E. J., and Peterson, L. C.: An 8-Century Tropical Atlantic SST Record from the Cariaco Basin: Baseline Variability, Twentieth-Century Warming, and Atlantic Hurricane Frequency, Paleoceanography, 22, https://doi.org/10.1029/2007PA001427, 2007.

Boës, X. and Fagel, N.: Relationships between Southern Chilean Varved Lake Sediments, Precipitation and ENSO for the Last 600 Years, Journal of Paleolimnology, 39, 237–252, https://doi.org/10.1007/s10933-007-9119-9, 2008.

Boucher, É., Guiot, J., and Chapron, E.: A Millennial Multi-Proxy Reconstruction of Summer PDSI for Southern South America, Climate of the Past, 7, 957–974, https://doi.org/10.5194/cp-7-957-2011, 2011.

Bradley, R.: Paleoclimatology. Reconstructing Climates of the Quaternary., Elsevier, 2015.

Brady, E., Stevenson, S., Bailey, D., Liu, Z., Noone, D., Nusbaumer, J., Otto-Bliesner, B. L., Tabor, C., Tomas, R., Wong, T., Zhang, J., and Zhu, J.: The Connected Isotopic Water Cycle in the Community Earth System Model Version 1, Journal of Advances in Modeling Earth Systems, 11, 2547–2566, https://doi.org/10.1029/2019MS001663, 2019.

Breitenmoser, P., Brönnimann, S., and Frank, D.: Forward Modelling of Tree-Ring Width and Comparison with a Global Network of Tree-Ring Chronologies, Climate of the Past, 10, 437–449, https://doi.org/10.5194/cp-10-437-2014, 2014.

Bretherton, C. S., Widmann, M., Dymnikov, V. P., Wallace, J. M., and Bladé, I.: The Effective Number of Spatial Degrees of Freedom of a Time-Varying Field, Journal of Climate, 12, 1990–2009, https://doi.org/10.1175/1520-0442(1999)012<1990:TENOSD>2.0.CO;2, 1999.

Bühler, J. C., Roesch, C., Kirschner, M., Sime, L., Holloway, M. D., and Rehfeld, K.: Comparison of the Oxygen Isotope Signatures in Speleothem Records and iHadCM3 Model Simulations for the Last Millennium, Preprint, Climate Modelling/Terrestrial Archives/Centennial-Decadal, https://doi.org/10.5194/cp-2020-121, 2020.

Bühler, J. C., Roesch, C., Kirschner, M., Sime, L., Holloway, M. D., and Rehfeld, K.: Comparison of the Oxygen Isotope Signatures in Speleothem Records and iHadCM3 Model Simulations for the Last Millennium, Climate of the Past, 17, 985–1004, https://doi.org/10.5194/cp-17-985-2021, 2021.

835 Bühler, J. C., Axelsson, J., Lechleitner, F. A., Fohlmeister, J., LeGrande, A. N., Midhun, M., Sjolte, J., Werner, M., Yoshimura, K., and Rehfeld, K.: Investigating Stable Oxygen and Carbon Isotopic Variability in Speleothem Records over the Last Millennium Using Multiple Isotope-Enabled Climate Models, Climate of the Past, 18, 1625–1654, https://doi.org/10.5194/cp-18-1625-2022, 2022.

Bühler, J. C., Axelsson, J., Rehfeld, K., LeGrande, A. N., Midhun, M., Sjolte, J., Werner, M., and Yoshimura, K.: Monthly climate variables of isotope-enabled climate model simulations over the last millennium (850-1849CE), https://doi.org/10.5281/ZENODO.6610684, 2022.

840 Bustamante, M., Cruz, F., Vuille, M., Apaéstegui, J., Strikis, N., Panizo, G., Novello, F., Deininger, M., Sifeddine, A., Cheng, H., Moquet, J., Guyot, J., Santos, R., Segura, H., and Edwards, R.: Holocene changes in monsoon precipitation in the Andes of NE Peru based on δ 18O speleothem records, Quaternary Science Reviews, 146, 274–287, https://doi.org/10.1016/j.quascirev.2016.05.023, 2016.

Campos, J. L. P. S., Cruz, F. W., Ambrizzi, T., Deininger, M., Vuille, M., Novello, V. F., and Strikis, N. M.: Coherent South American Monsoon Variability During the Last Millennium Revealed Through High-Resolution Proxy Records, Geophysical Research Letters, 46,
845 8261–8270, https://doi.org/10.1029/2019GL082513, 2019.

Campos, M. C., Chiessi, C. M., Novello, V. F., Crivellari, S., Campos, J. L. P. S., Albuquerque, A. L. S., Venancio, I. M., Santos, T. P., Melo, D. B., Cruz, F. W., Sawakuchi, A. O., and Mendes, V. R.: South American Precipitation Dipole Forced by Interhemispheric Temperature Gradient, Scientific Reports, 12, 10 527, https://doi.org/10.1038/s41598-022-14495-1, 2022.

Carvalho, L. M. V., Jones, C., and Liebmann, B.: The South Atlantic Convergence Zone: Intensity, Form, Persistence, and Relation-
850 ships with Intraseasonal to Interannual Activity and Extreme Rainfall, Journal of Climate, 17, 88–108, https://doi.org/10.1175/1520-0442(2004)017<0088:tsaczi>2.0.co;2, 2004.

Choblet, M. A., Bühler, J. C., Steiger, N. J., Novello, V. F., and Rehfeld, K.: Reconstructing climate fields with terrestrial climate archives, isotope-enabled GCMs and Data Assimilation, Copernicus GmbH, https://doi.org/10.5194/egusphere-egu23-2600, 2023.

Colose, C. M., LeGrande, A. N., and Vuille, M.: Hemispherically Asymmetric Volcanic Forcing of Tropical Hydroclimate during the Last
855 Millennium, Earth System Dynamics, 7, 681–696, https://doi.org/10.5194/esd-7-681-2016, 2016a.

Colose, C. M., LeGrande, A. N., and Vuille, M.: The Influence of Volcanic Eruptions on the Climate of Tropical South America during the Last Millennium in an Isotope-Enabled General Circulation Model, Climate of the Past, 12, 961–979, https://doi.org/10.5194/cp-12-961-2016, 2016b.

Comas-Bru, L., Rehfeld, K., Roesch, C., Amirnezhad-Mozhdehi, S., Harrison, S. P., Atsawawaranunt, K., Ahmad, S. M., Brahim, Y. A.,
860 Baker, A., Bosomworth, M., Breitenbach, S. F. M., Burstyn, Y., Columbu, A., Deininger, M., Demény, A., Dixon, B., Fohlmeister, J., Hatvani, I. G., Hu, J., Kaushal, N., Kern, Z., Labuhn, I., Lechleitner, F. A., Lorrey, A., Martrat, B., Novello, V. F., Oster, J., Pérez-Mejías, C., Scholz, D., Scroxton, N., Sinha, N., Ward, B. M., Warken, S., Zhang, H., and SISAL Working Group members: SISALv2: A Comprehensive Speleothem Isotope Database with Multiple Age–Depth Models, Earth System Science Data, 12, 2579–2606, https://doi.org/10.5194/essd-12-2579-2020, 2020.

865 Comboul, M., Emile-Geay, J., Hakim, G. J., and Evans, M. N.: Paleoclimate Sampling as a Sensor Placement Problem, Journal of Climate, 28, 7717–7740, https://doi.org/10.1175/JCLI-D-14-00802.1, 2015.

Compo, G. P., Whitaker, J. S., Sardeshmukh, P. D., Matsui, N., Allan, R. J., Yin, X., Gleason, B. E., Vose, R. S., Rutledge, G., Bessemoulin, P., Brönnimann, S., Brunet, M., Crouthamel, R. I., Grant, A. N., Groisman, P. Y., Jones, P. D., Kruk, M. C., Kruger, A. C., Marshall, G. J.,

Maugeri, M., Mok, H. Y., Nordli, Ø., Ross, T. F., Trigo, R. M., Wang, X. L., Woodruff, S. D., and Worley, S. J.: The Twentieth Century
Reanalysis Project, Quarterly Journal of the Royal Meteorological Society, 137, 1–28, https://doi.org/10.1002/qj.776, 2011.

Cook, E. R., Meko, D. M., Stahle, D. W., and Cleaveland, M. K.: Drought Reconstructions for the Continental United States*, Journal of
Climate, 12, 1145–1162, https://doi.org/10.1175/1520-0442(1999)012<1145:drftcu>2.0.co;2, 1999.

Craig, H.: Isotopic variations in meteoric waters, Science, 133, 1702–1703, 1961.

Cruz, F. W., Vuille, M., Burns, S. J., Wang, X., Cheng, H., Werner, M., Edwards, R. L., Karmann, I., Auler, A. S., and Nguyen, H.: Orbitally
driven east–west antiphasing of South American precipitation, Nature Geoscience, 2, 210–214, https://doi.org/10.1038/ngeo444, 2009.

Dansgaard, W.: Stable Isotopes in Precipitation, Tellus, 16, 436–468, https://doi.org/10.1111/j.2153-3490.1964.tb00181.x, 1964.

de Jong, R., von Gunten, L., Maldonado, A., and Grosjean, M.: Late Holocene Summer Temperatures in the Central Andes Reconstructed
from the Sediments of High-Elevation Laguna Chepical, Chile (32° S), Climate of the Past, 9, 1921–1932, https://doi.org/10.5194/cp-9-
1921-2013, 2013.

de Souza, J. G., Robinson, M., Maezumi, S. Y., Capriles, J., Hoggarth, J. A., Lombardo, U., Novello, V. F., Apaéstegui, J., Whitney, B.,
Urrego, D., Alves, D. T., Rostain, S., Power, M. J., Mayle, F. E., da Cruz, F. W., Hooghiemstra, H., and Iriarte, J.: Climate Change and
Cultural Resilience in Late Pre-Columbian Amazonia, Nature Ecology & Evolution, 3, 1007–1017, https://doi.org/10.1038/s41559-019-
0924-0, 2019.

Dee, S., Emile-Geay, J., Evans, M. N., Allam, A., Steig, E. J., and Thompson, D.: PRYSM: An Open-Source Framework for PRoxY
System Modeling, with Applications to Oxygen-Isotope Systems, Journal of Advances in Modeling Earth Systems, 7, 1220–1247,
https://doi.org/10.1002/2015MS000447, 2015.

Dee, S. G., Steiger, N. J., Emile-Geay, J., and Hakim, G. J.: On the utility of proxy system models for estimating climate states over the
common era, Journal of Advances in Modeling Earth Systems, 8, 1164–1179, https://doi.org/10.1002/2016ms000677, 2016.

Deininger, M., Ward, B. M., Novello, V. F., and Cruz, F. W.: Late Quaternary Variations in the South American Monsoon System as Inferred
by Speleothems—New Perspectives Using the SISAL Database, Quaternary, 2, 6, https://doi.org/10.3390/quat2010006, 2019.

DeLong, K. L., Flannery, J. A., Poore, R. Z., Quinn, T. M., Maupin, C. R., Lin, K., and Shen, C.-C.: A reconstruction of sea surface tem-
perature variability in the southeastern Gulf of Mexico from 1734 to 2008 CE using cross-dated Sr/Ca records from the coral Siderastrea
siderea, Paleoceanography, 29, 403–422, 2014.

Dirren, S. and Hakim, G. J.: Toward the assimilation of time-averaged observations, Geophysical research letters, 32, 2005.

Dunbar, R. B., Wellington, G. M., Colgan, M. W., and Glynn, P. W.: Eastern Pacific sea surface temperature since 1600 AD: The $\delta18O$ record
of climate variability in Galápagos corals, Paleoceanography, 9, 291–315, 1994.

Elbert, J., Wartenburger, R., von Gunten, L., Urrutia, R., Fischer, D., Fujak, M., Hamann, Y., Greber, N. D., and Grosjean, M.: Late Holocene
air temperature variability reconstructed from the sediments of Laguna Escondida, Patagonia, Chile (45°30′S), Palaeogeography, Palaeo-
climatology, Palaeoecology, 369, 482–492, https://doi.org/10.1016/j.palaeo.2012.11.013, 2013.

Elbert, J., Jacques-Coper, M., Van Daele, M., Urrutia, R., and Grosjean, M.: A 600 Years Warm-Season Temperature
Record from Varved Sediments of Lago Plomo, Northern Patagonia, Chile (47°S), Quaternary International, 377, 28–37,
https://doi.org/10.1016/j.quaint.2015.01.004, 2015.

Emile-Geay, J., McKay, N. P., Kaufman, D. S., von Gunten, L., Wang, J., Anchukaitis, K. J., Abram, N. J., Addison, J. A., Curran, M. A.,
Evans, M. N., Henley, B. J., Hao, Z., Martrat, B., McGregor, H. V., Neukom, R., Pederson, G. T., Stenni, B., Thirumalai, K., Werner, J. P.,
Xu, C., Divine, D. V., Dixon, B. C., Gergis, J., Mundo, I. A., Nakatsuka, T., Phipps, S. J., Routson, C. C., Steig, E. J., Tierney, J. E., Tyler,
J. J., Allen, K. J., Bertler, N. A., Björklund, J., Chase, B. M., Chen, M.-T., Cook, E., de Jong, R., DeLong, K. L., Dixon, D. A., Ekaykin,

A. A., Ersek, V., Filipsson, H. L., Francus, P., Freund, M. B., Frezzotti, M., Gaire, N. P., Gajewski, K., Ge, Q., Goosse, H., Gornostaeva, A., Grosjean, M., Horiuchi, K., Hormes, A., Husum, K., Isaksson, E., Kandasamy, S., Kawamura, K., Kilbourne, K. H., Koç, N., Leduc, G., Linderholm, H. W., Lorrey, A. M., Mikhalenko, V., Mortyn, P. G., Motoyama, H., Moy, A. D., Mulvaney, R., Munz, P. M., Nash, D. J., Oerter, H., Opel, T., Orsi, A. J., Ovchinnikov, D. V., Porter, T. J., Roop, H. A., Saenger, C., Sano, M., Sauchyn, D., Saunders, K. M., Seidenkrantz, M.-S., Severi, M., Shao, X., Sicre, M.-A., Sigl, M., Sinclair, K., St. George, S., St. Jacques, J.-M., Thamban, M., Kuwar Thapa, U., Thomas, E. R., Turney, C., Uemura, R., Viau, A. E., Vladimirova, D. O., Wahl, E. R., White, J. W., Yu, Z., Zinke, J., and PAGES2k Consortium: A Global Multiproxy Database for Temperature Reconstructions of the Common Era, Scientific Data, 4, 170 088, https://doi.org/10.1038/sdata.2017.88, 2017.

Erb, M. P., McKay, N. P., Steiger, N., Dee, S., Hancock, C., Ivanovic, R. F., Gregoire, L. J., and Valdes, P.: Reconstructing Holocene Temperatures in Time and Space Using Paleoclimate Data Assimilation, Climate of the Past, 18, 2599–2629, https://doi.org/10.5194/cp-18-2599-2022, 2022.

Evans, M. N., Tolwinski-Ward, S. E., Thompson, D. M., and Anchukaitis, K. J.: Applications of Proxy System Modeling in High Resolution Paleoclimatology, Quaternary Science Reviews, 76, 16–28, https://doi.org/10.1016/j.quascirev.2013.05.024, 2013.

Evensen, G.: Sequential Data Assimilation with a Nonlinear Quasi-Geostrophic Model Using Monte Carlo Methods to Forecast Error Statistics, Journal of Geophysical Research: Oceans, 99, 10 143–10 162, https://doi.org/10.1029/94JC00572, 1994.

Evensen, G.: The Ensemble Kalman Filter: Theoretical Formulation and Practical Implementation, Ocean Dynamics, 53, 343–367, https://doi.org/10.1007/s10236-003-0036-9, 2003.

Evensen, G., Vossepoel, F. C., and van Leeuwen, P. J.: Data Assimilation Fundamentals: A Unified Formulation of the State and Parameter Estimation Problem, Springer Textbooks in Earth Sciences, Geography and Environment, Springer International Publishing, Cham, https://doi.org/10.1007/978-3-030-96709-3, 2022.

Eyring, V., Cox, P. M., Flato, G. M., Gleckler, P. J., Abramowitz, G., Caldwell, P., Collins, W. D., Gier, B. K., Hall, A. D., Hoffman, F. M., et al.: Taking climate model evaluation to the next level, Nature Climate Change, 9, 102–110, 2019.

Fensterer, C., Scholz, D., Hoffmann, D., Spötl, C., Pajón, J. M., and Mangini, A.: Cuban stalagmite suggests relationship between Caribbean precipitation and the Atlantic Multidecadal Oscillation during the past 1.3 ka, The Holocene, 22, 1405–1412, https://doi.org/10.1177/0959683612449759, 2012.

Franke, J., Brönnimann, S., Bhend, J., and Brugnara, Y.: A Monthly Global Paleo-Reanalysis of the Atmosphere from 1600 to 2005 for Studying Past Climatic Variations, Scientific Data, 4, 170 076, https://doi.org/10.1038/sdata.2017.76, 2017.

Garreaud, R. D., Vuille, M., Compagnucci, R., and Marengo, J.: Present-Day South American Climate, Palaeogeography, Palaeoclimatology, Palaeoecology, 281, 180–195, https://doi.org/10.1016/j.palaeo.2007.10.032, 2009.

Garreaud, R. D., Boisier, J. P., Rondanelli, R., Montecinos, A., Sepúlveda, H. H., and Veloso-Aguila, D.: The Central Chile Mega Drought (2010–2018): A climate dynamics perspective, International Journal of Climatology, 40, 421–439, https://doi.org/10.1002/joc.6219, 2019.

Gioda, A. and Prieto, M. d. R.: Histoire des sécheresses andines ; Potosi, El Niño et le Petit âge glaciaire, La Météorologie, 1999, 33–42, https://doi.org/10.4267/2042/47082, 1999.

Gneiting, T. and Raftery, A. E.: Strictly Proper Scoring Rules, Prediction, and Estimation, Journal of the American Statistical Association, 102, 359–378, https://doi.org/10.1198/016214506000001437, 2007.

Grießinger, J., Langhamer, L., Schneider, C., Saß, B.-L., Steger, D., Skvarca, P., Braun, M. H., Meier, W. J.-H., Srur, A. M., and Hochreuther, P.: Imprints of Climate Signals in a 204 Year δ18O Tree-Ring Record of Nothofagus Pumilio From Perito Moreno Glacier, Southern Patagonia (50°S), Frontiers in Earth Science, 6, 2018.

945 Haase-Schramm, A., Böhm, F., Eisenhauer, A., Dullo, W.-C., Joachimski, M. M., Hansen, B., and Reitner, J.: Sr/Ca Ratios and Oxygen Isotopes from Sclerosponges: Temperature History of the Caribbean Mixed Layer and Thermocline during the Little Ice Age: SR/CA AND δ^{18}O FROM SCLEROSPONGES, Paleoceanography, 18, n/a–n/a, https://doi.org/10.1029/2002PA000830, 2003.

Hakim, G. J., Emile-Geay, J., Steig, E. J., Noone, D., Anderson, D. M., Tardif, R., Steiger, N., and Perkins, W. A.: The Last Millennium Climate Reanalysis Project: Framework and First Results, Journal of Geophysical Research: Atmospheres, 121, 6745–6764, https://doi.org/10.1002/2016JD024751, 2016.

950

Harris, C. R., Millman, K. J., van der Walt, S. J., Gommers, R., Virtanen, P., Cournapeau, D., Wieser, E., Taylor, J., Berg, S., Smith, N. J., Kern, R., Picus, M., Hoyer, S., van Kerkwijk, M. H., Brett, M., Haldane, A., del Río, J. F., Wiebe, M., Peterson, P., Gérard-Marchant, P., Sheppard, K., Reddy, T., Weckesser, W., Abbasi, H., Gohlke, C., and Oliphant, T. E.: Array programming with NumPy, Nature, 585, 357–362, https://doi.org/10.1038/s41586-020-2649-2, 2020a.

955 Harris, I., Osborn, T. J., Jones, P., and Lister, D.: Version 4 of the CRU TS monthly high-resolution gridded multivariate climate dataset, Scientific Data, 7, https://doi.org/10.1038/s41597-020-0453-3, 2020b.

Hoffmann, G., Ramirez, E., Taupin, J. D., Francou, B., Ribstein, P., Delmas, R., Dürr, H., Gallaire, R., Simões, J., Schotterer, U., Stievenard, M., and Werner, M.: Coherent Isotope History of Andean Ice Cores over the Last Century, Geophysical Research Letters, 30, https://doi.org/10.1029/2002GL014870, 2003.

960 Hoyer, S. and Hamman, J.: xarray: N-D labeled arrays and datasets in Python, J. Open Res. Software, 2017.

Humanes-Fuente, V., Ferrero, M. E., Muñoz, A. A., González-Reyes, Á., Requena-Rojas, E. J., Barichivich, J., Inga, J. G., and Layme-Huaman, E. T.: Two Centuries of Hydroclimatic Variability Reconstructed From Tree-Ring Records Over the Amazonian Andes of Peru, Journal of Geophysical Research: Atmospheres, 125, e2020JD032 565, https://doi.org/10.1029/2020JD032565, 2020.

Hunter, J. D.: Matplotlib: A 2D graphics environment, Computing in Science & Engineering, 9, 90–95, 965 https://doi.org/10.1109/MCSE.2007.55, 2007.

Huntley, H. S. and Hakim, G. J.: Assimilation of Time-Averaged Observations in a Quasi-Geostrophic Atmospheric Jet Model, Climate Dynamics, 35, 995–1009, https://doi.org/10.1007/s00382-009-0714-5, 2010.

IAEA/WMO: Global Network of Isotopes in Precipitation. The GNIP Database, http://www.iaea.org/water, accessible at: http://www.iaea.org/water, 2020.

970 Jiménez-Iñiguez, A., Ampuero, A., Valencia, B. G., Mayta, V. C., Cruz, F. W., Vuille, M., Novello, V. F., Misailidis Stríkis, N., Aranda, N., and Conicelli, B.: Stable isotope variability of precipitation and cave drip-water at Jumandy cave, western Amazon River basin (Ecuador), J. Hydrol. (Amst.), 610, 127 848, 2022.

Jiménez-Iñiguez, A., Ampuero, A., Valencia, B. G., Mayta, V. C., Cruz, F. W., Vuille, M., Novello, V. F., Stríkis, N. M., Aranda, N., and Conicelli, B.: Stable isotope variability of precipitation and cave drip-water at Jumandy cave, western Amazon River basin (Ecuador), 975 Journal of Hydrology, 610, 127 848, https://doi.org/10.1016/j.jhydrol.2022.127848, 2022.

Jungclaus, J. H., Bard, E., Baroni, M., Braconnot, P., Cao, J., Chini, L. P., Egorova, T., Evans, M., González-Rouco, J. F., Goosse, H., Hurtt, G. C., Joos, F., Kaplan, J. O., Khodri, M., Goldewijk, K. K., Krivova, N., LeGrande, A. N., Lorenz, S. J., Luterbacher, J., Man, W., Maycock, A. C., Meinshausen, M., Moberg, A., Muscheler, R., Nehrbass-Ahles, C., Otto-Bliesner, B. I., Phipps, S. J., Pongratz, J., Rozanov, E., Schmidt, G. A., Schmidt, H., Schmutz, W., Schurer, A., Shapiro, A. I., Sigl, M., Smerdon, J. E., Solanki, S. K., Timmreck, 980 C., Toohey, M., Usoskin, I. G., Wagner, S., Wu, C.-J., Yeo, K. L., Zanchettin, D., Zhang, Q., and Zorita, E.: The PMIP4 contribution to CMIP6–Part 3: The last millennium, scientific objective, and experimental design for the PMIP4 past1000 simulations, Geoscientific Model Development, 10, 4005–4033, https://doi.org/10.5194/gmd-10-4005-2017, 2017.

Kanner, L. C., Burns, S. J., Cheng, H., Edwards, R. L., and Vuille, M.: High-resolution variability of the South American summer monsoon over the last seven millennia: insights from a speleothem record from the central Peruvian Andes, Quaternary Science Reviews, 75, 1–10, https://doi.org/10.1016/j.quascirev.2013.05.008, 2013.

Kaushal, N., Lechleitner, F. A., Wilhelm, M., Bühler, J. C., Braun, K., Brahim, Y. A., Azennoud, K., Baker, A., Burstyn, Y., Comas-Bru, L., Goldsmith, Y., Harrison, S. P., Hatvani, I. G., Rehfeld, K., Ritzau, M., Skiba, V., Stoll, H. M., Szűcs, J. G., Treble, P. C., Azevedo, V., Baker, J. L., Chawchai, S., Columbu, A., Endres, L., Hu, J., Kern, Z., Kimbrough, A., Koç, K., Markowska, M., Martrat, B., Ahmad, S. M., Nehme, C., Novello, V. F., Pérez-Mejías, C., Ruan, J., Sekhon, N., Sinha, N., Tadros, C. V., Tiger, B. H., Warken, S., Wolf, A., and and, H. Z.: SISALv3: A global speleothem stable isotope and trace element database, https://doi.org/10.5194/essd-2023-364, 2023.

Kennett, D. J., Breitenbach, S. F. M., Aquino, V. V., Asmerom, Y., Awe, J., Baldini, J. U., Bartlein, P., Culleton, B. J., Ebert, C., Jazwa, C., Macri, M. J., Marwan, N., Polyak, V., Prufer, K. M., Ridley, H. E., Sodemann, H., Winterhalder, B., and Haug, G. H.: Development and Disintegration of Maya Political Systems in Response to Climate Change, Science, 338, 788–791, https://doi.org/10.1126/science.1226299, 2012.

Khider, D., Emile-Geay, J., Zhu, F., James, A., Landers, J., Ratnakar, V., and Gil, Y.: Pyleoclim: Paleoclimate Timeseries Analysis and Visualization With Python, Paleoceanography and Paleoclimatology, 37, e2022PA004 509, https://doi.org/10.1029/2022PA004509, 2022.

Kilbourne, K., Quinn, T., Webb, R., Guilderson, T., Nyberg, J., and Winter, A.: Paleoclimate proxy perspective on Caribbean climate since the year 1751: Evidence of cooler temperatures and multidecadal variability, Paleoceanography, 23, 2008.

King, J., Anchukaitis, K. J., Allen, K., Vance, T., and Hessl, A.: Trends and Variability in the Southern Annular Mode over the Common Era, Nature Communications, 14, 2324, https://doi.org/10.1038/s41467-023-37643-1, 2023.

King, J. M., Anchukaitis, K. J., Tierney, J. E., Hakim, G. J., Emile-Geay, J., Zhu, F., and Wilson, R.: A Data Assimilation Approach to Last Millennium Temperature Field Reconstruction Using a Limited High-Sensitivity Proxy Network, Journal of Climate, 34, 7091–7111, https://doi.org/10.1175/JCLI-D-20-0661.1, 2021.

Konecky, B. L., McKay, N. P., Churakova (Sidorova), O. V., Comas-Bru, L., Dassié, E. P., DeLong, K. L., Falster, G. M., Fischer, M. J., Jones, M. D., Jonkers, L., Kaufman, D. S., Leduc, G., Managave, S. R., Martrat, B., Opel, T., Orsi, A. J., Partin, J. W., Sayani, H. R., Thomas, E. K., Thompson, D. M., Tyler, J. J., Abram, N. J., Atwood, A. R., Cartapanis, O., Conroy, J. L., Curran, M. A., Dee, S. G., Deininger, M., Divine, D. V., Kern, Z., Porter, T. J., Stevenson, S. L., von Gunten, L., and Members, I. P.: The Iso2k Database: A Global Compilation of Paleo-δ^{18}O and δ^2H Records to Aid Understanding of Common Era Climate, Earth System Science Data, 12, 2261–2288, https://doi.org/10.5194/essd-12-2261-2020, 2020.

Lachniet, M. S., Bernal, J. P., Asmerom, Y., Polyak, V., and Piperno, D.: A 2400 yr Mesoamerican rainfall reconstruction links climate and cultural change, Geology, 40, 259–262, https://doi.org/10.1130/g32471.1, 2012.

Laepple, T. and Huybers, P.: Ocean Surface Temperature Variability: Large Model–Data Differences at Decadal and Longer Periods, Proceedings of the National Academy of Sciences, 111, 16 682–16 687, https://doi.org/10.1073/pnas.1412077111, 2014.

Laepple, T., Muench, T., and Dolman, A.: PaleoSpec: Spectral tools for the ECUS group, https://earthsystemdiagnostics.github.io/paleospec/, r package version 0.2.91, 2023a.

Laepple, T., Ziegler, E., Weitzel, N., Hébert, R., Ellerhoff, B., Schoch, P., Martrat, B., Bothe, O., Moreno-Chamarro, E., Chevalier, M., Herbert, A., and Rehfeld, K.: Regional but not global temperature variability underestimated by climate models at supradecadal timescales, Nat. Geosci., 16, 958–966, 2023b.

Lam, S. K., Pitrou, A., and Seibert, S.: Numba: A llvm-based python jit compiler, in: Proceedings of the Second Workshop on the LLVM Compiler Infrastructure in HPC, pp. 1–6, 2015.

Lewis, S. C. and LeGrande, A. N.: Stability of ENSO and Its Tropical Pacific Teleconnections over the Last Millennium, Climate of the Past, 11, 1347–1360, https://doi.org/10.5194/cp-11-1347-2015, 2015.

Libera, M. E. D., Novello, V. F., Cruz, F. W., Orrison, R., Vuille, M., Maezumi, S. Y., de Souza, J., Cauhy, J., Campos, J. L. P. S., Ampuero, A., Utida, G., Stríkis, N. M., Stumpf, C. F., Azevedo, V., Zhang, H., Edwards, R. L., and Cheng, H.: Paleoclimatic and paleoenvironmental changes in Amazonian lowlands over the last three millennia, Quaternary Science Reviews, 279, 107 383, https://doi.org/10.1016/j.quascirev.2022.107383, 2022.

Linsley, B. K., Dunbar, R. B., Wellington, G. M., and Mucciarone, D. A.: A coral-based reconstruction of Intertropical Convergence Zone variability over Central America since 1707, Journal of Geophysical Research: Oceans, 99, 9977–9994, 1994.

Lüning, S., Gałka, M., Bamonte, F. P., Rodríguez, F. G., and Vahrenholt, F.: The medieval climate anomaly in South America, Quaternary International, 508, 70–87, 2019.

Luterbacher, J., Xoplaki, E., Dietrich, D., Rickli, R., Jacobeit, J., Beck, C., Gyalistras, D., Schmutz, C., and Wanner, H.: Reconstruction of Sea Level Pressure Fields over the Eastern North Atlantic and Europe Back to 1500, Climate Dynamics, 18, 545–561, https://doi.org/10.1007/s00382-001-0196-6, 2002.

Luterbacher, J., Neukom, R., González-Rouco, F., Fernandez-Donado, L., Raible, C., and Zorita, E.: Reconstructed and Simulated Medieval Climate Anomaly in Southern South America, PAGES news, 19, 20–21, https://doi.org/10.22498/pages.19.1.20, 2011.

Marengo, J. A., Liebmann, B., Grimm, A. M., Misra, V., Silva Dias, P. L., Cavalcanti, I. F. A., Carvalho, L. M. V., Berbery, E. H., Ambrizzi, T., Vera, C. S., Saulo, A. C., Nogues-Paegle, J., Zipser, E., Seth, A., and Alves, L. M.: Recent developments on the South American monsoon system, International Journal of Climatology, 32, 1–21, https://doi.org/10.1002/joc.2254, 2010.

Medina, N. M. M., Cruz, F. W., Winter, A., Zhang, H., Ampuero, A., Vuille, M., Mayta, V. C., Campos, M. C., Rámirez, V. M., Utida, G., Zúñiga, A. C., and Cheng, H.: Atlantic ITCZ variability during the Holocene based on high-resolution speleothem isotope records from northern Venezuela, Quaternary Science Reviews, 307, 108 056, https://doi.org/https://doi.org/10.1016/j.quascirev.2023.108056, 2023.

Medina-Elizalde, M., Burns, S. J., Lea, D. W., Asmerom, Y., von Gunten, L., Polyak, V., Vuille, M., and Karmalkar, A.: High resolution stalagmite climate record from the Yucatán Peninsula spanning the Maya terminal classic period, Earth and Planetary Science Letters, 298, 255–262, https://doi.org/10.1016/j.epsl.2010.08.016, 2010.

Met Office: Cartopy: a cartographic python library with a Matplotlib interface, Exeter, Devon, https://scitools.org.uk/cartopy, 2010 - 2015.

Moquet, J. S., Cruz, F. W., Novello, V. F., Stríkis, N. M., Deininger, M., Karmann, I., Santos, R. V., Millo, C., Apaestegui, J., Guyot, J. L., Siffedine, A., Vuille, M., Cheng, H., Edwards, R. L., and Santini, W.: Calibration of Speleothem δ18O Records against Hydroclimate Instrumental Records in Central Brazil, Global and Planetary Change, 139, 151–164, https://doi.org/10.1016/j.gloplacha.2016.02.001, 2016.

Morales, M. S., Christie, D. A., Villalba, R., Argollo, J., Pacajes, J., Silva, J. S., Alvarez, C. A., Llancabure, J. C., and Soliz Gamboa, C. C.: Precipitation Changes in the South American Altiplano since 1300 AD Reconstructed by Tree-Rings, Climate of the Past, 8, 653–666, https://doi.org/10.5194/cp-8-653-2012, 2012.

Morales, M. S., Cook, E. R., Barichivich, J., Christie, D. A., Villalba, R., LeQuesne, C., Srur, A. M., Ferrero, M. E., González-Reyes, Á., Couvreux, F., et al.: Six hundred years of South American tree rings reveal an increase in severe hydroclimatic events since mid-20th century, Proceedings of the National Academy of Sciences, 117, 16 816–16 823, 2020.

Morales, M. S., Crispín-DelaCruz, D. B., Álvarez, C., Christie, D. A., Ferrero, M. E., Andreu-Hayles, L., Villalba, R., Guerra, A., Ticse-Otarola, G., Rodríguez-Ramírez, E. C., LLocclla-Martínez, R., Sanchez-Ferrer, J., and Requena-Rojas, E. J.: Drought Increase since the

Mid-20th Century in the Northern South American Altiplano Revealed by a 389-Year Precipitation Record, Climate of the Past, 19, 457–476, https://doi.org/10.5194/cp-19-457-2023, 2023.

1060 Nash, J. E. and Sutcliffe, J. V.: River Flow Forecasting through Conceptual Models Part I — A Discussion of Principles, Journal of Hydrology, 10, 282–290, https://doi.org/10.1016/0022-1694(70)90255-6, 1970.

Neukom, R. and Gergis, J.: Southern Hemisphere High-Resolution Palaeoclimate Records of the Last 2000 Years, The Holocene, 22, 501–524, https://doi.org/10.1177/0959683611427335, 2012.

Neukom, R., del Rosario Prieto, M., Moyano, R., Luterbacher, J., Pfister, C., Villalba, R., Jones, P. D., and Wanner, H.: An Extended
1065 Network of Documentary Data from South America and Its Potential for Quantitative Precipitation Reconstructions Back to the 16th Century, Geophysical Research Letters, 36, L12 703, https://doi.org/10.1029/2009GL038351, 2009.

Neukom, R., Luterbacher, J., Villalba, R., Küttel, M., Frank, D., Jones, P. D., Grosjean, M., Esper, J., Lopez, L., and Wanner, H.: Multi-Centennial Summer and Winter Precipitation Variability in Southern South America, Geophysical Research Letters, 37, https://doi.org/10.1029/2010GL043680, 2010.

1070 Neukom, R., Luterbacher, J., Villalba, R., Küttel, M., Frank, D., Jones, P. D., Grosjean, M., Wanner, H., Aravena, J.-C., Black, D. E., et al.: Multiproxy summer and winter surface air temperature field reconstructions for southern South America covering the past centuries, Climate Dynamics, 37, 35–51, 2011.

Neukom, R., Gergis, J., Karoly, D., Wanner, H., Curran, M., Elbert, J., González Rouco, J. F., Linsley, B., Moy, A., Mundo, I., Raible, C., Steig, E., van Ommen, T., Vance, T., Villalba, R., Zinke, J., and Frank, D.: Inter-Hemispheric Temperature Variability over the Last
1075 Millennium, Nature Climate Change, 4, https://doi.org/10.1038/nclimate2174, 2014.

Neukom, R., Steiger, N., Gómez-Navarro, J. J., Wang, J., and Werner, J. P.: No Evidence for Globally Coherent Warm and Cold Periods over the Preindustrial Common Era, Nature, 571, 550–554, https://doi.org/10.1038/s41586-019-1401-2, 2019.

Novello, V. F., Cruz, F. W., Karmann, I., Burns, S. J., Stríkis, N. M., Vuille, M., Cheng, H., Lawrence Edwards, R., Santos, R. V., Frigo, E., and Barreto, E. A. S.: Multidecadal Climate Variability in Brazil's Nordeste during the Last 3000 Years Based on Speleothem Isotope
1080 Records, Geophysical Research Letters, 39, https://doi.org/10.1029/2012GL053936, 2012.

Novello, V. F., Vuille, M., Cruz, F. W., Stríkis, N. M., de Paula, M. S., Edwards, R. L., Cheng, H., Karmann, I., Jaqueto, P. F., Trindade, R. I. F., Hartmann, G. A., and Moquet, J. S.: Centennial-Scale Solar Forcing of the South American Monsoon System Recorded in Stalagmites, Scientific Reports, 6, 24 762, https://doi.org/10.1038/srep24762, 2016.

Novello, V. F., Cruz, F. W., Moquet, J. S., Vuille, M., de Paula, M. S., Nunes, D., Edwards, R. L., Cheng, H., Karmann, I., Utida, G., Stríkis,
1085 N. M., and Campos, J. L. P. S.: Two Millennia of South Atlantic Convergence Zone Variability Reconstructed From Isotopic Proxies, Geophysical Research Letters, 45, 5045–5051, https://doi.org/10.1029/2017GL076838, 2018.

Novello, V. F., William da Cruz, F., Vuille, M., Pereira Silveira Campos, J. L., Stríkis, N. M., Apaéstegui, J., Moquet, J. S., Azevedo, V., Ampuero, A., Utida, G., Wang, X., Paula-Santos, G. M., Jaqueto, P., Ruiz Pessenda, L. C., Breecker, D. O., and Karmann, I.: Investigating $\delta13C$ Values in Stalagmites from Tropical South America for the Last Two Millennia, Quaternary Science Reviews, 255, 106 822,
1090 https://doi.org/10.1016/j.quascirev.2021.106822, 2021.

Okazaki, A., Miyoshi, T., Yoshimura, K., Greybush, S. J., and Zhang, F.: Revisiting Online and Offline Data Assimilation Comparison for Paleoclimate Reconstruction: An Idealized OSSE Study, Journal of Geophysical Research: Atmospheres, 126, e2020JD034 214, https://doi.org/10.1029/2020JD034214, 2021.

Oke, P. R., Schiller, A., Griffin, D. A., and Brassington, G. B.: Ensemble Data Assimilation for an Eddy-Resolving Ocean Model of the
1095 Australian Region, Quarterly Journal of the Royal Meteorological Society, 131, 3301–3311, https://doi.org/10.1256/qj.05.95, 2005.

Orrison, R., Vuille, M., Smerdon, J. E., Apaéstegui, J., Azevedo, V., Campos, J. L. P. S., Cruz, F. W., Della Libera, M. E., and Stríkis, N. M.: South American Summer Monsoon Variability over the Last Millennium in Paleoclimate Records and Isotope-Enabled Climate Models, Climate of the Past, 18, 2045–2062, https://doi.org/10.5194/cp-18-2045-2022, 2022.

Osman, M. B., Tierney, J. E., Zhu, J., Tardif, R., Hakim, G. J., King, J., and Poulsen, C. J.: Globally Resolved Surface Temperatures since the Last Glacial Maximum, Nature, 599, 239–244, https://doi.org/10.1038/s41586-021-03984-4, 2021.

PAGES 2k Consortium: [SI] Consistent Multidecadal Variability in Global Temperature Reconstructions and Simulations over the Common Era, Nature Geoscience, 12, 643–649, https://doi.org/10.1038/s41561-019-0400-0, 2019.

Parsons, L. A., Loope, G. R., Overpeck, J. T., Ault, T. R., Stouffer, R., and Cole, J. E.: Temperature and Precipitation Variance in CMIP5 Simulations and Paleoclimate Records of the Last Millennium, Journal of Climate, 30, 8885–8912, https://doi.org/10.1175/jcli-d-16-0863.1, 2017.

Parsons, L. A., LeRoy, S., Overpeck, J. T., Bush, M., Cárdenes-Sandí, G., and Saleska, S.: The Threat of Multi-Year Drought in Western Amazonia, Water Resources Research, 54, 5890–5904, https://doi.org/10.1029/2017wr021788, 2018.

Parsons, L. A., Amrhein, D. E., Sanchez, S. C., Tardif, R., Brennan, M. K., and Hakim, G. J.: Do Multi-Model Ensembles Improve Reconstruction Skill in Paleoclimate Data Assimilation?, Earth and Space Science, 8, e2020EA001 467, https://doi.org/10.1029/2020EA001467, 2021.

Pörtner, H.-O., Roberts, D. C., Poloczanska, E. S., Mintenbeck, K., Tignor, M., Alegría, A., Craig, M., Langsdorf, S., Löschke, S., Möller, V., et al.: IPCC, 2022: Summary for policymakers, 2022.

Prieto, M. d. R.: ENSO Signals in South America: Rains and Floods in the Paraná River Region during Colonial Times, Climatic Change, 83, 39–54, https://doi.org/10.1007/s10584-006-9188-1, 2007.

Prieto, M. d. R. and García Herrera, R.: Documentary Sources from South America: Potential for Climate Reconstruction, Palaeogeography, Palaeoclimatology, Palaeoecology, 281, 196–209, https://doi.org/10.1016/j.palaeo.2008.07.026, 2009.

Rohde, R. A. and Hausfather, Z.: The Berkeley Earth Land/Ocean Temperature Record, Earth System Science Data, 12, 3469–3479, https://doi.org/10.5194/essd-12-3469-2020, 2020.

Rojas, M., Arias, P. A., Flores-Aqueveque, V., Seth, A., and Vuille, M.: The South American Monsoon Variability over the Last Millennium in Climate Models, Climate of the Past, 12, 1681–1691, https://doi.org/10.5194/cp-12-1681-2016, 2016.

Saenger, C., Cohen, A. L., Oppo, D. W., Halley, R. B., and Carilli, J. E.: Surface-Temperature Trends and Variability in the Low-Latitude North Atlantic since 1552, Nature Geoscience, 2, 492–495, https://doi.org/10.1038/ngeo552, 2009.

Sanchez, S. C., Hakim, G. J., and Saenger, C. P.: Climate Model Teleconnection Patterns Govern the Niño-3.4 Response to Early Nineteenth-Century Volcanism in Coral-Based Data Assimilation Reconstructions, Journal of Climate, 34, 1863–1880, https://doi.org/10.1175/JCLI-D-20-0549.1, 2021.

Schneider, U., Fuchs, T., Meyer-Christoffer, A., and Rudolf, B.: Global precipitation analysis products of the GPCC, Global Precipitation Climatology Centre (GPCC), DWD, Internet Publikation, 112, 2008.

Schurer, A. P., Tett, S. F. B., and Hegerl, G. C.: Small influence of solar variability on climate over the past millennium, Nature Geoscience, 7, 104–108, https://doi.org/10.1038/ngeo2040, 2013.

Sekhon, N., Novello, V. F., Cruz, F. W., Wortham, B. E., Ribeiro, T. G., and Breecker, D. O.: Diurnal to seasonal ventilation in Brazilian caves, Global and Planetary Change, 197, 103 378, https://doi.org/10.1016/j.gloplacha.2020.103378, 2021.

Sigl, M., Winstrup, M., McConnell, J. R., Welten, K. C., Plunkett, G., Ludlow, F., Büntgen, U., Caffee, M., Chellman, N., Dahl-Jensen, D., et al.: Timing and climate forcing of volcanic eruptions for the past 2,500 years, Nature, 523, 543–549, 2015.

Sjolte, J., Adolphi, F., Vinther, B. M., Muscheler, R., Sturm, C., Werner, M., and Lohmann, G.: Seasonal Reconstructions Coupling Ice Core Data and an Isotope-Enabled Climate Model – Methodological Implications of Seasonality, Climate Modes and Selection of Proxy Data, Climate of the Past, 16, 1737–1758, https://doi.org/10.5194/cp-16-1737-2020, 2020.

Smerdon, J. E.: Climate Models as a Test Bed for Climate Reconstruction Methods: Pseudoproxy Experiments: Pseudoproxy Experiments, Wiley Interdisciplinary Reviews: Climate Change, 3, 63–77, https://doi.org/10.1002/wcc.149, 2012.

Stansell, N. D., Steinman, B. A., Abbott, M. B., Rubinov, M., and Roman-Lacayo, M.: Lacustrine Stable Isotope Record of Precipitation Changes in Nicaragua during the Little Ice Age and Medieval Climate Anomaly, Geology, 41, 151–154, https://doi.org/10.1130/G33736.1, 2013.

Steiger, N. and Hakim, G.: Multi-Timescale Data Assimilation for Atmosphere–Ocean State Estimates, Climate of the Past, 12, 1375–1388, https://doi.org/10.5194/cp-12-1375-2016, 2016.

Steiger, N. J., Hakim, G. J., Steig, E. J., Battisti, D. S., and Roe, G. H.: Assimilation of Time-Averaged Pseudoproxies for Climate Reconstruction, Journal of Climate, 27, 426–441, https://doi.org/10.1175/JCLI-D-12-00693.1, 2014.

Steiger, N. J., Smerdon, J. E., Cook, E. R., and Cook, B. I.: A Reconstruction of Global Hydroclimate and Dynamical Variables over the Common Era, Scientific Data, 5, 180 086, https://doi.org/10.1038/sdata.2018.86, 2018.

Stevenson, S., Otto-Bliesner, B. L., Brady, E. C., Nusbaumer, J., Tabor, C., Tomas, R., Noone, D. C., and Liu, Z.: Volcanic Eruption Signatures in the Isotope-Enabled Last Millennium Ensemble, Paleoceanography and Paleoclimatology, 34, 1534–1552, https://doi.org/10.1029/2019PA003625, 2019.

Swart, P. K., Dodge, R. E., and Hudson, H. J.: A 240-year stable oxygen and carbon isotopic record in a coral from South Florida: Implications for the prediction of precipitation in southern Florida, Palaios, pp. 362–375, 1996.

Tardif, R., Hakim, G. J., Perkins, W. A., Horlick, K. A., Erb, M. P., Emile-Geay, J., Anderson, D. M., Steig, E. J., and Noone, D.: Last Millennium Reanalysis with an Expanded Proxy Database and Seasonal Proxy Modeling, Climate of the Past, 15, 1251–1273, https://doi.org/10.5194/cp-15-1251-2019, 2019.

Thompson, L. G., Mosley-Thompson, E., Davis, M. E., Zagorodnov, V. S., Howat, I. M., Mikhalenko, V. N., and Lin, P.-N.: Annually Resolved Ice Core Records of Tropical Climate Variability over the Past ~1800 Years, Science, 340, 945–950, https://doi.org/10.1126/science.1234210, 2013.

Tierney, J. E., Abram, N. J., Anchukaitis, K. J., Evans, M. N., Giry, C., Kilbourne, K. H., Saenger, C. P., Wu, H. C., and Zinke, J.: Tropical sea surface temperatures for the past four centuries reconstructed from coral archives, Paleoceanography, 30, 226–252, https://doi.org/10.1002/2014pa002717, 2015.

Tierney, J. E., Zhu, J., King, J., Malevich, S. B., Hakim, G. J., and Poulsen, C. J.: Glacial Cooling and Climate Sensitivity Revisited, Nature, 584, 569–573, https://doi.org/10.1038/s41586-020-2617-x, 2020.

Tierney, J. E., Zhu, J., Li, M., Ridgwell, A., Hakim, G. J., Poulsen, C. J., Whiteford, R. D. M., Rae, J. W. B., and Kump, L. R.: Spatial Patterns of Climate Change across the Paleocene–Eocene Thermal Maximum, Proceedings of the National Academy of Sciences, 119, e2205326 119, https://doi.org/10.1073/pnas.2205326119, 2022.

Tindall, J. C., Valdes, P. J., and Sime, L. C.: Stable Water Isotopes in HadCM3: Isotopic Signature of El Niño–Southern Oscillation and the Tropical Amount Effect, Journal of Geophysical Research, 114, D04 111, https://doi.org/10.1029/2008JD010825, 2009.

Utida, G., Cruz, F. W., Vuille, M., Ampuero, A., Novello, V. F., Maksic, J., Sampaio, G., Cheng, H., Zhang, H., Dias de Andrade, F. R., and Edwards, R. L.: Spatiotemporal ITCZ Dynamics during the Last Three Millennia in Northeastern Brazil and Related Impacts in Modern Human History, Preprint, Proxy Use-Development-Validation/Terrestrial Archives/Holocene, https://doi.org/10.5194/cp-2023-2, 2023.

Valler, V., Brugnara, Y., Franke, J., and Brönnimann, S.: Assimilating Monthly Precipitation Data in a Paleoclimate Data Assimilation Framework, Climate of the Past, 16, 1309–1323, https://doi.org/10.5194/cp-16-1309-2020, 2020.

Valler, V., Franke, J., Brugnara, Y., Samakinwa, E., Hand, R., Lundstad, E., Burgdorf, A.-M., Lipfert, L., Friedman, A. R., and Brönnimann, S.: ModE-RA: a global monthly paleo-reanalysis of the modern era 1421 to 2008, Scientific Data, 11, https://doi.org/10.1038/s41597-023-02733-8, 2024.

Van Rossum, G. and De Boer, J.: Interactively testing remote servers using the Python programming language, CWI quarterly, 4, 283–303, 1991.

Vetra-Carvalho, S., van Leeuwen, P. J., Nerger, L., Barth, A., Altaf, M. U., Brasseur, P., Kirchgessner, P., and Beckers, J.-M.: State-of-the-Art Stochastic Data Assimilation Methods for High-Dimensional Non-Gaussian Problems, Tellus A: Dynamic Meteorology and Oceanography, 70, 1–43, https://doi.org/10.1080/16000870.2018.1445364, 2018.

Vicente-Serrano, S. M., Beguería, S., and López-Moreno, J. I.: A Multiscalar Drought Index Sensitive to Global Warming: The Standardized Precipitation Evapotranspiration Index, Journal of Climate, 23, 1696–1718, https://doi.org/10.1175/2009JCLI2909.1, 2010.

Virtanen, P., Gommers, R., Oliphant, T. E., Haberland, M., Reddy, T., Cournapeau, D., Burovski, E., Peterson, P., Weckesser, W., Bright, J., van der Walt, S. J., Brett, M., Wilson, J., Millman, K. J., Mayorov, N., Nelson, A. R. J., Jones, E., Kern, R., Larson, E., Carey, C. J., Polat, İ., Feng, Y., Moore, E. W., VanderPlas, J., Laxalde, D., Perktold, J., Cimrman, R., Henriksen, I., Quintero, E. A., Harris, C. R., Archibald, A. M., Ribeiro, A. H., Pedregosa, F., van Mulbregt, P., and SciPy 1.0 Contributors: SciPy 1.0: Fundamental Algorithms for Scientific Computing in Python, Nature Methods, 17, 261–272, https://doi.org/10.1038/s41592-019-0686-2, 2020.

von Gunten, L., Grosjean, M., Rein, B., Urrutia, R., and Appleby, P.: A quantitative high-resolution summer temperature reconstruction based on sedimentary pigments from Laguna Aculeo, central Chile, back to AD 850, The Holocene, 19, 873–881, https://doi.org/10.1177/0959683609336573, 2009.

Vuille, M. and Werner, M.: Stable isotopes in precipitation recording South American summer monsoon and ENSO variability: observations and model results, Climate Dynamics, 25, 401–413, https://doi.org/10.1007/s00382-005-0049-9, 2005.

Vuille, M., Bradley, R. S., Werner, M., Healy, R., and Keimig, F.: Modeling d18O in precipitation over the tropical Americas: 1. Interannual variability and climatic controls, Journal of Geophysical Research: Atmospheres, 108, https://doi.org/10.1029/2001jd002038, 2003.

Vuille, M., Burns, S. J., Taylor, B. L., Cruz, F. W., Bird, B. W., Abbott, M. B., Kanner, L. C., Cheng, H., and Novello, V. F.: A Review of the South American Monsoon History as Recorded in Stable Isotopic Proxies over the Past Two Millennia, Climate of the Past, 8, 1309–1321, https://doi.org/10.5194/cp-8-1309-2012, 2012.

Wang, J., Emile-Geay, J., Guillot, D., Smerdon, J. E., and Rajaratnam, B.: Evaluating Climate Field Reconstruction Techniques Using Improved Emulations of Real-World Conditions, Climate of the Past, 10, 1–19, https://doi.org/10.5194/cp-10-1-2014, 2014.

Wang, X., Edwards, R. L., Auler, A. S., Cheng, H., Kong, X., Wang, Y., Cruz, F. W., Dorale, J. A., and Chiang, H.-W.: Hydroclimate Changes across the Amazon Lowlands over the Past 45,000 Years, Nature, 541, 204–207, https://doi.org/10.1038/nature20787, 2017.

Ward, B. M., Wong, C. I., Novello, V. F., McGee, D., Santos, R. V., Silva, L. C., Cruz, F. W., Wang, X., Edwards, R. L., and Cheng, H.: Reconstruction of Holocene coupling between the South American Monsoon System and local moisture variability from speleothem δ18O and 87Sr/86Sr records, Quaternary Science Reviews, 210, 51–63, https://doi.org/10.1016/j.quascirev.2019.02.019, 2019.

Werner, M., Haese, B., Xu, X., Zhang, X., Butzin, M., and Lohmann, G.: Glacial–Interglacial Changes in $H_2^{18}O$, HDO and Deuterium Excess – Results from the Fully Coupled ECHAM5/MPI-OM Earth System Model, Geoscientific Model Development, 9, 647–670, https://doi.org/10.5194/gmd-9-647-2016, 2016.

Wes McKinney: Data Structures for Statistical Computing in Python, in: Proceedings of the 9th Python in Science Conference, edited by Stéfan van der Walt and Jarrod Millman, pp. 56 – 61, https://doi.org/10.25080/Majora-92bf1922-00a, 2010.

Wilks, D. S.: Forecast verification, in: International geophysics, vol. 100, pp. 301–394, Elsevier, 2011.

Winter, A., Miller, T., Kushnir, Y., Sinha, A., Timmermann, A., Jury, M. R., Gallup, C., Cheng, H., and Edwards, R. L.: Evidence for 800years of North Atlantic multi-decadal variability from a Puerto Rican speleothem, Earth and Planetary Science Letters, 308, 23–28, https://doi.org/10.1016/j.epsl.2011.05.028, 2011.

Wong, M. L., Wang, X., Latrubesse, E. M., He, S., and Bayer, M.: Variations in the South Atlantic Convergence Zone over the mid-to-late Holocene inferred from speleothem D18O in central Brazil, Quaternary Science Reviews, 270, 107 178, https://doi.org/10.1016/j.quascirev.2021.107178, 2021.

Wortham, B. E., Wong, C. I., Silva, L. C. R., McGee, D., Montañez, I. P., Troy Rasbury, E., Cooper, K. M., Sharp, W. D., Glessner, J. J. G., and Santos, R. V.: Assessing Response of Local Moisture Conditions in Central Brazil to Variability in Regional Monsoon Intensity Using Speleothem 87Sr/86Sr Values, Earth and Planetary Science Letters, 463, 310–322, https://doi.org/10.1016/j.epsl.2017.01.034, 2017.

Yoshimura, K., Kanamitsu, M., Noone, D., and Oki, T.: Historical Isotope Simulation Using Reanalysis Atmospheric Data, Journal of Geophysical Research: Atmospheres, 113, https://doi.org/10.1029/2008JD010074, 2008.

Zhou, J. and Lau, K.: Does a monsoon climate exist over South America?, Journal of climate, 11, 1020–1040, 1998.

Supplement A: ~~Additional Figures~~

1225 ~~Detailed spatiotemporal availability~~

Supplement S1: **Proxy record Supplement**

S1.1 **Detailed spatiotemporal availability**
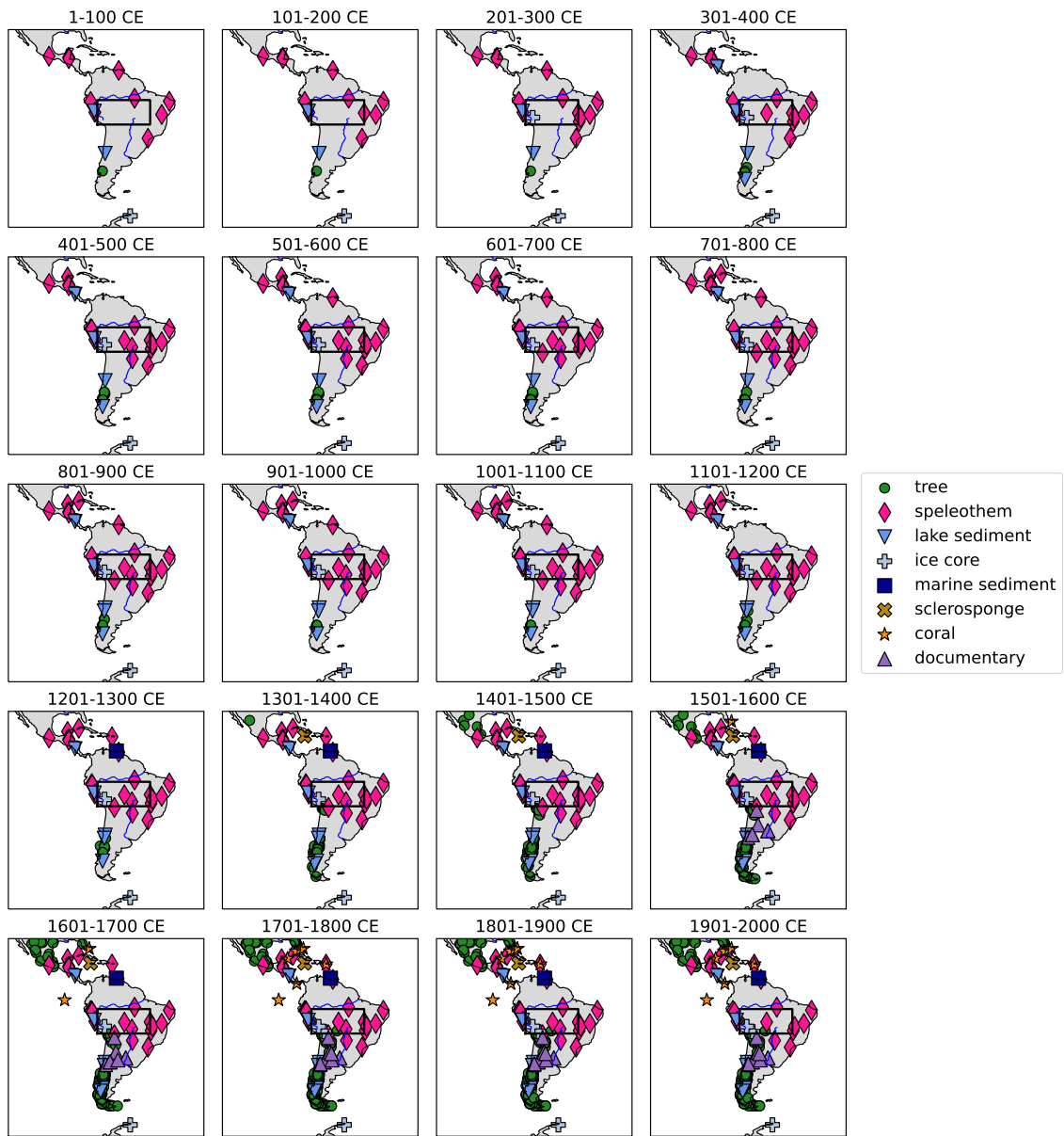
SF 1.1. Spatiotemporal availability of the proxy records for each century . The black box represents the core region of the South American Summer Monsoon (Vuille et al., 2012)

S1.2 Proxy record lists

For an overview of all proxy records employed in this regional climate field reconstruction, the proxy records are grouped by climate archive type and presented in tabular form. In the *database* column, the proxy record databases from which the values were taken are named, in case the record is part of one. Additionally the original publications are cited in the *source* column. For the citations of proxy records that were part of a database, the reader is referred to the publications presenting the proxy record databases. The level of detail in the tables varies by climate archive type, as the information from column with unique entries (e.g. the proxy variable, PSM type, Seasonality or SNR) has been transferred to explanatory text above the tables to limit the size of the tables. All data processing steps can be retraced and reproduced with the Jupyter Notebooks accompanying this publication.

Mean anomaly fields (Figure 3) for austral summer reconstruction

S1.2.1 Speleothems

Same as Figure 3 for the austral summer (DJF) reconstruction. Stippling indicates grid cells where the difference to the Last Millennium values is not significant according to a Welch's t-test ($\alpha > 0.01$). The proxy variables are δ^{18}O of aragonite and δ^{18}O of calcite for all processed speleothem time series. For all speleothems, the same *precipitation weighting*-type PSM has been used, thus rendering the application of some additional seasonality restrictions unnecessary. The SNR is computed from the variance of the time series by assuming the same SNR for all speleothems (See Section S2.2). Whereas the speleothem time series have relatively high median temporal resolutions, all time series are resampled to 10 years resolution to conservatively account for smoothing effects in the karst.

Mean anomaly fields (Figure 3) for reconstruction with different proxy error definition

For caves with multiple records of similar resolution, composites were computed according to Novello et al. (2021) (step 2 and 3 in section 3.3) by applying the following steps to the time series of various records in one cave during the overlap period 1) resampling all proxy time series to annual resolution, 2) standardizing the time series (zero-mean & standard deviation equal to one) 3) computing the mean of the overlapping values 4) destandardizing the mean time series using the mean and standard deviation of the time series which is longer. Further steps detailed in section 3.3 of Novello et al. (2021) are not applied, as these involve age model ensembles, which have not been used in this study. The practical computation of speleothem composites can be retraced in the Jupyter Notebooks accompanying this publication.

Nr	Site name	Location (Lat,Lon)	Time (CE)	Resolution time scale [yrs]	Database (ID in database)	Source	Comment
1	Dos Anas cave	22.4,276.0	746-2000	2	SISALv3 (443)	Fensterer et al. (2012)	
2	Tzabnah cave	20.7,270.3	487-2004	2	SISALv3 (147)	Medina-Elizalde et al. (2010)	
3	Perdida cave	18.0,293.0	1208-2003	2	SISALv3 (378)	Winter et al. (2011)	
4	Juxtlahuaca cave	17.4,260.8	0-2010	2	SISALv3 (286)	Lachniet et al. (2012)	
5	Macal Chasm	16.9,270.9	0-1992	3	SISALv3 (178)	Akers et al. (2016)	
6	Yok Balum cave	16.2,270.9	0-2005	1	SISALv3 (209)	Kennett et al. (2012)	Used longest record from location
7	Caripe Cave	10.2,296.4	0-1993	2	-	Medina et al. (2023)	
8	Paraiso cave	-4.1,304.6	0-1998	7	SISALv3 (424)	Wang et al. (2017)	
9	Trapiá cave	-5.6,322.3	0-1932	3	-	Utida et al. (2023)	
10	Shatuca cave	-5.7,282.1	0-1984	8	SISALv3 (434)	Bustamante et al. (2016)	
11	Palestina cave	-5.9,282.6	413-1850	5	SISALv3 (94)	Apaéstegui et al. (2014)	
12	Cascayunga Cave	-6.4,282.9	1088-1999	1	-	Bird et al. (2011b)	
13	Huagapo cave	-11.3,284.2	3-1993	2	SISALv3 (597,598)	Kanner et al. (2013)	Composite
14	Mata Virgem cave	-11.6,312.5	166-1814	1	-	Azevedo et al. (2019)	Used Mata Virgem 1 record
15	Cuíca cave	-11.7,299.4	338-2013	2	SISALv3 (752)	Libera et al. (2022)	
16	Diva cave	-12.4,318.4	2-1999	4	SISALv3 (113,146,203)	Novello et al. (2012)	Composite
17	São Matheus/Bernardo cave	-13.8,313.6	264-1998	1	SISALv3 (430,431)	Novello et al. (2018)	Composite
18	Pau d'Alho cave	-15.2,303.2	491-1860	1	SISALv3 (128)	Novello et al. (2016)	
19	Tamboril cave	-16.0,313.0	272-1982	2	SISALv3 (97)	Wortham et al. (2017)	
20	Umajalanta cave	-18.1,294.2	620-1863	2	SISALv3 (499,497,498,518)	Apaéstegui et al. (2018)	Composite
21	Jaraguá cave	-21.1,303.4	422-2000	3	SISALv3 (449)	Novello et al. (2018)	Composite as part of SISAL
22	Cristal Cave	-24.5,311.4	0-2006	2	-	Vuille et al. (2012)	

Table S1.1. Speleothem proxy records description table

Same as Figure 3 applying a proxy error variance equal to the prior variance instead of the SNR=0.5 proxy error definition. Stippling indicates grid cells where the difference to the Last Millennium values is not significant according to a Welch's t-test ($\alpha > 0.01$).

S1.2.2 Lake sediment records

~~Centennial climate anomalies~~

Only lake sediment records directly related to the isotopic composition of precipitation (and thus not mostly affected by additional evaporation) or already calibrated to temperature have been included. To make this distinction, the original publications have been consulted and records have been accordingly selected. This restriction excluded most lake sediment records available in the Iso2k database (Konecky et al., 2020). All lake sediment records are used on a time scale of five years, to account for the effect of bioturbation in the sedimentation process. For all lake sediments, the same SNR value has been assumed, also for temperature calibrated records which come with an error variance.

Nr	Site name	Location (Lat,Lon)	Time (CE)	Resolution	Proxy variable	PSM	Seasonality	Database (ID in database)	Source
1	Lago El Grancho	11.9,274.1	341-2004	4	$\delta^{18}O$	prec. weighted	None	Iso2k (263)	Stansell et al. (2013)
2	Laguna Pumacocha	-10.7,283.9	0-2007	2	$\delta^{18}O$	prec. weighted	None	Iso2k (343)	Bird et al. (2011a)
3	Laguna Chepical	-32.3,289.5	0-2005	1	tsurf	season	11,12,1,2	Pages2k (SAm_30)	de Jong et al. (2013)
4	Laguna Aculeo	-33.8,289.1	856-1997	1	tsurf	season	12,1,2	Pages2k (SAm_3)	von Gunten et al. (2009)
5	Laguna Escondida	-45.5,288.2	400-2008	1	tsurf	direct	None	Pages2k (SAm_31)	Elbert et al. (2013)
6	Lago Plomo	-47.0,287.1	1384-2001	1	tsurf	season	9,10,11,12,1,2	Elbert et al. (2015)	Elbert et al. (2015)
7	Lago Puyehue	-40.7,287.55	1408-1997	1	tsurf/spei	linear	-	Neukom and Gergis (2012)	Boës and Fagel (2008)

Table S1.2. ~~Reconstructed mean anomaly fields for precipitation with respect to the 850 - 1850 CE mean value (annual reconstruction). Stippling indicates grid cells where the difference to the Last Millennium values is not significant according to a Welch's t-test ($\alpha > 0.01$).~~ Lake sediment proxy records description table

~~Reconstructed mean anomaly fields for surface temperature with respect to the 850 - 1850 CE mean value (annual reconstruction). Stippling indicates grid cells where the difference to the Last Millennium values is not significant according to a Welch's t-test ($\alpha > 0.01$).~~

S1.2.3 Sclerosponge

~~Reconstructed mean anomaly fields for SPEI with respect to the 850 - 1850 CE mean value (annual reconstruction). Before computing centennial means, the SPEI time series have been standardized with respect to the 850 - 1850 CE mean. Stippling indicates grid cells where the difference to the Last Millennium values is not significant according to a Welch's t-test ($\alpha > 0.01$).~~ For the conversion of the sclerosponge values from Montego Bay, Jamaica, to temperature, the formula presented in Haase-Schramm et al. (was used. From the two provided records, we selected the record which was located closer the sea surface (see original publication for details). The time series values were resampled to five years to account for the non-annual resolution of the record.

Nr	Site name	Location (Lat,Lon)	Time (CE)	Resolution	Proxy variable	PSM	Seasonality	SNR	Database (ID in database)	Source
1	Montego Bay, Jamaica	18.5,282.0	1356-1991	5	tsurf	direct	None	assumed	Pages2k (150)	Haase-Schramm et al. (2003)

Table S1.3. Sclerosponge proxy record description table

Mean anomaly fields (Figure 3) for reconstruction only using speleothem proxy records

S1.2.4 Marine sediment

Same as Figure 3 but for the reconstruction that only uses speleothems as proxy record input data. Stippling indicates grid cells
1285 where the difference to the Last Millennium values is not significant according to a Welch's t-test ($\alpha > 0.01$).

Mean anomaly fields (Figure 3) for reconstruction excluding speleothem proxy records

The Cariaco Basin record from Black et al. (2007) was the only marine sediment included in our regional climate field reconstruction, as other marine sediment from South and Central America only provide a longer than decadal resolution. Due to the exceptionally high sedimentation rate in the Cariaco Basin, the record was treated as an annual record according to its temporal resolution.

Nr	Site name	Location (Lat,Lon)	Time (CE)	Resolution	Proxy variable	PSM	Seasonality	SNR	Database (ID in database)	Source
1	Cariaco Basin	10.8,295.2	1221-1990	1	tsurf	season	3,4,5	assumed	Pages2k (11)	Black et al. (2007)

Table S1.4. Same as Figure 3 but for the reconstruction that uses all proxy records except the speleothems as Marine sediment proxy record input data. Stippling indicates grid cells where the difference to the Last Millennium values is not significant according to a Welch's t-test ($\alpha > 0.01$). description table

1290 **Additional SASM index figures**

S1.2.5 Ice cores

For all ice core δ^{18}O record locations, the precipitation weighting PSM has been applied, rendering the definition of a seasonality unnecessary. For all ice core proxy records, an SNR value was assumed to compute the error variance.
Same as Figure 4 including the single model reconstructions using all proxy records (dotted lines). The black line is the
1295 multi-model ensemble reconstruction (mean of single prior reconstructions).

Nr	Site name	Location (Lat,Lon)	Time (CE)	Proxy variable	Database (ID in database)	Source	Comment
1	Quelccaya Ice Cap	-13.9,289.2	226-2009	$\delta^{18}O$	Pages2k (SAm_026)	Thompson et al. (2013)	
2	Illimani	-16.6,292.2	1771-1998	D	Iso2k (485)	Hoffmann et al. (2003)	Deuterium converted to $\delta^{18}O$ with factor 1/8
3	James Ross Island	-64.2,302.3	0-2007	D	Pages2k (Ant_10)	Abram et al. (2013)	Deuterium converted to $\delta^{18}O$ with factor 1/8

Table S1.5. ~~Same as Figure 4 for the austral summer (DJF) reconstruction with extended y-axes ranges. The PHYDA reconstruction displayed here is a specific austral summer reconstruction, whereas LMRv2.1 is only provided at an annual time scale.~~ Ice core proxy records description table

S1.2.6 Corals

All coral proxy records were used on an annual time scale. For the PSM, the linear PSM for temperature was used, thus all records were calibrated to temperature. Calibration values (including SNR estimates) were calculated for the annual and seasonal reconstruction/calibration separately.

Nr	Site name	Location (Lat,Lon)	Time (CE)	Resolution	Proxy variable	SNR (Ann.,DJF)	Database (ID in database)	Source
1	Gingerbread Bahamas	25.8,281.4	1552-1991	1	calcification	0.2, 0.15	PAGES2K-Ocn_065	Saenger et al. (2009)
2	Alinas Reef, Biscayne National Park, Florida	25.4,279.8	1751-1986	1	$\delta^{18}O$	0.1,0.13	Iso2K-255	Swart et al. (1996)
3	Dry Tortugas	24.6,277.7	1733-2008	1	Sr_Ca	0.55,0.97	PAGES2K-Ocn_070	DeLong et al. (2014)
4	Punta Maroma, Mexico	20.8,273.3	1773-2009	1	calcification	0.88,0.4	PAGES2K-Ocn_073	Tierney et al. (2015)
5	Turrumote Reef, Puerto Rico	17.9,293.0	1751-2004	1	$\delta^{18}O$	0.73,0.59	PAGES2K-Ocn_111	Kilbourne et al. (2008)
6	Secas Island, Panama	8.0,278.0	1707-1984	1	$\delta^{18}O$	0.27,0.23	PAGES2K-Ocn_104	Linsley et al. (1994)
7	Urvina Bay	-0.4,268.8	1607-1981	1	$\delta^{18}O$	0.61,0.34	PAGES2K-Ocn_087	Dunbar et al. (1994)

Table S1.6. ~~Same as Figure 4 for the *all proxies* reconstruction and the model simulations. The time period has been limited to the period 850-1850 CE as this is the time span covered by the model simulations.~~ Coral proxy records description table

1300 S1.2.7 Documentary records

All employed documentary indices were taken from the NOAA database (https://www.ncei.noaa.gov/access/paleo-search/study/8703) and were presented in Neukom et al. (2009). No seasonality restriction was imposed for using the data as the calibration to instrumental variables for the linear PSM was computed for the annual and summer season separately. All documentary records were used on an annual time scale.

1305 S1.2.8 Trees

The employed tree records are described solely in text form rather than tabular format due to their large quantity. The proxy data from trees was mainly taken from three proxy record databases according to the selection criteria outlined in the main text. This selection resulted in 203 tree proxy time series from the South American Drought Atlas (Morales et al., 2020), 42 from

Nr	Site name	Proxy variable	Location (Lat,Lon)	Time (CE)	SNR (Ann.,DJF)	Database	Source
1	Potosi	precipitation index	-19.6,294.3	1585-2005	0.32, 0.22	NOAA	Neukom et al. (2009)
2	Dulce	river runoff index	-27.0,295.0	1750-1977	0.27,0.29	NOAA	Neukom et al. (2009)
3	Tucuman	precipitation index	-27.0,295.0	1548-2005	0.65,0.36	NOAA	Neukom et al. (2009)
4	Santiago del Estero	precipitation index	-27.8,195.7	1750-2005	0.47,0.38	NOAA	Neukom et al. (2009)
5	Santa Fe and Corrientes	precipitation index	-30.0,300.0	1590-2006	0.73,0.59	NOAA	Neukom et al. (2009)
6	Mendoza	river runoff index	-32.0,292.0	1599-2000	0.27,0.21	NOAA	Neukom et al. (2009)
7	Mendoza	precipitation index	-32.0,292.0	1600-1985	0.42,0.34	NOAA	Neukom et al. (2009)
8	Central Andes	snow depth index	-33.0,290.0	1760-1996	0.64,0.54	NOAA	Neukom et al. (2009)
9	Santiago de Chile	precipitation index	-33.3,289.7	1540-2006	0.49,0.45	NOAA	Neukom et al. (2009)
10	Parana	river runoff index	-30.0,300.0	1590-1993	0.3,0.33	NOAA	Neukom et al. (2009)
11	Cordoba	precipitation index	-31.0,296.0	1700-2005	0.42,0.27	NOAA	Neukom et al. (2009)

Table S1.7. Documentary records description table

Breitenmoser et al. (2014), as used in and published alongside Steiger et al. (2014), and 5 records from the Pages2k database
1310 (Emile-Geay et al., 2017). We checked for potential overlaps between these proxy databases and excluded double/triple records.
As the SADA database only extends back to 1400CE, six records from it have been replaced by the longer original record data
which are available in the NOAA database (see code of this publication for exact documentation). All these data bases use
tree ring width as a proxy from trees, and not Maximum Wood Density (MXD). In addition to these tree ring data sources, we
used four single records/tree ring composites , namely from the central Altiplano (Morales et al., 2012), the northern altiplano
1315 (Morales et al., 2023), the western Amazon (Humanes-Fuente et al., 2020) and near the Perito Moreno glacier in Patagonia
(Grießinger et al., 2018). For this last tree proxy record, the proxy variable is δ^{18}O in wood and not tree ring width, but this
record has also been calibrated to instrumental variables as all other tree ring records, because precipitation δ^{18}O can not be
directly related to δ^{18}O in wood. No seasonality restriction was imposed for using the data as the calibration to instrumental
variables for the linear PSM was computed for the annual and summer season separately. All used tree records have annual
1320 resolution.

~~Additional power spectra~~

Supplement S2: Methodology

S2.1   Algorithm sketches
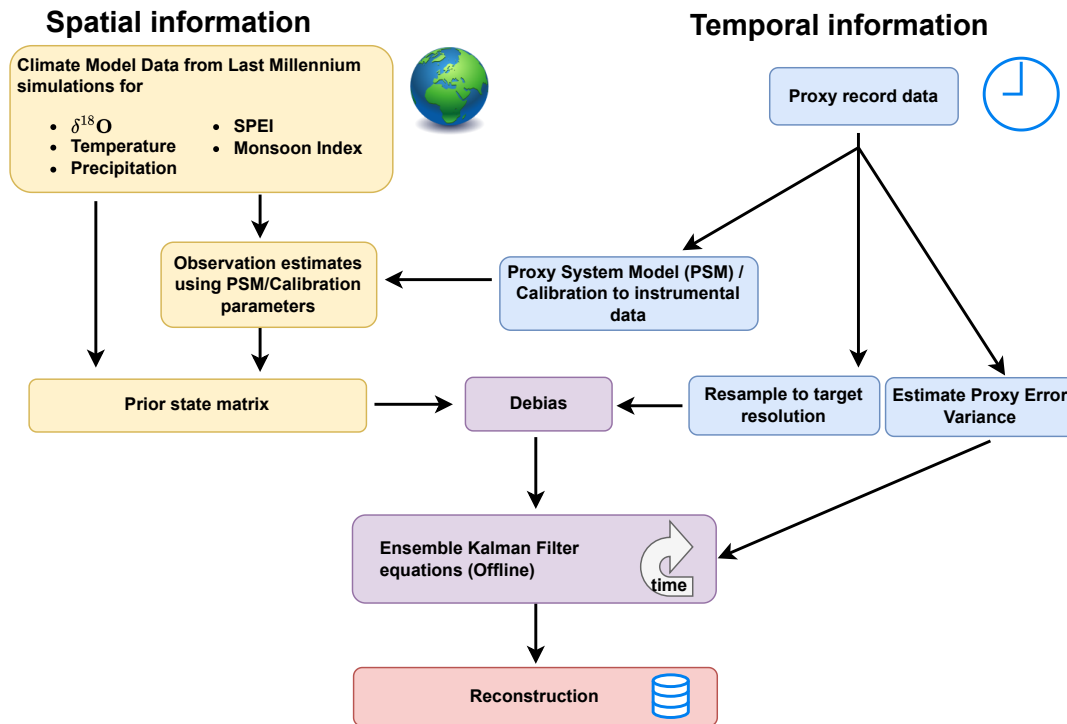
SF 2.1. ~~**Spectra of reconstructed monsoon** δ^{18}**O index**~~Algorithm sketch for multi-timescale Paleoclimate Data Assimilation Algorithm.
See main text for a description of ~~Figure 6~~the individual steps.

~~**Spectra of SASM indices in model simulations**. The spectra for SASM precipitation and δ^{18}O have been computed as in Figure 6, but limited to the period 850-1850 CE, because this is the time period covered by the model simulations. In addition, all time series have been standardized, as the model simulations have more overall variability (higher variance). Standardizing the time series allows to highlight the different scaling of the simulation and reconstruction spectra.~~

~~Climate anomalies in PHYDA and LMRv2.1~~

1325 ~~Same Anomaly Fields as Figure 3 for the PHYDA reconstruction (Steiger et al., 2018), which includes temperature and SPEI among its reconstructed variables, but not precipitation and δ^{18}O. Stippling indicates grid cells where the difference to the Last Millennium values is not significant according to a Welch's t-test ($\alpha > 0.01$).~~

$$\mathbf{X}^f = \begin{pmatrix} \mathbf{X}_{120} \\ \mathbf{X}_{50} \\ \dots \\ \mathbf{X}_{930} \end{pmatrix} \Rightarrow \left.\begin{pmatrix} \overbrace{\mathbf{X}_{120} \quad \mathbf{X}_{121} \quad \dots \quad \mathbf{X}_{129}}^{\text{block size=10 years}} \\ \mathbf{X}_{50} \quad \mathbf{X}_{51} \quad \dots \quad \mathbf{X}_{59} \\ \dots \quad \dots \quad \dots \quad \dots \\ \mathbf{X}_{930} \quad \mathbf{X}_{931} \quad \dots \quad \mathbf{X}_{939} \end{pmatrix}\right\} N_y \text{ ensemble members}$$

SF 2.2. Illustration of how single-time scale PaleoDA prior, consisting of a random collection of climate fields, is extended into a matrix which also contains the subsequent years for multi-time scale PaleoDA. Each $\mathbf{X}_i$ corresponds to the mean climate field of one simulation year, the index denotes the year of the simulation that was randomly selected for creating the ensemble. The $\mathbf{X}_i$ could also be depicted explicitly as a vector, thus rendering the matrix three-dimensional. In the multi-time scale PaleoDA, rows of the matrix are averaged over several years in order to assimilate multiyear means.

Correlations in the model simulations (prior) for NEB

~~**Correlation of**~~ δ^{18}~~**O mean in the Nordeste**~~ ~~(black box, Lat: -15-0°, Lon: 313-327°)~~ To facilitate the assignment to ~~climate variables δ^{18}O, precipitation~~the blocks, ~~temperature~~ the non-annually resolved proxy records are resampled to 5 and ~~SPEI of individual grid cells~~ 10 year resolutions as described in the ~~five isotope-enabled climate model simulations. The correlations have been computed with the annual mean values of the simulated climate variables~~main text.

SF 2.3. ~~Same Anomaly Fields as Figure 3 for the LMRv2.1 reconstruction (Tardif et al., 2019), which includes temperature~~ Assignment of non-annually resolved proxy records to 5 and ~~precipitation among its reconstructed variables, but not SPEI~~ 10 year time scales (e.g. lake records and δ^{18}O~~speleothems in our reconstruction). Stippling indicates grid cells where~~ During the ~~difference to~~ multi-time scale PaleoDA, the ~~Last Millennium~~ values ~~is not significant according~~ of these types of proxies are assigned to ~~a Welch's t-test~~ the 5 or 10 year block means ~~(α > 0.01)~~see Figure SF 2.2 instead of annual values.

Correlations in the model simulations (prior) for NEB

~~**Correlation of**~~ δ^{18}~~**O mean in the Nordeste**~~ ~~(black box, Lat: -15-0°, Lon: 313-327°)~~ To facilitate the assignment to ~~climate variables δ^{18}O, precipitation~~the blocks, ~~temperature~~ the non-annually resolved proxy records are resampled to 5 and ~~SPEI of individual grid cells~~ 10 year resolutions as described in the ~~five isotope-enabled climate model simulations. The correlations have been computed with the annual mean values of the simulated climate variables~~main text.

S2.2 Observation error estimation from the Signal-to-Noise Ratio (SNR)

Correlations in the model simulations (prior) for SASM region

We estimate the observation error variance $\mathbf{R}$ (Equation 2) for each proxy record from an assumed signal-to-noise ratio (SNR).

Correlation of precipitation mean in core SASM region (black box, Lat: -17.5 – -5°, Lon: 287.5-312.5°) to climate variables δ^{18}O, precipitation, temperature and SPEI of individual grid cells in the five isotope-enabled climate model simulations. The correlations have been computed with the annual mean values of the simulated climate variables. The SNR is defined as the ratio of the standard deviations of the unperturbed time series T and the white noise N:

$$\mathrm{SNR} := \frac{\mathrm{std}(T)}{\mathrm{std}(N)} \tag{S2.1}$$

As the observation error variance $\mathbf{R}$ is by definition equal to the squared standard deviation of the noise N, we get for $\mathbf{R}$

$$\mathbf{R} = \mathrm{std}(N)^2 = \mathrm{var}(N) \tag{S2.2}$$

$$\Rightarrow SNR = \frac{\mathrm{std}(T)}{\sqrt{\mathbf{R}}} \tag{S2.3}$$

$$\Rightarrow \mathbf{R} = \frac{\mathrm{var}(T)}{\mathrm{SNR}^2} \tag{S2.4}$$

The variance of T is not known directly because the proxy record time series Y represents the noisy time series $T + N$, whose variance can be used to compute $\mathrm{var}(T)$. When assuming that N and T are uncorrelated, their variances are additive.

$$\mathrm{std}(T+N) = \sqrt{\mathrm{var}(T+N)} \tag{S2.5}$$

$$= \sqrt{\mathrm{var}(T) + \mathrm{var}(N) + \mathrm{cov}(T,N)} = \sqrt{\mathrm{var}(T) + \mathrm{var}(N)} \tag{S2.6}$$

$$= \sqrt{\mathrm{var}(T) + \mathbf{R}} \tag{S2.7}$$

$$\Rightarrow \mathrm{var}(T) = \mathrm{var}(T+N) - \mathbf{R} \tag{S2.8}$$

Using the relationship from equation S2.8 in equation S2.4 we get

$$\mathbf{R} = \frac{\mathrm{var}(T+N) - \mathbf{R}}{SNR^2} \tag{S2.9}$$

$$\Rightarrow \mathbf{R} = \frac{\mathrm{var}(T+N)}{1 + SNR^2} = \frac{\mathrm{var}(Y)}{1 + SNR^2} \tag{S2.10}$$

Using equation S3.1, the observation error $\mathbf{R}$ can be estimated from the variance of the proxy record time series and by assuming a specific SNR value for the proxy records, which does not need to be the same for all proxy records.

Supplement S3: Validation of reconstruction

S3.1 Spatial reconstruction skill using gridded instrumental data

To evaluate the spatial reconstruction skill of our reconstructions, we compare these to gridded instrumental datasets, Berkeley Earth (Rohde and Hausfather, 2020) for temperature and CRUTS 4 (Harris et al., 2020b) for precipitation. A reference SPEI dataset is computed from CRUTS 4 using Thornthwaite's method for estimating potential evapotranspiration. The validation periods are 1920 - 2000 CE for temperature and 1950 - 2000 CE for precipitation and the SPEI, due to limited local instrumental, radiosonde and satellite precipitation data during the first half of the 20th century. Until the second half of the 20th century, South America lacked extensive weather station coverage, with only a few stations mainly situated in coastal regions and the Southern part of the continent (See Figure 1 in Harris et al., 2020b). Estimates of precipitation, which is a more localized phenomenon than temperature, are particularly affected by this limited station coverage. Precipitation estimates are considered more reliable since the deployment of the global radiosonde network in 1958 and satellite-derived rainfall estimates from the late 1970s (Garreaud et al., 2009). Consequently, the time period suitable for meaningful calibrations/validations using instrumental precipitation data is usually restricted to the second half of the 20th century (e.g. Morales et al., 2020). The validation period is, thus, the same as the calibration period of the tree rings and corals, which can be considered problematic. Unlike other climate field reconstruction techniques such as PCR (e.g. Neukom et al., 2010, 2011), PaleoDA with linear statistical PSMs does not strictly require the separation of calibration/validation data for two reasons. Firstly, the statistical PSM estimates regression parameters using local observational data, which are then applied to independent model simulation data. The model simulation data's mean and spatial covariances are not debiased with respect to the observational data, and thus importantly influence the reconstruction. In contrast, techniques like Point by Point regression (e.g. Morales et al., 2020) estimate a linear regression model for each reconstructed grid cell, resulting in more instrumentally tuned reconstructions. Secondly, the calibration process predicts proxy records from instrumental data, while the validation process predicts instrumental data from proxy records. This non-symmetry introduces information loss. Additionally, using multiple variables as predictors simultaneously in the reconstruction can potentially introduce errors through inadequate covariances in the prior.

As skill metrics, we choose the widely employed Pearson correlation and the Continuous Ranked Probability Skill Score (CRPSS) (Wilks, 2011). The correlation is a simple similarity metric with range $[-1, 1]$, which rewards a correct phasing of the reconstructed signal with respect to the observational data. In the correlation plots, we further denote significant correlations according to an effective p-value < 0.05. The effective p-value takes into account the smaller number of degrees of freedom in autocorrelated time series (Bretherton et al., 1999). Note, that, in a strict sense, correlations require detrended time series. We choose to not detrend the time series to also evaluate the skill of the reconstruction to capture trends, similar to previous PaleoDA reconstructions (e.g. Tardif et al., 2019; Steiger et al., 2018) In contrast, the CRPSS is considered a strictly proper scoring metric (Gneiting and Raftery, 2007) because it takes into account the posterior reconstruction distribution instead of the ensemble mean. We assume Gaussian statistics and, thus, characterize it via the ensemble mean and standard deviation. The CRPSS is the skill score version of the Continuous Ranked Probability Score (CRPS) and is computed as 1-CRPS$_{\text{rec}}$/CRPS$_{\text{ref}}$, where CRPS$_{\text{ref}}$ is the CRPS value for a reference distribution. CRPS rewards small biases, correct variances and ensemble

spread. For the reference CRPS score, we take the ensemble statistics of the uninformed prior ensemble as in Steiger et al. (2018). The CRPSS values lie in the range $(-\infty, 1]$, where positive values denote reconstructions more skillful than the prior.

1390 As the CRPSS values are computed for each validation time step, we compute the temporal mean of these values and denote them as CRPSS. Both metrics do not take observational uncertainties into account. For all skill scores, we have initially also considered applying a low-pass filter to the time series before applying the skill metrics, as we estimate our reconstruction to be more meaningful on longer than annual time scales. However, we have finally refrained from this idea as the validation period is pretty short (80 and 50 years) and for correlation, higher absolute correlations and effective p-values are expected due to the filtering introducing auto-correlation.
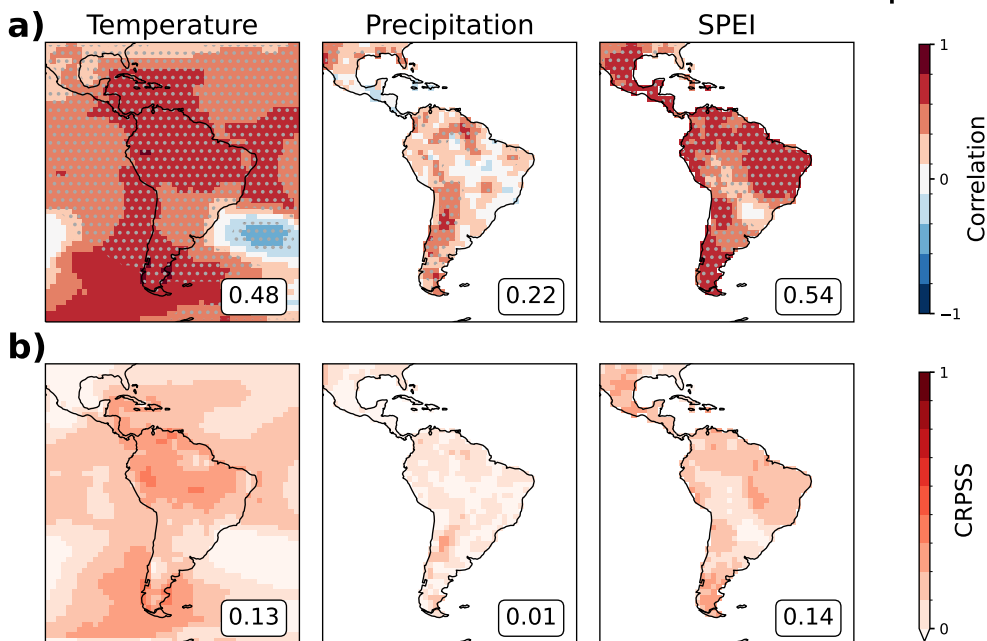
SF 3.1. Comparison to validation data sets over calibration period: validation skill metrics from comparing our reconstruction to the Berkeley Earth surface temperature dataset (Rohde and Hausfather, 2020) for the years 1920 - 2000 CE, the CRUTS 4 precipitation dataset (Harris et al., 2020b) for the years 1950 - 2000 CE and SPEI calculated using temperature and precipitation from the CRUTS 4 dataset for the years 1950 - 2000 CE. Precipitation skill is only evaluated on land as the instrumental dataset only provides precipitation over land. The panels in a) show the correlation with stippling indicating effective p-values smaller than 0.05. The panels in b) show the results for the CRPSS. The values in the lower right corner denote the mean skill score. See text for details. The spatial reconstruction skill for the reconstruction of austral summer (DJF) is displayed in Figure SF 3.2.

1395

Comparison to validation datasets over calibration period (DJF)
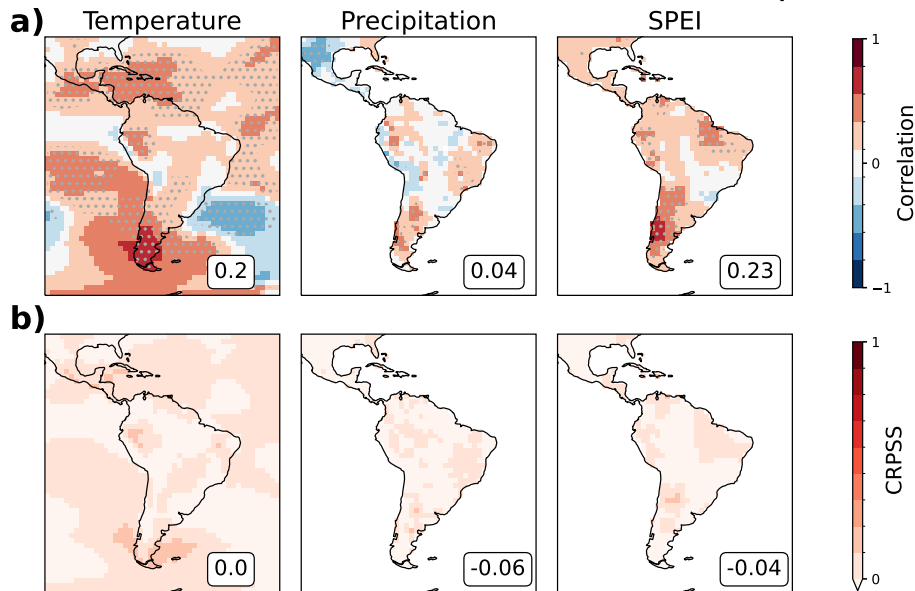
SF 3.2. Validation skill metrics from comparing our austral summer (DJF) reconstruction to instrumental data. See caption of Figure SF 3.1 for details.

Figure SF 3.1 shows the skill metric results for the annual reconstruction. Significant positive correlations are found for almost all terrestrial locations in the surface temperature and SPEI reconstruction (mean values 0.48 and ~~0.56), whereas for precipitation positive significant correlation is only found in the Andes and parts of northern and eastern South America (mean value 0.20)~~ 0.54). Due to the increasing temperature trend of the current warm period (CWP), such high correlations can be expected, also for SPEI, which depends on temperature via evapotranspiration. For precipitation ~~, we~~ positive significant correlations are mainly found in the Andes and parts of northern and eastern South America (mean value 0.22). We find the highest similarities close to the proxy record locations, in particular the Andes, which reflects the local character of precipitation changes and the lack of a clear trend in precipitation during the 20th century. CRPSS values for temperature and SPEI are mostly positive (mean 0.13 and ~~0.15~~0.14), whereas for precipitation positive values stay close to zero (mean ~~0.00~~0.01).

The skill metric values for the austral summer reconstruction (DJF) are shown in Figure SF 3.2. The values are consistently lower than for the annual means, with the highest similarity encountered for the Southern Cone. We suppose, that despite calibrating the tree rings and corals to austral summer means, their proxy record locations are less representative for the whole continent compared to annual means. In the presentation of the results, we thus focus on the annual reconstruction.

Note, that this type of 20th century validation mainly reflects the skill of reconstructing the continent's hydroclimate through tree proxy data, the most abundant annually dated climate archive in our database during the instrumental era. The speleothems, which are a key archive for reconstructing the entire past two millennia, are only used on a decadal time scale and thus only contribute very little to reconstructions during the 20th century. Moreover, the focus on our data analysis will lie on decadal

to centennial climate changes. The instrumental record is too short to validate the reconstructions skill on these time scales. Finally, it needs to be accounted that in most climate field reconstructions, the number of proxy records available in the validation/calibration period is usually order of magnitudes larger than in the preceding centuries. Hence, the obtained skill is not necessarily representative for the rest of the reconstruction period.

S3.2 Precipitation in the core monsoon region

A central aspect of this study consists of reconstructing the variability of the SASM according to the definition of Vuille et al. (2012), who proposed computing the mean precipitation in the core monsoon region (5°S–17.5°S/72.5°W–47.5°W, see black rectangle in Figure 1) as an indicator of monsoon strength. The SASM reaches its peak intensity during the austral summer months (DJF). Nevertheless, we focus on annual mean precipitation values in the core monsoon region for the validation, as we consider our annual reconstruction to be more reliable (see Section S3.1). Figure SF 3.4 shows the reconstructed mean precipitation anomaly in the core monsoon region compared to the values computed from the instrumental datasets CRUTS 4 (Harris et al., 2020b) and GPCC (Schneider et al., 2008) for the 20th century.

One important uncertainty in this type of validation is the inconsistency of different precipitation validation datasets, which is even more apparent when including the data from the 20CR reanalysis project (Compo et al., 2011)(SF 3.5). Computing the pointwise correlation between the datasets for the annual mean precipitation values (SF 3.3 highlights, that in the core monsoon region, the low density of meteorological stations also discussed in Section S3.1 leads to lower similarity compared to the rest of the continent.

It is apparent that our reconstruction does not capture short-term precipitation fluctuations and clearly underestimates precipitation variability for the short instrumental period, as it stays in the range of [-5,5] mm/month, whereas the instrumental data fluctuates in the range [-20,20] mm/month. The intensity of these fluctuations also shows considerable disagreement between the two instrumental datasets during the first half of the 20th century.

Table S3.1 presents the skill scores for the reconstructed monsoon index depending on whether all proxy records, only tree data, or all proxy records without the tree data is used. These scores have been computed for the calibration period, but also the entire 20th century. Overall, the skill scores are low and inconclusive. In contrast to what one would expect, the tree data, which is calibrated to instrumental temperature, precipitation, and SPEI data, yields the lowest skill scores. The tree data, which is mainly located in the central and southern Andes and thus outside the core monsoon region does not seem to be a good predictor for mean precipitation changes in the core monsoon region. This emphasizes the need to add precipitation sensitive proxies within, or at least closer to the core monsoon region. In our study, additional value is gained through the inclusion of speleothem records, but which are not highly resolved enough for a validation during the short instrumental period. This assessment emphasizes that the reconstructed precipitation changes likely do not accurately capture short-term variations in precipitation. We assume that the recorded changes are more likely to reflect long-term trends, which cannot be adequately validated due to the limited duration of instrumental data. Due to its limitations and despite its frequent use in PaleoDA, the instrumental validation exercise is thus not a proper tool for our reconstruction.

Correlations between different precipation datasets
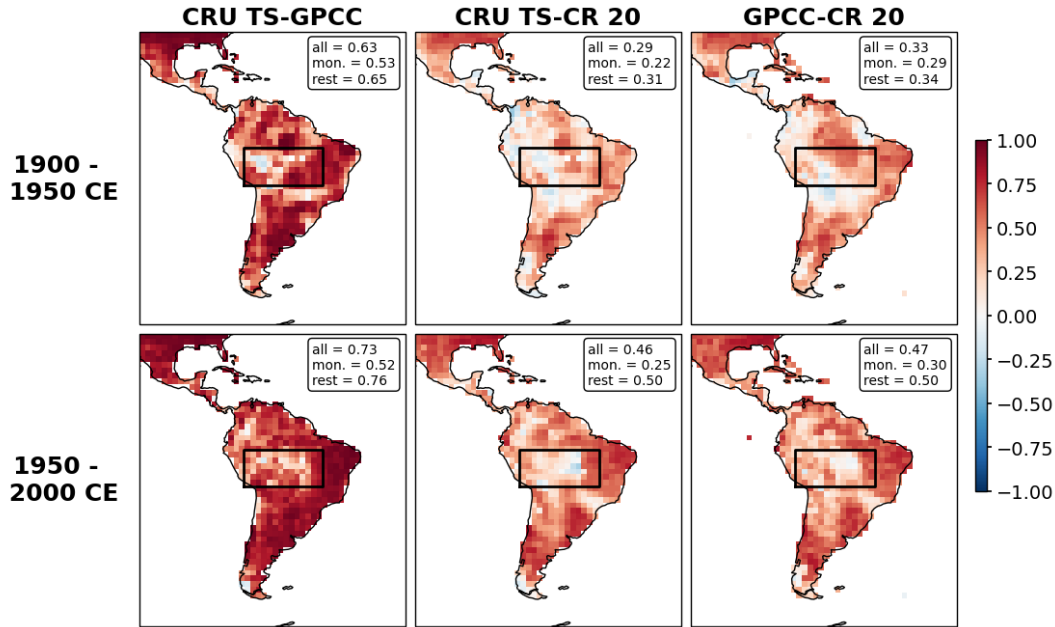
SF 3.3. Correlation of annual mean precipitation values in the CRU (Harris et al., 2020b), GPCC (Schneider et al., 2008) and 20CR (Compo et al., 2011) datasets. The correlation is computed separately for the period 1900-1950 CE, prior to the onset of radiosonde precipitation monitoring (1958), and for the second half of the 20th century. The inset box computes the average correlation for all grid cells (all), for the core monsoon region (mon.) and for all grid cells except the core monsoon region (rest).

		1950 - 2000 CE		1901 - 2000 CE	
		CRUTS 4	GPCC	CRUTS 4	GPCC
All proxy records	Corr	0.16 0.18	0.03 0.07	0.08 0.1	0.01 0.03
	CRPSS	-0.01	-0.04 -0.02	-0.04 -0.03	-0.03
Only trees	Corr	-0.06	-0.14	-0.10	-0.08
	CRPSS	-0.07	-0.06	-0.09	-0.05
No trees	Corr	0.18 0.20	0.10 0.11	0.15 0.18	0.08
	CRPSS	-0.05 -0.04	-0.07 -0.03	-0.05	-0.03

Table S3.1. Skill scores for the annual reconstruction of precipitation in the core monsoon region of the SASM during the 20th century with respect to CRUTS 4 (Harris et al., 2020b) and GPCC (Schneider et al., 2008). For the experiments of the first row, all proxy records have been used, in the second row only tree data has been employed and in the third row the tree data has been explicitly excluded. The correlation values are presented without effective p-values, as none was significant ($\alpha < 0.05$).
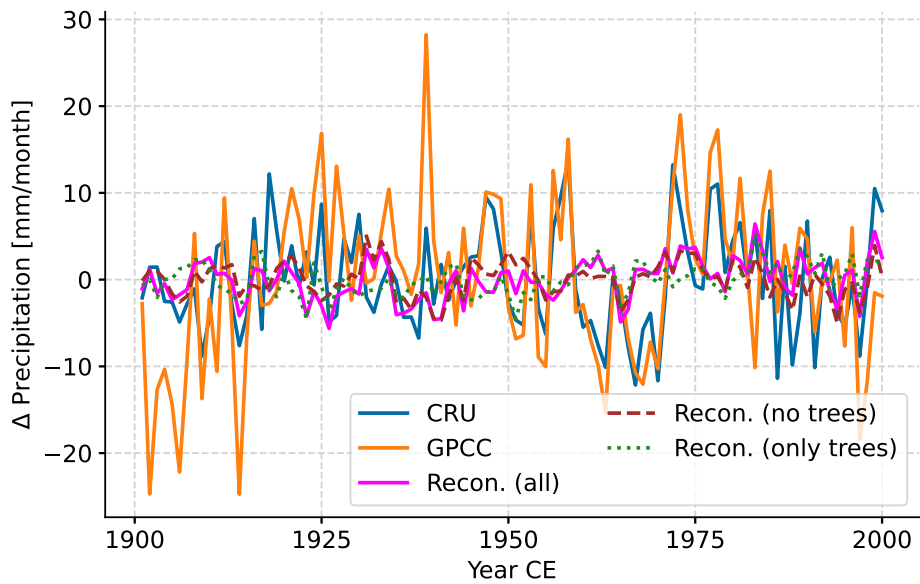
SF 3.4. Annual precipitation anomaly in the core monsoon region $(5° − 17.5°$ S $/ 72.5° − 47.5°$ W) for the years 1901 - 2000 CE in the CRUTS 4 and GPCC datasets and our reconstruction (including all proxy records). For all time series the mean of the period 1901 - 2000 CE was subtracted.
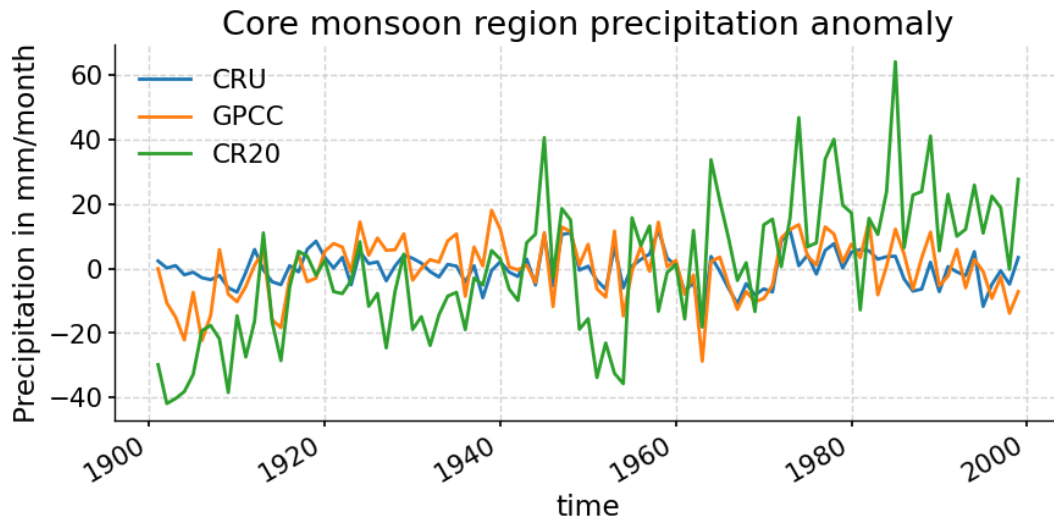
SF 3.5. Annual core monsoon region precipitation anomaly from CRU (Harris et al., 2020b), GPCC (Schneider et al., 2008) and 20CR (Compo et al., 2011)
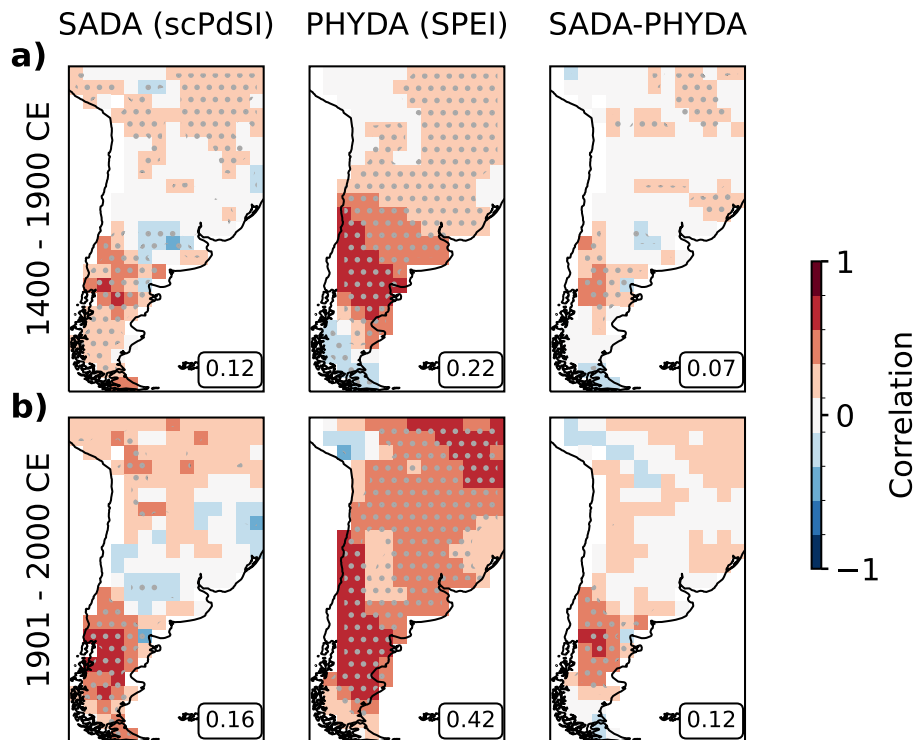
SF 3.6. Evaluation of correlation of the reconstructed annual SPEI to scPDSI from the SADA (Morales et al., 2020) and SPEI from the PHYDA (Steiger et al., 2018) (left and center panels). The right panel compares the correlation of scPDSI in SADA and PDSI in PHYDA. Grid cells with effective p-values <0.05 are indicated by stippling. The upper row (a) shows the correlation for the period 1400 - 1900 CE and the lower row (b) for the period 1901 - 2000 CE. The SADA and PHYDA datasets have been regridded to the spatial resolution of our reconstruction.

S3.3   Drought Index validation for the Southern Cone

A reference reconstruction of dry and wet conditions for Southern South America in the period 1400 - 2000 CE is the South American Drought Atlas (SADA) (Morales et al., 2020), whose input tree ring data is also partially employed our study. The SADA reconstructs the self-calibrated PDSI (scPDSI) using Point-by-Point Regression, a climate field reconstruction technique that is more calibrated towards local instrumental data. The SADA can be considered the most elaborate drought index reconstruction for the region. Although our reconstruction does not include scPDSI as a reconstructed variable, we compute the correlation to our reconstructed SPEI drought index to assess their similarity (Figure SF 3.4). Despite scPDSI and PDSI capturing different types of droughts, we expect similarity in the phasing of drier and wetter periods due to using similar input data. Additionally, the reconstructed SPEI is compared to the SPEI from the PHYDA reconstruction (Steiger et al., 2018),

1455 which also employs PaleoDA as a reconstruction technique using a subset of the SADA tree data. In PHYDA, where both SPEI and PDSI are reconstructed, both indices are highly correlated (not shown), we thus consider that in PHYDA both indices can be used interchangeably.

The largest similarity in terms of significant positive correlation for our reconstruction and SADA can be found close to the tree data locations in the Andes, especially Patagonia. The lowest similarity is found in the Pampas and the La Plata

1460 basin. Comparing the similarity of our reconstruction to SADA to the similarity of SADA and PHYDA, we find higher mean correlations than for PHYDA (0.12 vs 0.07 for the period 1400-1900 CE and ~~0.14~~ 0.16 vs 0.12 for the period 1901-2000 CE). The correlations between our reconstruction and PHYDA are ~~high~~ higher and spatially extensive for the entire Southern Cone (~~0.25 and 0.41~~ 0.22 and 0.42), except for southern Patagonia. This reflects that both employ the same reconstruction technique, and in part the same proxy and model data, as PHYDA is based on the CESM model, whose isotope-enabled version is also

1465 part of our multi-model ensemble.

Supplement S4.: Observation error estimation from the Signal-to-Noise Ratio (SNR)

We estimate the observation error variance $\mathbf{R}$ (Equation 2) for each proxy record from an assumed signal-to-noise ratio (SNR).

The SNR is defined as the ratio of the standard deviations of the unperturbed time series T and the white noise N:

$$\mathrm{SNR} := \frac{\mathrm{std}(T)}{\mathrm{std}(N)}$$

As the observation error variance $\mathbf{R}$ is by definition equal to the squared standard deviation of the noise N, we get for $\mathbf{R}$

$$\mathbf{R} = \mathrm{std}(N)^2 = \mathrm{var}(N)$$

$$\Rightarrow SNR = \frac{\mathrm{std}(T)}{\sqrt{\mathbf{R}}}$$

$$\Rightarrow \mathbf{R} = \frac{\mathrm{var}(T)}{SNR^2}$$

The variance of T is not known directly because the proxy record time series Y represents the noisy time series $T+N$, whose variance can be used to compute $\mathrm{var}(T)$. When assuming that N and T are uncorrelated, their variances are additive.

$$\mathrm{std}(T+N) = \sqrt{\mathrm{var}(T+N)}$$

$$= \sqrt{\mathrm{var}(T) + \mathrm{var}(N) + \mathrm{cov}(T,N)} = \sqrt{\mathrm{var}(T) + \mathrm{var}(N)}$$

$$= \sqrt{\mathrm{var}(T) + \mathbf{R}}$$

$$\Rightarrow \mathrm{var}(T) = \mathrm{var}(T+N) - \mathbf{R}$$

Using the relationship from equation S2.8 in equation S2.4 we get

$$\mathbf{R} = \frac{\mathrm{var}(T+N) - \mathbf{R}}{SNR^2}$$

$$\Rightarrow \mathbf{R} = \frac{\mathrm{var}(T+N)}{1+SNR^2} = \frac{\mathrm{var}(Y)}{1+SNR^2}$$

Using equation S3.1, the observation error $\mathbf{R}$ can be estimated from the variance of the proxy record time series and by assuming a specific SNR value for the proxy records, which does not need to be the same for all proxy records.

Supplement S4.: Proxy record lists

For an overview of all proxy records employed in this regional climate field reconstruction, the proxy records are grouped by climate archive type and presented in tabular form. In the *database* column, the proxy record databases from which the values were taken are named, in case the record is part of one. Additionally the original publications are cited in the *source* column. For the citations of proxy records that were part of a database, the reader is referred to the publications presenting the proxy

record databases. The level of detail in the tables varies by climate archive type, as the information from column with unique entries (e.g. the proxy variable, PSM type, Seasonality or SNR) has been transferred to explanatory text above the tables to limit the size of the tables. All data processing steps can be retraced and reproduced with the Jupyter Notebooks accompanying this publication.

S3.1 Speleothems

The proxy variables are $\delta^{18}O$ of aragonite and $\delta^{18}O$ of calcite for all processed speleothem time series. For all speleothems, the same *precipitation weighting*-type PSM has been used, thus rendering the application of some additional seasonality restrictions unnecessary. The SNR is computed from the variance of the time series by assuming the same SNR for all speleothems (See Section S2.2). Whereas the speleothem time series have relatively high median temporal resolutions, all time series are resampled to 10 years resolution to conservatively account for smoothing effects in the karst.

Supplement S4: Additional Result Figures

For caves with multiple records of similar resolution, composites were computed according to Novello et al. (2021) (step 2 and 3 in section 3.3) by applying the following steps to the time series of various records in one cave during the overlap period 1) resampling all proxy time series to annual resolution, 2) standardizing the time series (zero-mean & standard deviation equal to one) 3) computing the mean of the overlapping values 4) destandardizing the mean time series using the mean and standard deviation of the time series which is longer. Further steps detailed in section 3.3 of Novello et al. (2021) are not applied, as these involve age model ensembles, which have not been used in this study. The practical computation of speleothem composites can be retraced in the Jupyter Notebooks accompanying this publication.

Mean anomaly fields (Figure 3) for austral summer reconstruction

Speleothem proxy records description table

SF 4.1. Same as Figure 3 for the austral summer (DJF) reconstruction. Stippling indicates grid cells where the difference to the Last Millennium values is not significant according to a Welch's t-test ($\alpha > 0.01$).

Mean anomaly fields (Figure 3) for reconstruction with different proxy error definition
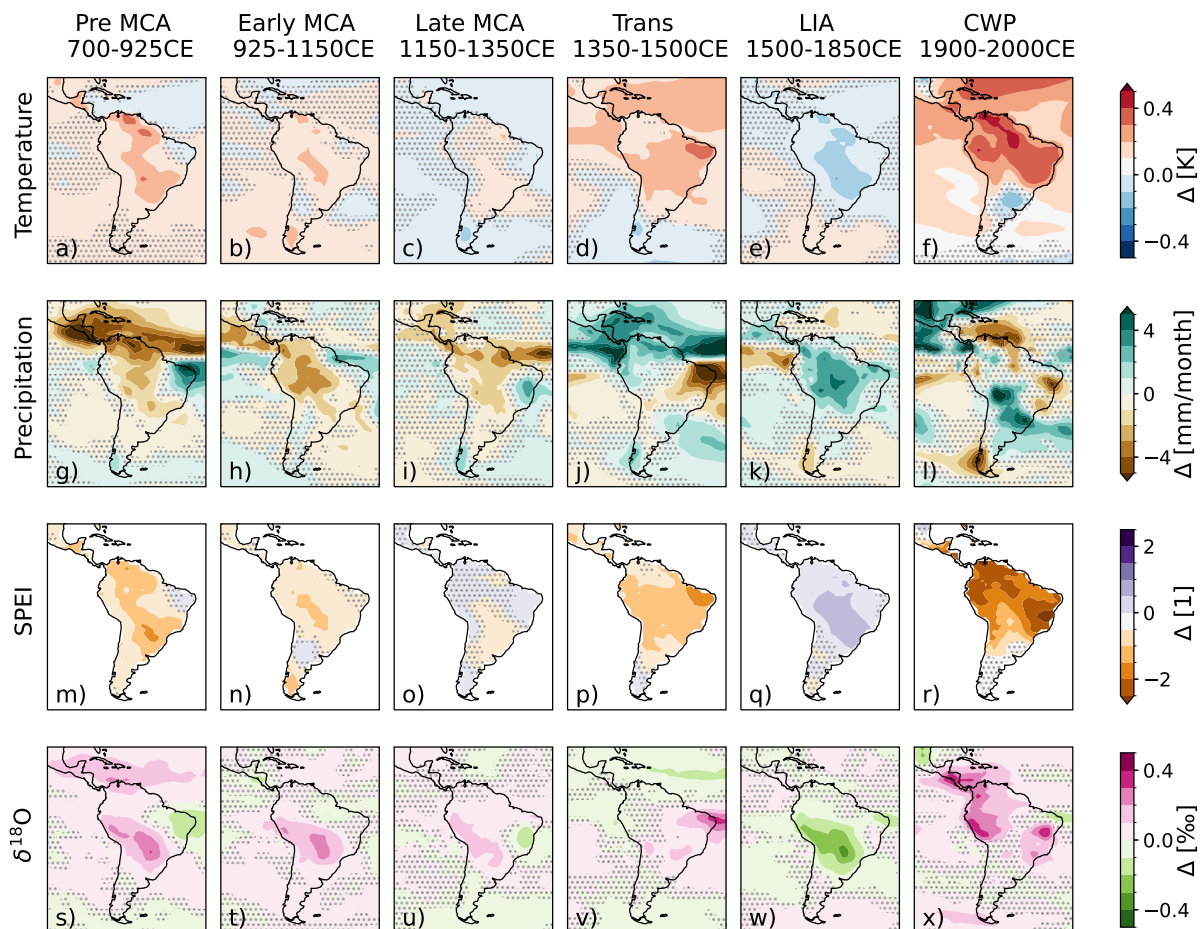
SF 4.2. Same as Figure 3 applying a proxy error variance equal to the prior variance instead of the SNR=0.5 proxy error definition. Stippling indicates grid cells where the difference to the Last Millennium values is not significant according to a Welch's t-test ($\alpha > 0.01$).

S4.1 ~~Lake sediment records~~

~~Only lake sediment records directly related to the isotopic composition of precipitation (and thus not mostly affected by additional evaporation) or already calibrated to temperature have been included. To make this distinction, the original publications have been consulted and records have been accordingly selected. This restriction excluded most lake sediment records available in the Iso2k database (Konecky et al., 2020). All lake sediment records are used on a time scale of five years, to account for the effect of bioturbation in the sedimentation process. For all lake sediments, the same SNR value has been assumed, also for temperature calibrated records which come with an error variance.~~

1515

1520 **Mean anomaly fields (Figure 3) for reconstruction only using speleothem proxy records**
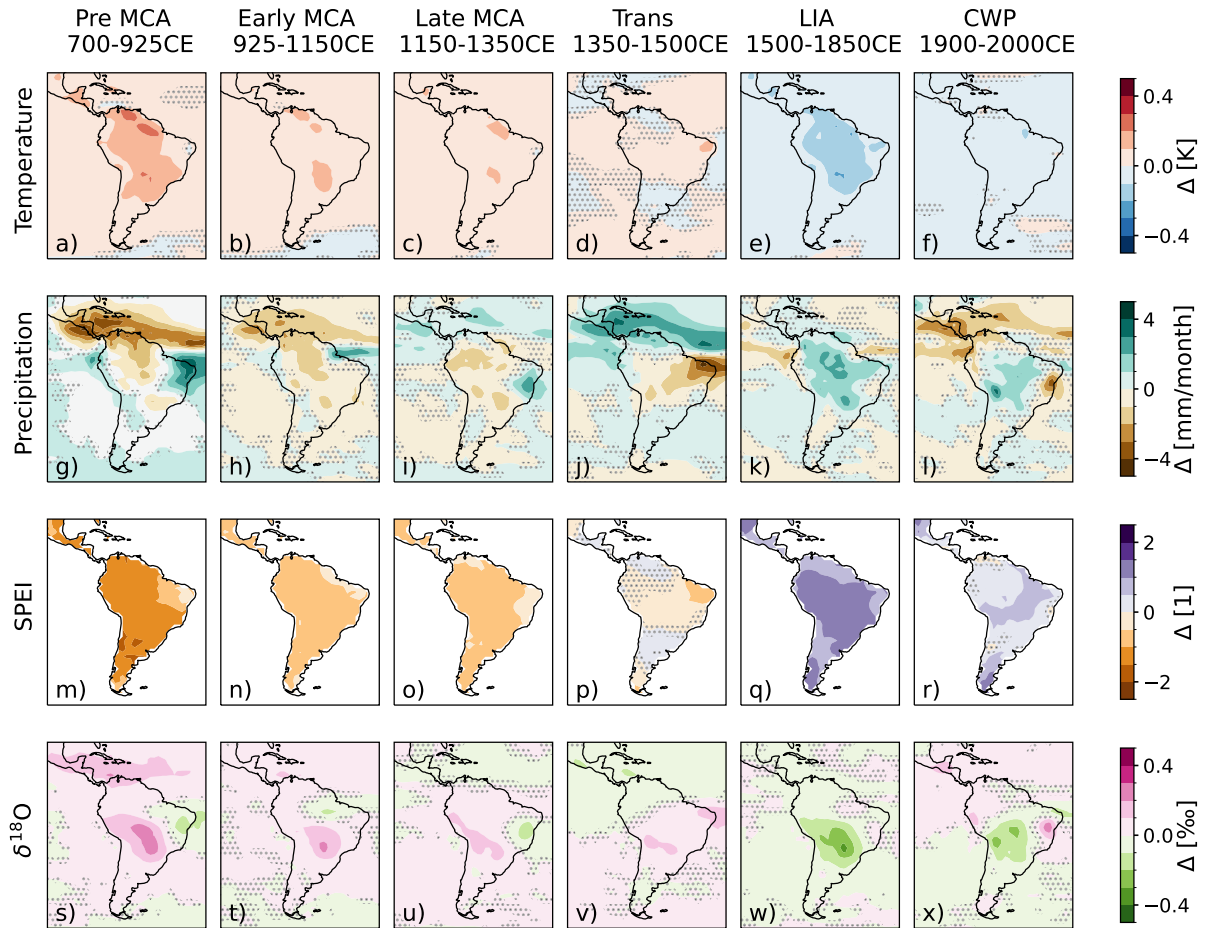
SF 4.3. Same as Figure 3 but for the reconstruction that only uses speleothems as proxy record input data. Stippling indicates grid cells where the difference to the Last Millennium values is not significant according to a Welch's t-test ($\alpha > 0.01$).

S4.1 ~~Sclerosponge~~
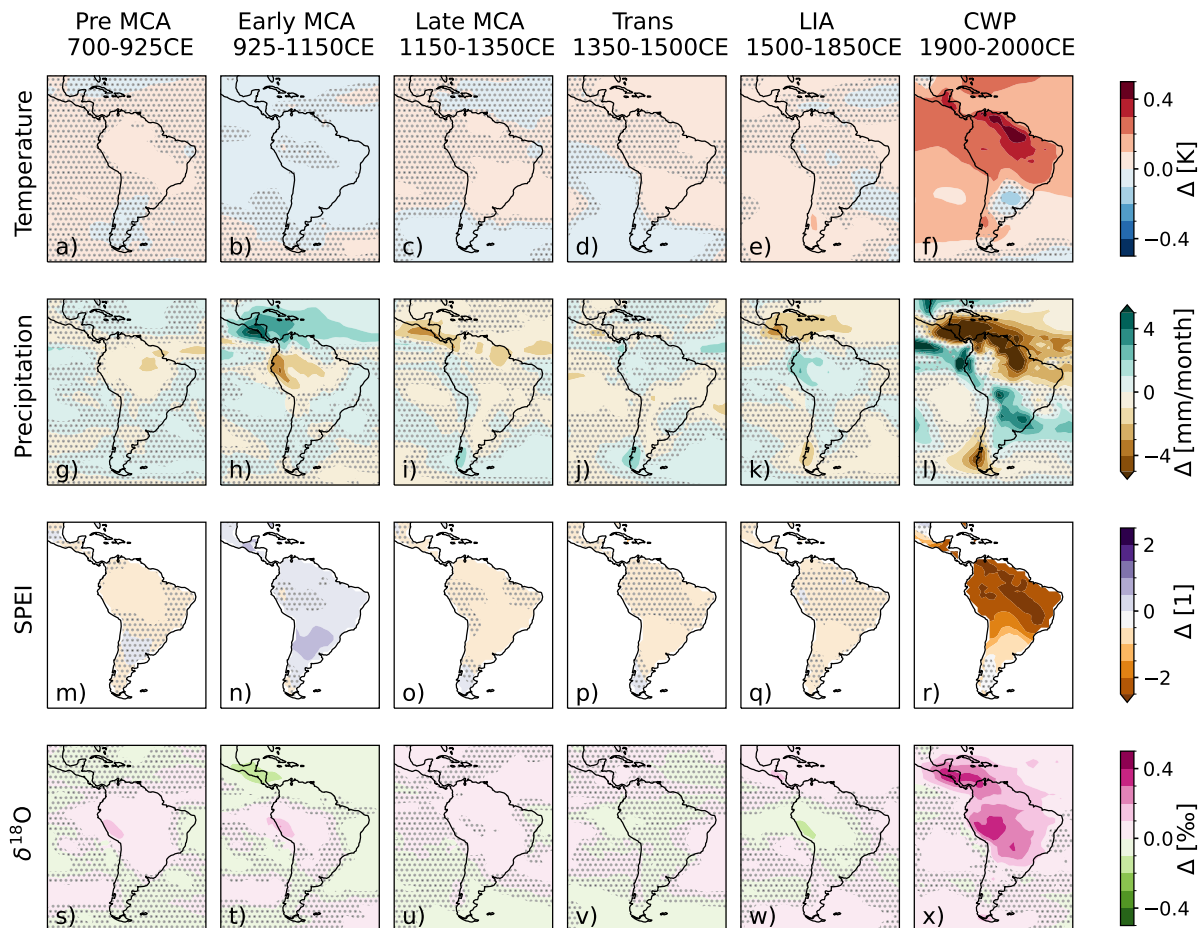
SF 4.4. Same as Figure 3 but for the reconstruction that uses all proxy records except the speleothems as proxy record input data. Stippling indicates grid cells where the difference to the Last Millennium values is not significant according to a Welch's t-test ($\alpha > 0.01$).

For the conversion of the sclerosponge values from Montego Bay, Jamaica, to temperature, the formula presented in Haase-Schramm et al. (2003) was used. From the two provided records, we selected the record which was located closer the sea surface (see original publication for details). The time series values were resampled to five years to account for the non-annual resolution of the record.

Additional SASM index figures

S4.1 Marine sediment

The Cariaco Basin record from Black et al. (2007) was the only marine sediment included in our regional climate field reconstruction, as other marine sediment from South and Central America only provide a longer than decadal resolution. Due to the exceptionally high sedimentation rate in the Cariaco Basin, the record was treated as an annual record according to its temporal resolution.

Anomalies in the core monsoon region (DJF mean)
(5°S–17.5°S/72.5°W–47.5°W)
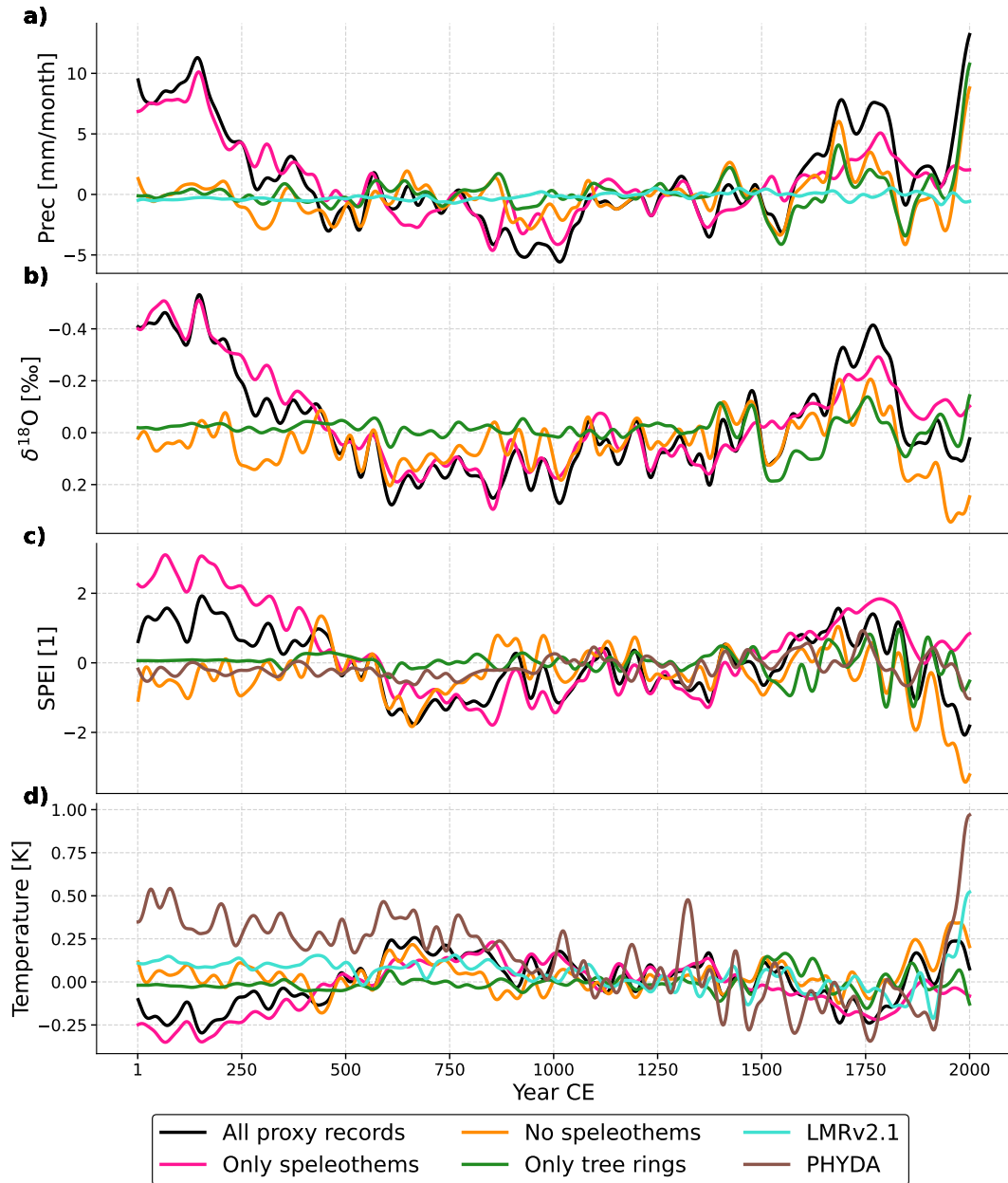
SF 4.5. Same as Figure 4 for the austral summer (DJF) reconstruction with extended y-axes ranges. The PHYDA reconstruction displayed here is a specific austral summer reconstruction, whereas LMRv2.1 is only provided at an annual time scale.
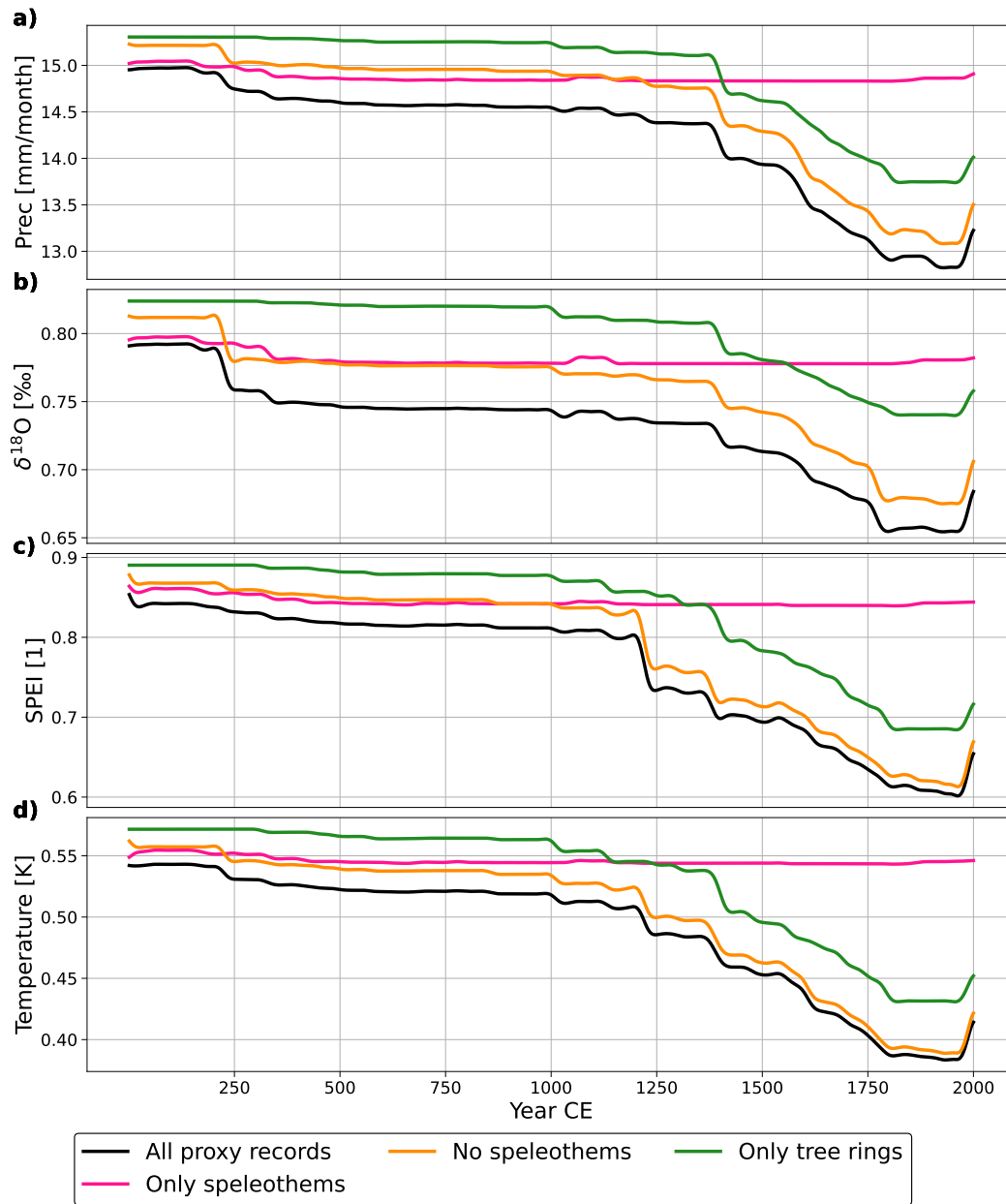
SF 4.6. Reconstruction uncertainty for the indices from Figure 4 defined as the standard deviation of the posterior ensemble. Here, we display the mean of the standard deviations of the five single model reconstructions, although also other multi-model ensemble error definitions in terms of the propagation of uncertainty are conceivable.
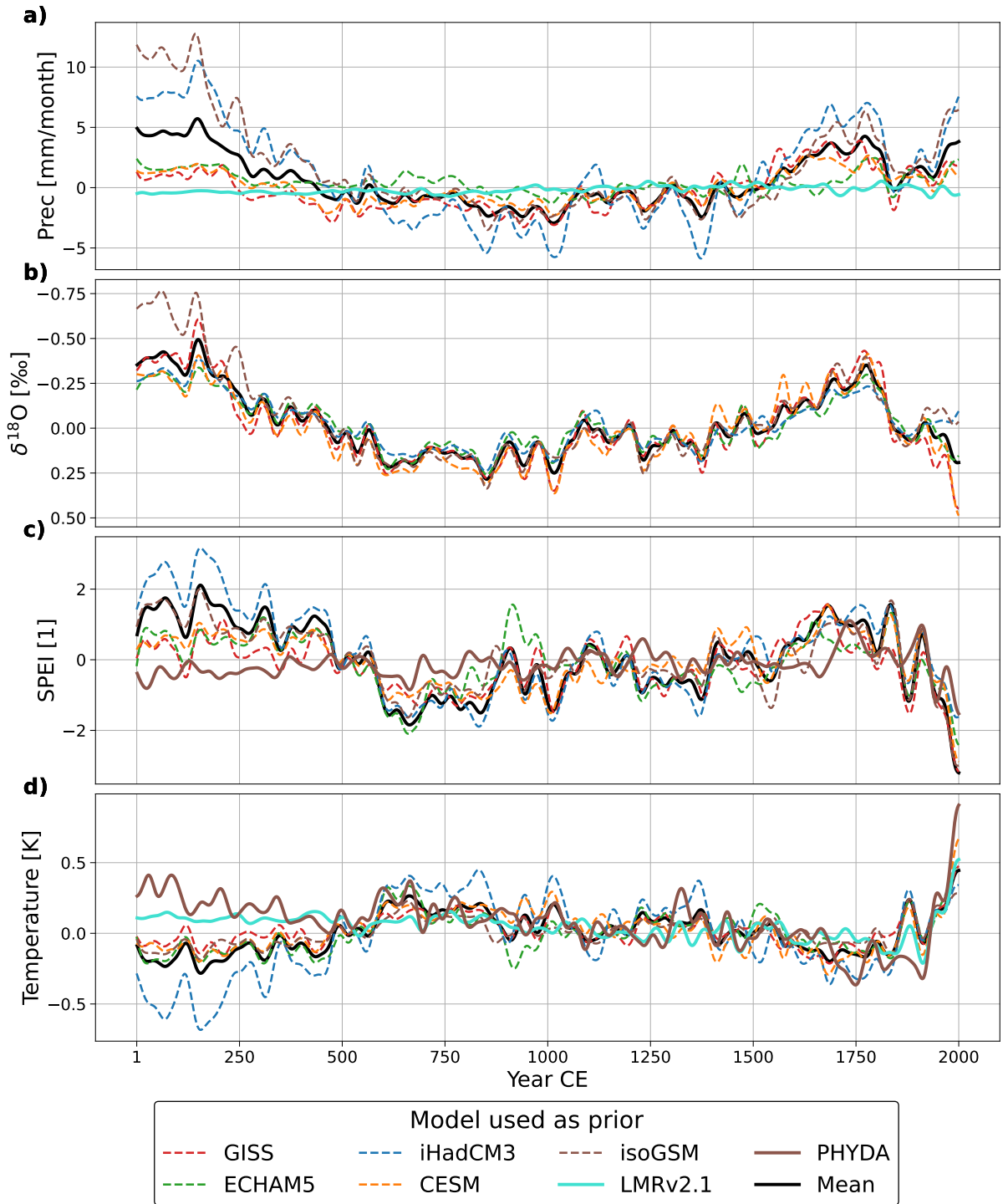
SF 4.7. ~~Sclerosponge~~ Same as Figure 4 including the single model reconstructions using all proxy ~~record description table~~ records (dotted lines). The black line is the multi-model ensemble reconstruction (mean of single prior reconstructions).

Anomalies in the core monsoon region
(5°S–17.5°S/72.5°W–47.5°W)
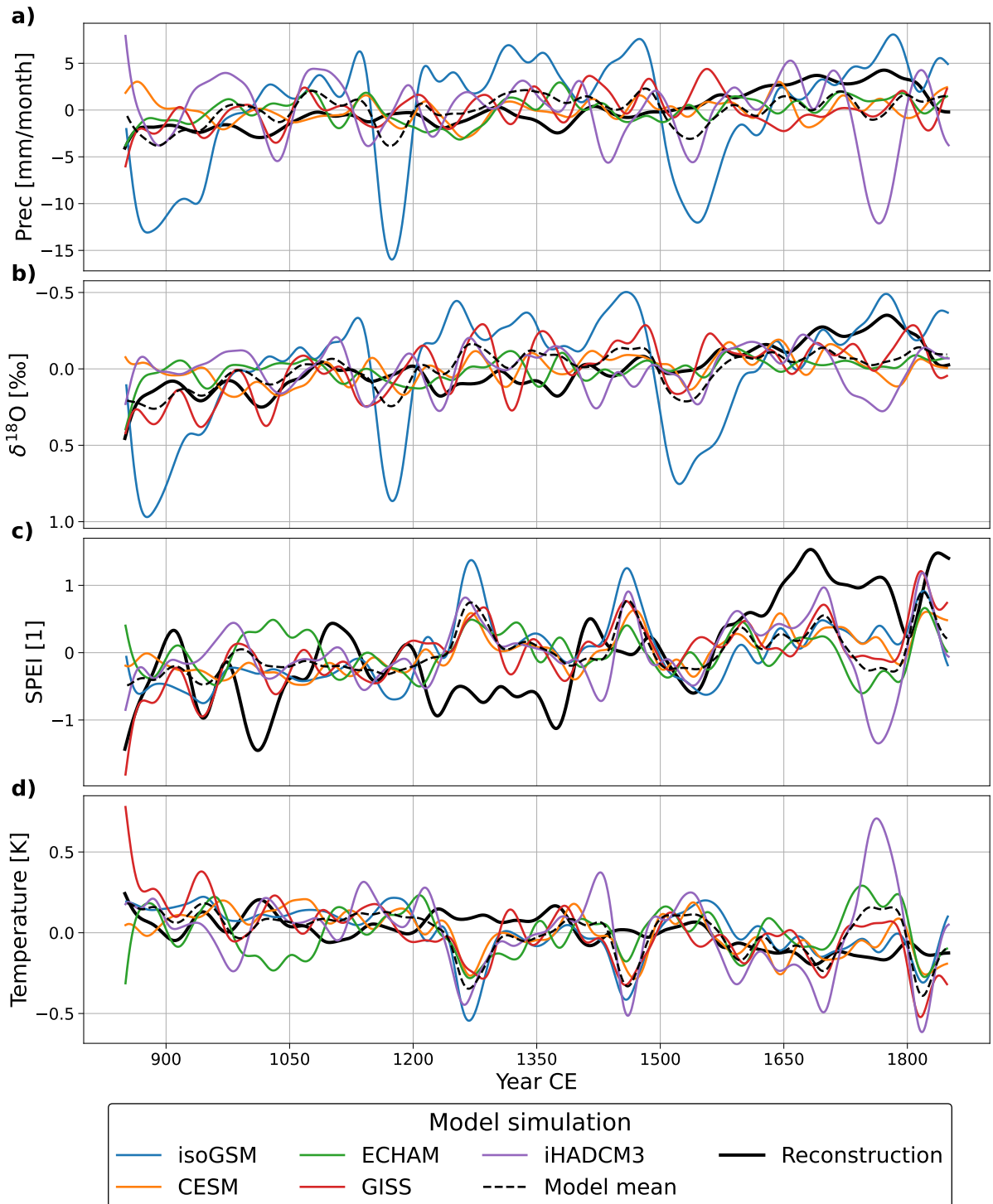
SF 4.8. Same as Figure 4 for the *all proxies* reconstruction and the model simulations. The time period has been limited to the period 850-1850 CE as this is the time span covered by the model simulations.

Additional power spectra

S4.1 Ice cores
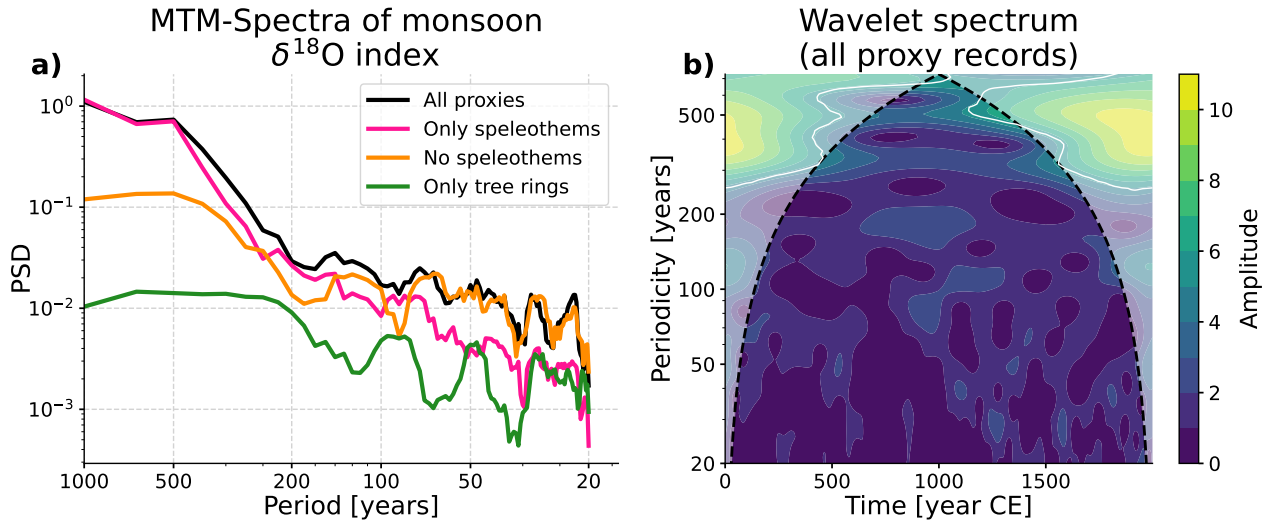
SF 4.9. **Spectra of reconstructed monsoon** δ^{18}**O index**. See description of Figure 6.

1535 ~~For all ice core δ^{18}O record locations, the precipitation weighting PSM has been applied, rendering the definition of a seasonality unnecessary. For all ice core proxy records, an SNR value was assumed to compute the error variance.~~

SF 4.10. Spectra of SASM indices in model simulations. The spectra for SASM precipitation and δ^{18}O have been computed as in Figure 6, but limited to the period 850-1850 CE, because this is the time period covered by the model simulations. In addition, all time series have been standardized, as the model simulations have more overall variability (higher variance). Standardizing the time series allows to highlight the different scaling of the simulation and reconstruction spectra.

SF 4.11. ~~Ice core proxy records description table~~Same Anomaly Fields as Figure 3 for the PHYDA reconstruction (Steiger et al., 2018), which includes temperature and SPEI among its reconstructed variables, but not precipitation and $\delta^{18}O$. Stippling indicates grid cells where the difference to the Last Millennium values is not significant according to a Welch's t-test ($\alpha > 0.01$).

SF 4.12. Same Anomaly Fields as Figure 3 for the LMRv2.1 reconstruction (Tardif et al., 2019), which includes temperature and precipitation among its reconstructed variables, but not SPEI and $\delta^{18}O$. Stippling indicates grid cells where the difference to the Last Millennium values is not significant according to a Welch's t-test ($\alpha > 0.01$).

S4.1 ~~Corals~~

Correlations in the model simulations (prior) for NEB

1540 ~~All coral proxy records were used on an annual time scale. For the PSM, the linear PSM for temperature was used, thus all records were calibrated to temperature. Calibration values (including SNR estimates) were calculated for the annual and seasonal reconstruction/calibration separately.~~

~~Coral proxy records description table~~

Correlation to δ^{18}O
in North Eastern Brazil
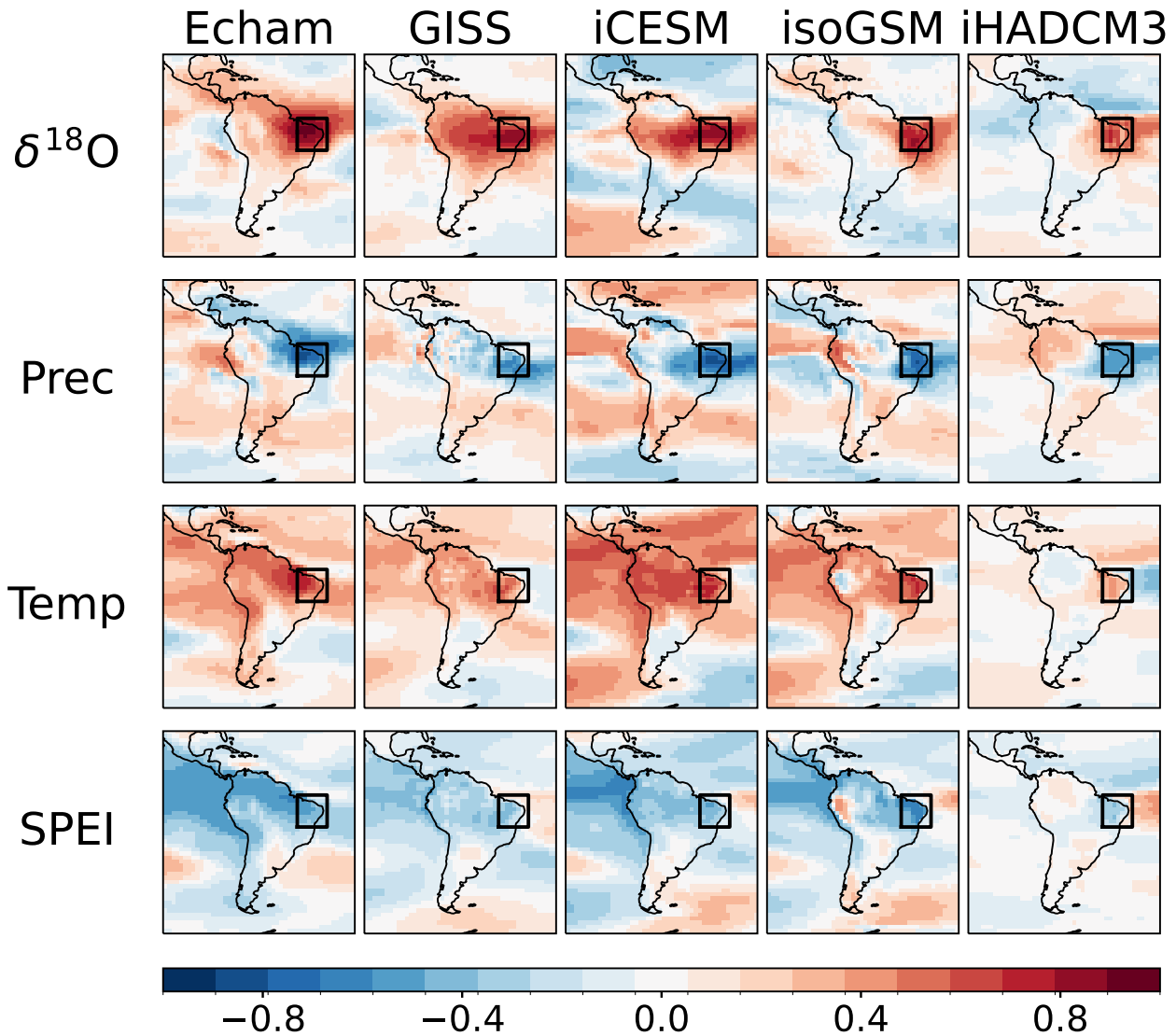
SF 4.13. **Correlation of δ^{18}O mean in the Nordeste** (black box, Lat: -15-0°, Lon: 313-327°) to climate variables δ^{18}O, precipitation, temperature and SPEI of individual grid cells in the five isotope-enabled climate model simulations. The correlations have been computed with the annual mean values of the simulated climate variables.

1545   **S4.1**   ~~Trees~~
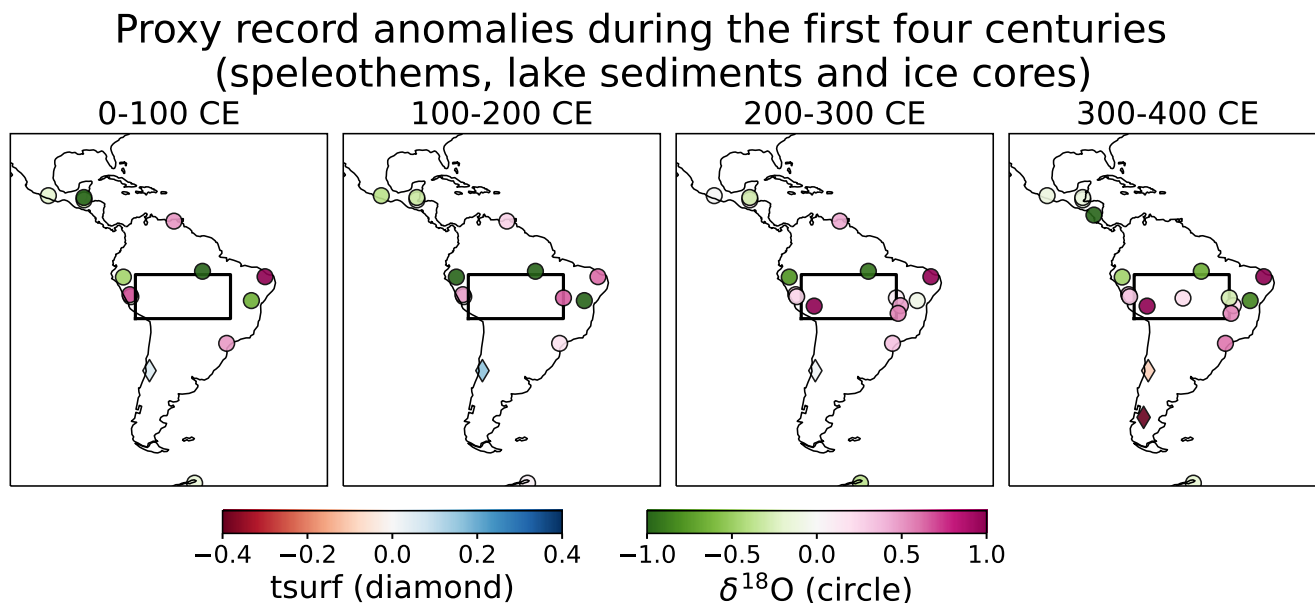
SF 4.14. Proxy record anomalies during the first four centuries of the CE with respect to the Last Millennium mean.

~~The employed tree records are described solely in text form rather than tabular format due to their large quantity. The proxy data from trees was mainly taken from three proxy record databases according to the selection criteria outlined in the main text. This selection resulted in 203 tree proxy time series from the South American Drought Atlas (Morales et al., 2020), 42 from Breitenmoser et al. (2014), as used in and published alongside Steiger et al. (2014), and 5 records from the Pages2k database (Emile-Geay et al., 2017). We checked for potential overlaps between these proxy databases and excluded double/triple records. As the SADA database only extends back to 1400CE, six records from it have been replaced by the longer original record data which are available in the NOAA database (see code of this publication for exact documentation). All these data bases use tree ring width as a proxy from trees, and not Maximum Wood Density (MXD). In addition to these tree ring data sources, we used four single records/tree ring composites , namely from the central Altiplano (Morales et al., 2012), the northern altiplano (Morales et al., 2023), the western Amazon (Humanes-Fuente et al., 2020) and near the Perito Moreno glacier in Patagonia (Grießinger et al., 2018). For this last tree proxy record, the proxy variable is δ^{18}O in wood and not tree ring width, but this record has also been calibrated to instrumental variables as all other tree ring records, because precipitation δ^{18}O can not be directly related to δ^{18}O in wood. No seasonality restriction was imposed for using the data as the calibration to instrumental variables for the linear PSM was computed for the annual and summer season separately. All used tree records have annual resolution.~~

Correlation to SASM precipitation
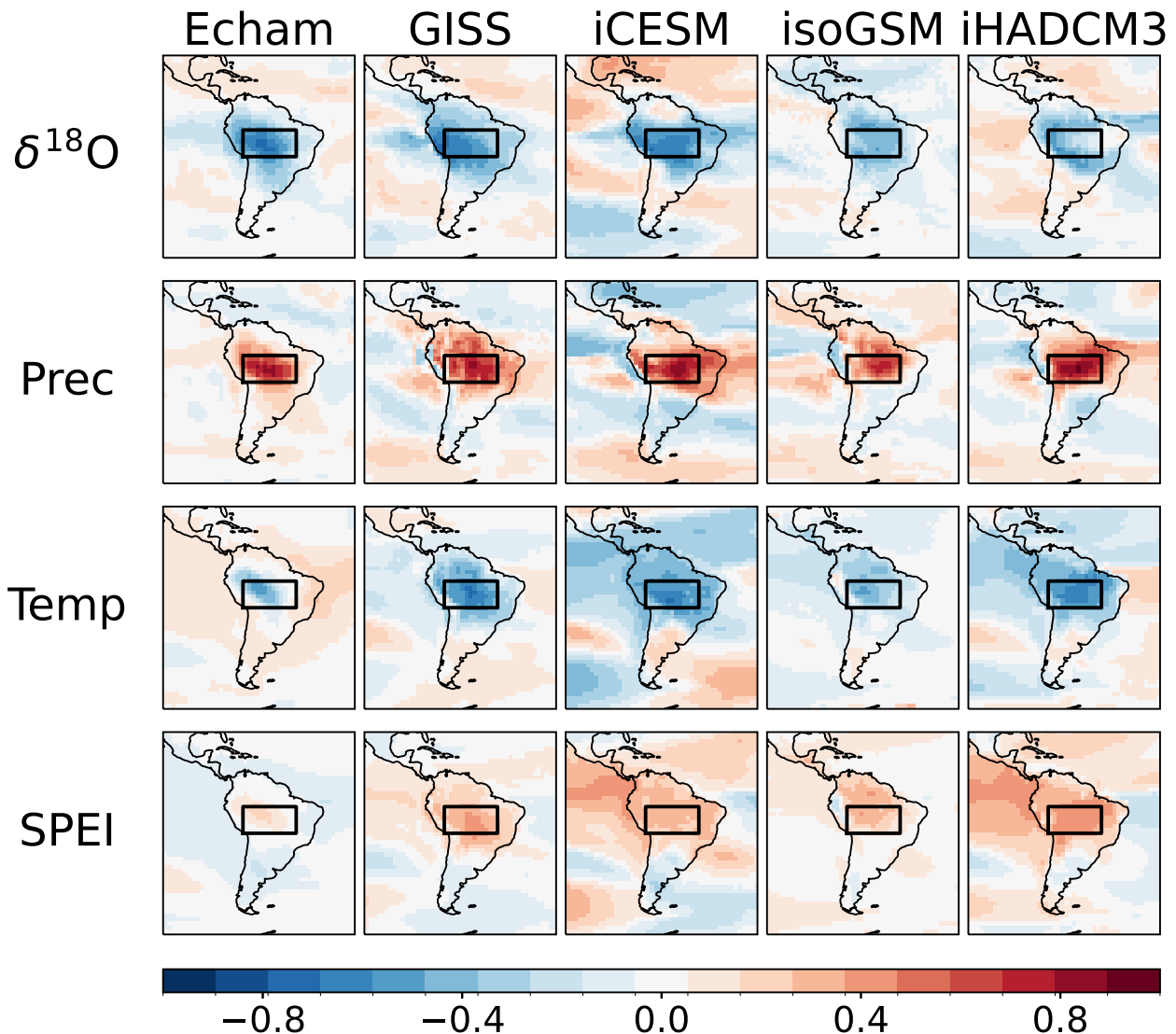
SF 4.15. Correlation of precipitation mean in core SASM region (black box, Lat: -17.5 - -5°, Lon: 287.5-312.5°) to climate variables $\delta^{18}O$, precipitation, temperature and SPEI of individual grid cells in the five isotope-enabled climate model simulations. The correlations have been computed with the annual mean values of the simulated climate variables.

Supplement: References

Abram, N. J., Mulvaney, R., Wolff, E. W., Triest, J., Kipfstuhl, S., Trusel, L. D., Vimeux, F., Fleet, L., and Arrowsmith, C.: Acceleration of snow melt in an Antarctic Peninsula ice core during the twentieth century, Nature Geoscience, 6, 404–411, https://doi.org/10.1038/ngeo1787, 2013.

Aceituno, P., del Rosario Prieto, M., Solari, M. E., Martínez, A., Poveda, G., and Falvey, M.: The 1877–1878 El Niño episode: associated impacts in South America, Climatic Change, 92, 389–416, https://doi.org/10.1007/s10584-008-9470-5, 2008.

Adams, J.: climate indices, an open source Python library providing reference implementations of commonly used climate indices, https://github.com/monocongo/climate_indices, 2017.

Akers, P. D., Brook, G. A., Railsback, L. B., Liang, F., Iannone, G., Webster, J. W., Reeder, P. P., Cheng, H., and Edwards, R. L.: An extended and higher-resolution record of climate and land use from stalagmite MC01 from Macal Chasm, Belize, revealing connections between major dry events, overall climate variability, and Maya sociopolitical changes, Palaeogeography, Palaeoclimatology, Palaeoecology, 459, 268–288, https://doi.org/10.1016/j.palaeo.2016.07.007, 2016.

Ampuero, A., Stríkis, N. M., Apaéstegui, J., Vuille, M., Novello, V. F., Espinoza, J. C., Cruz, F. W., Vonhof, H., Mayta, V. C., Martins, V. T. S., Cordeiro, R. C., Azevedo, V., and Sifeddine, A.: The Forest Effects on the Isotopic Composition of Rainfall in the Northwestern Amazon Basin, Journal of Geophysical Research: Atmospheres, 125, https://doi.org/10.1029/2019jd031445, 2020.

Anchukaitis, K. J. and Smerdon, J. E.: Progress and Uncertainties in Global and Hemispheric Temperature Reconstructions of the Common Era, Quaternary Science Reviews, 286, 107 537, https://doi.org/10.1016/j.quascirev.2022.107537, 2022.

Annan, J. D., Hargreaves, J. C., and Mauritsen, T.: A New Global Surface Temperature Reconstruction for the Last Glacial Maximum, Climate of the Past, 18, 1883–1896, https://doi.org/10.5194/cp-18-1883-2022, 2022.

Apaéstegui, J., Cruz, F. W., Sifeddine, A., Vuille, M., Espinoza, J. C., Guyot, J. L., Khodri, M., Strikis, N., Santos, R. V., Cheng, H., Edwards, L., Carvalho, E., and Santini, W.: Hydroclimate Variability of the Northwestern Amazon Basin near the Andean Foothills of Peru Related to the South American Monsoon System during the Last 1600 Years, Climate of the Past, 10, 1967–1981, https://doi.org/10.5194/cp-10-1967-2014, 2014.

Apaéstegui, J., Cruz, F. W., Vuille, M., Fohlmeister, J., Espinoza, J. C., Sifeddine, A., Strikis, N., Guyot, J. L., Ventura, R., Cheng, H., and Edwards, R. L.: Precipitation Changes over the Eastern Bolivian Andes Inferred from Speleothem (δ18O) Records for the Last 1400 Years, Earth and Planetary Science Letters, 494, 124–134, https://doi.org/10.1016/j.epsl.2018.04.048, 2018.

Atsawawaranunt, K., Comas-Bru, L., Amirnezhad Mozhdehi, S., Deininger, M., Harrison, S. P., Baker, A., Boyd, M., Kaushal, N., Ahmad, S. M., Ait Brahim, Y., Arienzo, M., Bajo, P., Braun, K., Burstyn, Y., Chawchai, S., Duan, W., Hatvani, I. G., Hu, J., Kern, Z., Labuhn, I., Lachniet, M., Lechleitner, F. A., Lorrey, A., Pérez-Mejías, C., Pickering, R., Scroxton, N., and SISAL Working Group Members: The SISAL Database: A Global Resource to Document Oxygen and Carbon Isotope Records from Speleothems, Earth System Science Data, 10, 1687–1713, https://doi.org/10.5194/essd-10-1687-2018, 2018.

Ault, T. R., Cole, J. E., and St. George, S.: The amplitude of decadal to multidecadal variability in precipitation simulated by state-of-the-art climate models, Geophysical Research Letters, 39, https://doi.org/10.1029/2012gl053424, 2012.

Azevedo, V., Stríkis, N. M., Santos, R. A., de Souza, J. G., Ampuero, A., Cruz, F. W., de Oliveira, P., Iriarte, J., Stumpf, C. F., Vuille, M., Mendes, V. R., Cheng, H., and Edwards, R. L.: Medieval Climate Variability in the Eastern Amazon-Cerrado Regions and Its Archeological Implications, Scientific Reports, 9, 20 306, https://doi.org/10.1038/s41598-019-56852-7, 2019.

Bakker, P., Goosse, H., and Roche, D. M.: Internal climate variability and spatial temperature correlations during the past 2000 years, Climate of the Past, 18, 2523–2544, 2022.

Beguería, S., Vicente-Serrano, S. M., Reig, F., and Latorre, B.: Standardized Precipitation Evapotranspiration Index (SPEI) Revisited: Parameter Fitting, Evapotranspiration Models, Tools, Datasets and Drought Monitoring, International Journal of Climatology, 34, 3001–3023, https://doi.org/10.1002/joc.3887, 2014.

Bernal, J., Cruz, F. W., Stríkis, N. M., Wang, X., Deininger, M., Catunda, M. C. A., Ortega-Obregón, C., Cheng, H., Edwards, R. L., and Auler, A. S.: High-resolution Holocene South American monsoon history recorded by a speleothem from Botuverá Cave, Brazil, Earth and Planetary Science Letters, 450, 186–196, https://doi.org/10.1016/j.epsl.2016.06.008, 2016.

Bhend, J., Franke, J., Folini, D., Wild, M., and Brönnimann, S.: An Ensemble-Based Approach to Climate Reconstructions, Climate of the Past, 8, 963–976, https://doi.org/10.5194/cp-8-963-2012, 2012.

Bird, B. W., Abbott, M. B., Rodbell, D. T., and Vuille, M.: Holocene Tropical South American Hydroclimate Revealed from a Decadally Resolved Lake Sediment δ18O Record, Earth and Planetary Science Letters, 310, 192–202, https://doi.org/10.1016/j.epsl.2011.08.040, 2011a.

Bird, B. W., Abbott, M. B., Vuille, M., Rodbell, D. T., Stansell, N. D., and Rosenmeier, M. F.: A 2,300-Year-Long Annually Resolved Record of the South American Summer Monsoon from the Peruvian Andes, Proceedings of the National Academy of Sciences, 108, 8583–8588, https://doi.org/10.1073/pnas.1003719108, 2011b.

Bishop, C. H., Etherton, B. J., and Majumdar, S. J.: Adaptive Sampling with the Ensemble Transform Kalman Filter. Part I: Theoretical Aspects, Monthly Weather Review, 129, 420–436, https://doi.org/10.1175/1520-0493(2001)129<0420:ASWTET>2.0.CO;2, 2001.

Black, D. E., Abahazi, M. A., Thunell, R. C., Kaplan, A., Tappa, E. J., and Peterson, L. C.: An 8-Century Tropical Atlantic SST Record from the Cariaco Basin: Baseline Variability, Twentieth-Century Warming, and Atlantic Hurricane Frequency, Paleoceanography, 22, https://doi.org/10.1029/2007PA001427, 2007.

Boës, X. and Fagel, N.: Relationships between Southern Chilean Varved Lake Sediments, Precipitation and ENSO for the Last 600 Years, Journal of Paleolimnology, 39, 237–252, https://doi.org/10.1007/s10933-007-9119-9, 2008.

Boucher, É., Guiot, J., and Chapron, E.: A Millennial Multi-Proxy Reconstruction of Summer PDSI for Southern South America, Climate of the Past, 7, 957–974, https://doi.org/10.5194/cp-7-957-2011, 2011.

Bradley, R.: Paleoclimatology. Reconstructing Climates of the Quaternary., Elsevier, 2015.

Brady, E., Stevenson, S., Bailey, D., Liu, Z., Noone, D., Nusbaumer, J., Otto-Bliesner, B. L., Tabor, C., Tomas, R., Wong, T., Zhang, J., and Zhu, J.: The Connected Isotopic Water Cycle in the Community Earth System Model Version 1, Journal of Advances in Modeling Earth Systems, 11, 2547–2566, https://doi.org/10.1029/2019MS001663, 2019.

Breitenmoser, P., Brönnimann, S., and Frank, D.: Forward Modelling of Tree-Ring Width and Comparison with a Global Network of Tree-Ring Chronologies, Climate of the Past, 10, 437–449, https://doi.org/10.5194/cp-10-437-2014, 2014.

Bretherton, C. S., Widmann, M., Dymnikov, V. P., Wallace, J. M., and Bladé, I.: The Effective Number of Spatial Degrees of Freedom of a Time-Varying Field, Journal of Climate, 12, 1990–2009, https://doi.org/10.1175/1520-0442(1999)012<1990:TENOSD>2.0.CO;2, 1999.

Bühler, J. C., Roesch, C., Kirschner, M., Sime, L., Holloway, M. D., and Rehfeld, K.: Comparison of the Oxygen Isotope Signatures in Speleothem Records and iHadCM3 Model Simulations for the Last Millennium, Preprint, Climate Modelling/Terrestrial Archives/Centennial-Decadal, https://doi.org/10.5194/cp-2020-121, 2020.

Bühler, J. C., Roesch, C., Kirschner, M., Sime, L., Holloway, M. D., and Rehfeld, K.: Comparison of the Oxygen Isotope Signatures in Speleothem Records and iHadCM3 Model Simulations for the Last Millennium, Climate of the Past, 17, 985–1004, https://doi.org/10.5194/cp-17-985-2021, 2021.

Bühler, J. C., Axelsson, J., Lechleitner, F. A., Fohlmeister, J., LeGrande, A. N., Midhun, M., Sjolte, J., Werner, M., Yoshimura, K., and Rehfeld, K.: Investigating Stable Oxygen and Carbon Isotopic Variability in Speleothem Records over the Last Millennium Using Multiple Isotope-Enabled Climate Models, Climate of the Past, 18, 1625–1654, https://doi.org/10.5194/cp-18-1625-2022, 2022.

Bühler, J. C., Axelsson, J., Rehfeld, K., LeGrande, A. N., Midhun, M., Sjolte, J., Werner, M., and Yoshimura, K.: Monthly climate variables of isotope-enabled climate model simulations over the last millennium (850-1849CE), https://doi.org/10.5281/ZENODO.6610684, 2022.

Bustamante, M., Cruz, F., Vuille, M., Apaéstegui, J., Strikis, N., Panizo, G., Novello, F., Deininger, M., Sifeddine, A., Cheng, H., Moquet, J., Guyot, J., Santos, R., Segura, H., and Edwards, R.: Holocene changes in monsoon precipitation in the Andes of NE Peru based on δ 18O speleothem records, Quaternary Science Reviews, 146, 274–287, https://doi.org/10.1016/j.quascirev.2016.05.023, 2016.

Campos, J. L. P. S., Cruz, F. W., Ambrizzi, T., Deininger, M., Vuille, M., Novello, V. F., and Strikis, N. M.: Coherent South American Monsoon Variability During the Last Millennium Revealed Through High-Resolution Proxy Records, Geophysical Research Letters, 46, 8261–8270, https://doi.org/10.1029/2019GL082513, 2019.

Campos, M. C., Chiessi, C. M., Novello, V. F., Crivellari, S., Campos, J. L. P. S., Albuquerque, A. L. S., Venancio, I. M., Santos, T. P., Melo, D. B., Cruz, F. W., Sawakuchi, A. O., and Mendes, V. R.: South American Precipitation Dipole Forced by Interhemispheric Temperature Gradient, Scientific Reports, 12, 10 527, https://doi.org/10.1038/s41598-022-14495-1, 2022.

Carvalho, L. M. V., Jones, C., and Liebmann, B.: The South Atlantic Convergence Zone: Intensity, Form, Persistence, and Relationships with Intraseasonal to Interannual Activity and Extreme Rainfall, Journal of Climate, 17, 88–108, https://doi.org/10.1175/1520-0442(2004)017<0088:tsaczi>2.0.co;2, 2004.

Choblet, M. A., Bühler, J. C., Steiger, N. J., Novello, V. F., and Rehfeld, K.: Reconstructing climate fields with terrestrial climate archives, isotope-enabled GCMs and Data Assimilation, Copernicus GmbH, https://doi.org/10.5194/egusphere-egu23-2600, 2023.

Colose, C. M., LeGrande, A. N., and Vuille, M.: Hemispherically Asymmetric Volcanic Forcing of Tropical Hydroclimate during the Last Millennium, Earth System Dynamics, 7, 681–696, https://doi.org/10.5194/esd-7-681-2016, 2016a.

Colose, C. M., LeGrande, A. N., and Vuille, M.: The Influence of Volcanic Eruptions on the Climate of Tropical South America during the Last Millennium in an Isotope-Enabled General Circulation Model, Climate of the Past, 12, 961–979, https://doi.org/10.5194/cp-12-961-2016, 2016b.

Comas-Bru, L., Rehfeld, K., Roesch, C., Amirnezhad-Mozhdehi, S., Harrison, S. P., Atsawawaranunt, K., Ahmad, S. M., Brahim, Y. A., Baker, A., Bosomworth, M., Breitenbach, S. F. M., Burstyn, Y., Columbu, A., Deininger, M., Demény, A., Dixon, B., Fohlmeister, J., Hatvani, I. G., Hu, J., Kaushal, N., Kern, Z., Labuhn, I., Lechleitner, F. A., Lorrey, A., Martrat, B., Novello, V. F., Oster, J., Pérez-Mejías, C., Scholz, D., Scroxton, N., Sinha, N., Ward, B. M., Warken, S., Zhang, H., and SISAL Working Group members: SISALv2: A Comprehensive Speleothem Isotope Database with Multiple Age–Depth Models, Earth System Science Data, 12, 2579–2606, https://doi.org/10.5194/essd-12-2579-2020, 2020.

Comboul, M., Emile-Geay, J., Hakim, G. J., and Evans, M. N.: Paleoclimate Sampling as a Sensor Placement Problem, Journal of Climate, 28, 7717–7740, https://doi.org/10.1175/JCLI-D-14-00802.1, 2015.

Compo, G. P., Whitaker, J. S., Sardeshmukh, P. D., Matsui, N., Allan, R. J., Yin, X., Gleason, B. E., Vose, R. S., Rutledge, G., Bessemoulin, P., Brönnimann, S., Brunet, M., Crouthamel, R. I., Grant, A. N., Groisman, P. Y., Jones, P. D., Kruk, M. C., Kruger, A. C., Marshall, G. J.,

Maugeri, M., Mok, H. Y., Nordli, Ø., Ross, T. F., Trigo, R. M., Wang, X. L., Woodruff, S. D., and Worley, S. J.: The Twentieth Century Reanalysis Project, Quarterly Journal of the Royal Meteorological Society, 137, 1–28, https://doi.org/10.1002/qj.776, 2011.

Cook, E. R., Meko, D. M., Stahle, D. W., and Cleaveland, M. K.: Drought Reconstructions for the Continental United States*, Journal of Climate, 12, 1145–1162, https://doi.org/10.1175/1520-0442(1999)012<1145:drftcu>2.0.co;2, 1999.

Craig, H.: Isotopic variations in meteoric waters, Science, 133, 1702–1703, 1961.

Cruz, F. W., Vuille, M., Burns, S. J., Wang, X., Cheng, H., Werner, M., Edwards, R. L., Karmann, I., Auler, A. S., and Nguyen, H.: Orbitally driven east–west antiphasing of South American precipitation, Nature Geoscience, 2, 210–214, https://doi.org/10.1038/ngeo444, 2009.

Dansgaard, W.: Stable Isotopes in Precipitation, Tellus, 16, 436–468, https://doi.org/10.1111/j.2153-3490.1964.tb00181.x, 1964.

de Jong, R., von Gunten, L., Maldonado, A., and Grosjean, M.: Late Holocene Summer Temperatures in the Central Andes Reconstructed from the Sediments of High-Elevation Laguna Chepical, Chile (32° S), Climate of the Past, 9, 1921–1932, https://doi.org/10.5194/cp-9-1921-2013, 2013.

de Souza, J. G., Robinson, M., Maezumi, S. Y., Capriles, J., Hoggarth, J. A., Lombardo, U., Novello, V. F., Apaéstegui, J., Whitney, B., Urrego, D., Alves, D. T., Rostain, S., Power, M. J., Mayle, F. E., da Cruz, F. W., Hooghiemstra, H., and Iriarte, J.: Climate Change and Cultural Resilience in Late Pre-Columbian Amazonia, Nature Ecology & Evolution, 3, 1007–1017, https://doi.org/10.1038/s41559-019-0924-0, 2019.

Dee, S., Emile-Geay, J., Evans, M. N., Allam, A., Steig, E. J., and Thompson, D.: PRYSM: An Open-Source Framework for PRoxY System Modeling, with Applications to Oxygen-Isotope Systems, Journal of Advances in Modeling Earth Systems, 7, 1220–1247, https://doi.org/10.1002/2015MS000447, 2015.

Dee, S. G., Steiger, N. J., Emile-Geay, J., and Hakim, G. J.: On the utility of proxy system models for estimating climate states over the common era, Journal of Advances in Modeling Earth Systems, 8, 1164–1179, https://doi.org/10.1002/2016ms000677, 2016.

Deininger, M., Ward, B. M., Novello, V. F., and Cruz, F. W.: Late Quaternary Variations in the South American Monsoon System as Inferred by Speleothems—New Perspectives Using the SISAL Database, Quaternary, 2, 6, https://doi.org/10.3390/quat2010006, 2019.

DeLong, K. L., Flannery, J. A., Poore, R. Z., Quinn, T. M., Maupin, C. R., Lin, K., and Shen, C.-C.: A reconstruction of sea surface temperature variability in the southeastern Gulf of Mexico from 1734 to 2008 CE using cross-dated Sr/Ca records from the coral Siderastrea siderea, Paleoceanography, 29, 403–422, 2014.

Dirren, S. and Hakim, G. J.: Toward the assimilation of time-averaged observations, Geophysical research letters, 32, 2005.

Dunbar, R. B., Wellington, G. M., Colgan, M. W., and Glynn, P. W.: Eastern Pacific sea surface temperature since 1600 AD: The δ18O record of climate variability in Galápagos corals, Paleoceanography, 9, 291–315, 1994.

Elbert, J., Wartenburger, R., von Gunten, L., Urrutia, R., Fischer, D., Fujak, M., Hamann, Y., Greber, N. D., and Grosjean, M.: Late Holocene air temperature variability reconstructed from the sediments of Laguna Escondida, Patagonia, Chile (45°30′S), Palaeogeography, Palaeoclimatology, Palaeoecology, 369, 482–492, https://doi.org/10.1016/j.palaeo.2012.11.013, 2013.

Elbert, J., Jacques-Coper, M., Van Daele, M., Urrutia, R., and Grosjean, M.: A 600 Years Warm-Season Temperature Record from Varved Sediments of Lago Plomo, Northern Patagonia, Chile (47°S), Quaternary International, 377, 28–37, https://doi.org/10.1016/j.quaint.2015.01.004, 2015.

Emile-Geay, J., McKay, N. P., Kaufman, D. S., von Gunten, L., Wang, J., Anchukaitis, K. J., Abram, N. J., Addison, J. A., Curran, M. A., Evans, M. N., Henley, B. J., Hao, Z., Martrat, B., McGregor, H. V., Neukom, R., Pederson, G. T., Stenni, B., Thirumalai, K., Werner, J. P., Xu, C., Divine, D. V., Dixon, B. C., Gergis, J., Mundo, I. A., Nakatsuka, T., Phipps, S. J., Routson, C. C., Steig, E. J., Tierney, J. E., Tyler, J. J., Allen, K. J., Bertler, N. A., Björklund, J., Chase, B. M., Chen, M.-T., Cook, E., de Jong, R., DeLong, K. L., Dixon, D. A., Ekaykin,

A. A., Ersek, V., Filipsson, H. L., Francus, P., Freund, M. B., Frezzotti, M., Gaire, N. P., Gajewski, K., Ge, Q., Goosse, H., Gornostaeva, A., Grosjean, M., Horiuchi, K., Hormes, A., Husum, K., Isaksson, E., Kandasamy, S., Kawamura, K., Kilbourne, K. H., Koç, N., Leduc, G., Linderholm, H. W., Lorrey, A. M., Mikhalenko, V., Mortyn, P. G., Motoyama, H., Moy, A. D., Mulvaney, R., Munz, P. M., Nash, D. J., Oerter, H., Opel, T., Orsi, A. J., Ovchinnikov, D. V., Porter, T. J., Roop, H. A., Saenger, C., Sano, M., Sauchyn, D., Saunders, K. M., Seidenkrantz, M.-S., Severi, M., Shao, X., Sicre, M.-A., Sigl, M., Sinclair, K., St. George, S., St. Jacques, J.-M., Thamban, M., Kuwar Thapa, U., Thomas, E. R., Turney, C., Uemura, R., Viau, A. E., Vladimirova, D. O., Wahl, E. R., White, J. W., Yu, Z., Zinke, J., and PAGES2k Consortium: A Global Multiproxy Database for Temperature Reconstructions of the Common Era, Scientific Data, 4, 170 088, https://doi.org/10.1038/sdata.2017.88, 2017.

Erb, M. P., McKay, N. P., Steiger, N., Dee, S., Hancock, C., Ivanovic, R. F., Gregoire, L. J., and Valdes, P.: Reconstructing Holocene Temperatures in Time and Space Using Paleoclimate Data Assimilation, Climate of the Past, 18, 2599–2629, https://doi.org/10.5194/cp-18-2599-2022, 2022.

Evans, M. N., Tolwinski-Ward, S. E., Thompson, D. M., and Anchukaitis, K. J.: Applications of Proxy System Modeling in High Resolution Paleoclimatology, Quaternary Science Reviews, 76, 16–28, https://doi.org/10.1016/j.quascirev.2013.05.024, 2013.

Evensen, G.: Sequential Data Assimilation with a Nonlinear Quasi-Geostrophic Model Using Monte Carlo Methods to Forecast Error Statistics, Journal of Geophysical Research: Oceans, 99, 10 143–10 162, https://doi.org/10.1029/94JC00572, 1994.

Evensen, G.: The Ensemble Kalman Filter: Theoretical Formulation and Practical Implementation, Ocean Dynamics, 53, 343–367, https://doi.org/10.1007/s10236-003-0036-9, 2003.

Evensen, G., Vossepoel, F. C., and van Leeuwen, P. J.: Data Assimilation Fundamentals: A Unified Formulation of the State and Parameter Estimation Problem, Springer Textbooks in Earth Sciences, Geography and Environment, Springer International Publishing, Cham, https://doi.org/10.1007/978-3-030-96709-3, 2022.

Eyring, V., Cox, P. M., Flato, G. M., Gleckler, P. J., Abramowitz, G., Caldwell, P., Collins, W. D., Gier, B. K., Hall, A. D., Hoffman, F. M., et al.: Taking climate model evaluation to the next level, Nature Climate Change, 9, 102–110, 2019.

Fensterer, C., Scholz, D., Hoffmann, D., Spötl, C., Pajón, J. M., and Mangini, A.: Cuban stalagmite suggests relationship between Caribbean precipitation and the Atlantic Multidecadal Oscillation during the past 1.3 ka, The Holocene, 22, 1405–1412, https://doi.org/10.1177/0959683612449759, 2012.

Franke, J., Brönnimann, S., Bhend, J., and Brugnara, Y.: A Monthly Global Paleo-Reanalysis of the Atmosphere from 1600 to 2005 for Studying Past Climatic Variations, Scientific Data, 4, 170 076, https://doi.org/10.1038/sdata.2017.76, 2017.

Garreaud, R. D., Vuille, M., Compagnucci, R., and Marengo, J.: Present-Day South American Climate, Palaeogeography, Palaeoclimatology, Palaeoecology, 281, 180–195, https://doi.org/10.1016/j.palaeo.2007.10.032, 2009.

Garreaud, R. D., Boisier, J. P., Rondanelli, R., Montecinos, A., Sepúlveda, H. H., and Veloso-Aguila, D.: The Central Chile Mega Drought (2010–2018): A climate dynamics perspective, International Journal of Climatology, 40, 421–439, https://doi.org/10.1002/joc.6219, 2019.

Gioda, A. and Prieto, M. d. R.: Histoire des sécheresses andines ; Potosi, El Niño et le Petit âge glaciaire, La Météorologie, 1999, 33–42, https://doi.org/10.4267/2042/47082, 1999.

Gneiting, T. and Raftery, A. E.: Strictly Proper Scoring Rules, Prediction, and Estimation, Journal of the American Statistical Association, 102, 359–378, https://doi.org/10.1198/016214506000001437, 2007.

Grießinger, J., Langhamer, L., Schneider, C., Saß, B.-L., Steger, D., Skvarca, P., Braun, M. H., Meier, W. J.-H., Srur, A. M., and Hochreuther, P.: Imprints of Climate Signals in a 204 Year δ18O Tree-Ring Record of Nothofagus Pumilio From Perito Moreno Glacier, Southern Patagonia (50°S), Frontiers in Earth Science, 6, 2018.

Haase-Schramm, A., Böhm, F., Eisenhauer, A., Dullo, W.-C., Joachimski, M. M., Hansen, B., and Reitner, J.: Sr/Ca Ratios and Oxygen Isotopes from Sclerosponges: Temperature History of the Caribbean Mixed Layer and Thermocline during the Little Ice Age: SR/CA AND δ^{18} O FROM SCLEROSPONGES, Paleoceanography, 18, n/a–n/a, https://doi.org/10.1029/2002PA000830, 2003.

1735 Hakim, G. J., Emile-Geay, J., Steig, E. J., Noone, D., Anderson, D. M., Tardif, R., Steiger, N., and Perkins, W. A.: The Last Millennium Climate Reanalysis Project: Framework and First Results, Journal of Geophysical Research: Atmospheres, 121, 6745–6764, https://doi.org/10.1002/2016JD024751, 2016.

Harris, C. R., Millman, K. J., van der Walt, S. J., Gommers, R., Virtanen, P., Cournapeau, D., Wieser, E., Taylor, J., Berg, S., Smith, N. J., Kern, R., Picus, M., Hoyer, S., van Kerkwijk, M. H., Brett, M., Haldane, A., del Río, J. F., Wiebe, M., Peterson, P., Gérard-Marchant,
1740 P., Sheppard, K., Reddy, T., Weckesser, W., Abbasi, H., Gohlke, C., and Oliphant, T. E.: Array programming with NumPy, Nature, 585, 357–362, https://doi.org/10.1038/s41586-020-2649-2, 2020a.

Harris, I., Osborn, T. J., Jones, P., and Lister, D.: Version 4 of the CRU TS monthly high-resolution gridded multivariate climate dataset, Scientific Data, 7, https://doi.org/10.1038/s41597-020-0453-3, 2020b.

Hoffmann, G., Ramirez, E., Taupin, J. D., Francou, B., Ribstein, P., Delmas, R., Dürr, H., Gallaire, R., Simões, J., Schotterer, U., Stieve-
1745 nard, M., and Werner, M.: Coherent Isotope History of Andean Ice Cores over the Last Century, Geophysical Research Letters, 30, https://doi.org/10.1029/2002GL014870, 2003.

Hoyer, S. and Hamman, J.: xarray: N-D labeled arrays and datasets in Python, J. Open Res. Software, 2017.

Humanes-Fuente, V., Ferrero, M. E., Muñoz, A. A., González-Reyes, Á., Requena-Rojas, E. J., Barichivich, J., Inga, J. G., and Layme-Huaman, E. T.: Two Centuries of Hydroclimatic Variability Reconstructed From Tree-Ring Records Over the Amazonian Andes of Peru,
1750 Journal of Geophysical Research: Atmospheres, 125, e2020JD032 565, https://doi.org/10.1029/2020JD032565, 2020.

Hunter, J. D.: Matplotlib: A 2D graphics environment, Computing in Science & Engineering, 9, 90–95, https://doi.org/10.1109/MCSE.2007.55, 2007.

Huntley, H. S. and Hakim, G. J.: Assimilation of Time-Averaged Observations in a Quasi-Geostrophic Atmospheric Jet Model, Climate Dynamics, 35, 995–1009, https://doi.org/10.1007/s00382-009-0714-5, 2010.

1755 IAEA/WMO: Global Network of Isotopes in Precipitation. The GNIP Database, http://www.iaea.org/water, accessible at: http://www.iaea.org/water, 2020.

Jiménez-Iñiguez, A., Ampuero, A., Valencia, B. G., Mayta, V. C., Cruz, F. W., Vuille, M., Novello, V. F., Misailidis Stríkis, N., Aranda, N., and Conicelli, B.: Stable isotope variability of precipitation and cave drip-water at Jumandy cave, western Amazon River basin (Ecuador), J. Hydrol. (Amst.), 610, 127 848, 2022.

1760 Jiménez-Iñiguez, A., Ampuero, A., Valencia, B. G., Mayta, V. C., Cruz, F. W., Vuille, M., Novello, V. F., Stríkis, N. M., Aranda, N., and Conicelli, B.: Stable isotope variability of precipitation and cave drip-water at Jumandy cave, western Amazon River basin (Ecuador), Journal of Hydrology, 610, 127 848, https://doi.org/10.1016/j.jhydrol.2022.127848, 2022.

Jungclaus, J. H., Bard, E., Baroni, M., Braconnot, P., Cao, J., Chini, L. P., Egorova, T., Evans, M., González-Rouco, J. F., Goosse, H., Hurtt, G. C., Joos, F., Kaplan, J. O., Khodri, M., Goldewijk, K. K., Krivova, N., LeGrande, A. N., Lorenz, S. J., Luterbacher, J., Man,
1765 W., Maycock, A. C., Meinshausen, M., Moberg, A., Muscheler, R., Nehrbass-Ahles, C., Otto-Bliesner, B. I., Phipps, S. J., Pongratz, J., Rozanov, E., Schmidt, G. A., Schmidt, H., Schmutz, W., Schurer, A., Shapiro, A. I., Sigl, M., Smerdon, J. E., Solanki, S. K., Timmreck, C., Toohey, M., Usoskin, I. G., Wagner, S., Wu, C.-J., Yeo, K. L., Zanchettin, D., Zhang, Q., and Zorita, E.: The PMIP4 contribution to CMIP6–Part 3: The last millennium, scientific objective, and experimental design for the PMIP4 past1000 simulations, Geoscientific Model Development, 10, 4005–4033, https://doi.org/10.5194/gmd-10-4005-2017, 2017.

Kanner, L. C., Burns, S. J., Cheng, H., Edwards, R. L., and Vuille, M.: High-resolution variability of the South American summer monsoon over the last seven millennia: insights from a speleothem record from the central Peruvian Andes, Quaternary Science Reviews, 75, 1–10, https://doi.org/10.1016/j.quascirev.2013.05.008, 2013.

Kaushal, N., Lechleitner, F. A., Wilhelm, M., Bühler, J. C., Braun, K., Brahim, Y. A., Azennoud, K., Baker, A., Burstyn, Y., Comas-Bru, L., Goldsmith, Y., Harrison, S. P., Hatvani, I. G., Rehfeld, K., Ritzau, M., Skiba, V., Stoll, H. M., Szűcs, J. G., Treble, P. C., Azevedo, V., Baker, J. L., Chawchai, S., Columbu, A., Endres, L., Hu, J., Kern, Z., Kimbrough, A., Koç, K., Markowska, M., Martrat, B., Ahmad, S. M., Nehme, C., Novello, V. F., Pérez-Mejías, C., Ruan, J., Sekhon, N., Sinha, N., Tadros, C. V., Tiger, B. H., Warken, S., Wolf, A., and and, H. Z.: SISALv3: A global speleothem stable isotope and trace element database, https://doi.org/10.5194/essd-2023-364, 2023.

Kennett, D. J., Breitenbach, S. F. M., Aquino, V. V., Asmerom, Y., Awe, J., Baldini, J. U., Bartlein, P., Culleton, B. J., Ebert, C., Jazwa, C., Macri, M. J., Marwan, N., Polyak, V., Prufer, K. M., Ridley, H. E., Sodemann, H., Winterhalder, B., and Haug, G. H.: Development and Disintegration of Maya Political Systems in Response to Climate Change, Science, 338, 788–791, https://doi.org/10.1126/science.1226299, 2012.

Khider, D., Emile-Geay, J., Zhu, F., James, A., Landers, J., Ratnakar, V., and Gil, Y.: Pyleoclim: Paleoclimate Timeseries Analysis and Visualization With Python, Paleoceanography and Paleoclimatology, 37, e2022PA004 509, https://doi.org/10.1029/2022PA004509, 2022.

Kilbourne, K., Quinn, T., Webb, R., Guilderson, T., Nyberg, J., and Winter, A.: Paleoclimate proxy perspective on Caribbean climate since the year 1751: Evidence of cooler temperatures and multidecadal variability, Paleoceanography, 23, 2008.

King, J., Anchukaitis, K. J., Allen, K., Vance, T., and Hessl, A.: Trends and Variability in the Southern Annular Mode over the Common Era, Nature Communications, 14, 2324, https://doi.org/10.1038/s41467-023-37643-1, 2023.

King, J. M., Anchukaitis, K. J., Tierney, J. E., Hakim, G. J., Emile-Geay, J., Zhu, F., and Wilson, R.: A Data Assimilation Approach to Last Millennium Temperature Field Reconstruction Using a Limited High-Sensitivity Proxy Network, Journal of Climate, 34, 7091–7111, https://doi.org/10.1175/JCLI-D-20-0661.1, 2021.

Konecky, B. L., McKay, N. P., Churakova (Sidorova), O. V., Comas-Bru, L., Dassié, E. P., DeLong, K. L., Falster, G. M., Fischer, M. J., Jones, M. D., Jonkers, L., Kaufman, D. S., Leduc, G., Managave, S. R., Martrat, B., Opel, T., Orsi, A. J., Partin, J. W., Sayani, H. R., Thomas, E. K., Thompson, D. M., Tyler, J. J., Abram, N. J., Atwood, A. R., Cartapanis, O., Conroy, J. L., Curran, M. A., Dee, S. G., Deininger, M., Divine, D. V., Kern, Z., Porter, T. J., Stevenson, S. L., von Gunten, L., and Members, I. P.: The Iso2k Database: A Global Compilation of Paleo-δ^{18}O and δ^2H Records to Aid Understanding of Common Era Climate, Earth System Science Data, 12, 2261–2288, https://doi.org/10.5194/essd-12-2261-2020, 2020.

Lachniet, M. S., Bernal, J. P., Asmerom, Y., Polyak, V., and Piperno, D.: A 2400 yr Mesoamerican rainfall reconstruction links climate and cultural change, Geology, 40, 259–262, https://doi.org/10.1130/g32471.1, 2012.

Laepple, T. and Huybers, P.: Ocean Surface Temperature Variability: Large Model–Data Differences at Decadal and Longer Periods, Proceedings of the National Academy of Sciences, 111, 16 682–16 687, https://doi.org/10.1073/pnas.1412077111, 2014.

Laepple, T., Muench, T., and Dolman, A.: PaleoSpec: Spectral tools for the ECUS group, https://earthsystemdiagnostics.github.io/paleospec/, r package version 0.2.91, 2023a.

Laepple, T., Ziegler, E., Weitzel, N., Hébert, R., Ellerhoff, B., Schoch, P., Martrat, B., Bothe, O., Moreno-Chamarro, E., Chevalier, M., Herbert, A., and Rehfeld, K.: Regional but not global temperature variability underestimated by climate models at supradecadal timescales, Nat. Geosci., 16, 958–966, 2023b.

Lam, S. K., Pitrou, A., and Seibert, S.: Numba: A llvm-based python jit compiler, in: Proceedings of the Second Workshop on the LLVM Compiler Infrastructure in HPC, pp. 1–6, 2015.

Lewis, S. C. and LeGrande, A. N.: Stability of ENSO and Its Tropical Pacific Teleconnections over the Last Millennium, Climate of the Past, 11, 1347–1360, https://doi.org/10.5194/cp-11-1347-2015, 2015.

Libera, M. E. D., Novello, V. F., Cruz, F. W., Orrison, R., Vuille, M., Maezumi, S. Y., de Souza, J., Cauhy, J., Campos, J. L. P. S., Ampuero, A., Utida, G., Stríkis, N. M., Stumpf, C. F., Azevedo, V., Zhang, H., Edwards, R. L., and Cheng, H.: Paleoclimatic and paleoenvironmental changes in Amazonian lowlands over the last three millennia, Quaternary Science Reviews, 279, 107 383, https://doi.org/10.1016/j.quascirev.2022.107383, 2022.

Linsley, B. K., Dunbar, R. B., Wellington, G. M., and Mucciarone, D. A.: A coral-based reconstruction of Intertropical Convergence Zone variability over Central America since 1707, Journal of Geophysical Research: Oceans, 99, 9977–9994, 1994.

Lüning, S., Gałka, M., Bamonte, F. P., Rodríguez, F. G., and Vahrenholt, F.: The medieval climate anomaly in South America, Quaternary International, 508, 70–87, 2019.

Luterbacher, J., Xoplaki, E., Dietrich, D., Rickli, R., Jacobeit, J., Beck, C., Gyalistras, D., Schmutz, C., and Wanner, H.: Reconstruction of Sea Level Pressure Fields over the Eastern North Atlantic and Europe Back to 1500, Climate Dynamics, 18, 545–561, https://doi.org/10.1007/s00382-001-0196-6, 2002.

Luterbacher, J., Neukom, R., González-Rouco, F., Fernandez-Donado, L., Raible, C., and Zorita, E.: Reconstructed and Simulated Medieval Climate Anomaly in Southern South America, PAGES news, 19, 20–21, https://doi.org/10.22498/pages.19.1.20, 2011.

Marengo, J. A., Liebmann, B., Grimm, A. M., Misra, V., Silva Dias, P. L., Cavalcanti, I. F. A., Carvalho, L. M. V., Berbery, E. H., Ambrizzi, T., Vera, C. S., Saulo, A. C., Nogues-Paegle, J., Zipser, E., Seth, A., and Alves, L. M.: Recent developments on the South American monsoon system, International Journal of Climatology, 32, 1–21, https://doi.org/10.1002/joc.2254, 2010.

Medina, N. M. M., Cruz, F. W., Winter, A., Zhang, H., Ampuero, A., Vuille, M., Mayta, V. C., Campos, M. C., Rámirez, V. M., Utida, G., Zúñiga, A. C., and Cheng, H.: Atlantic ITCZ variability during the Holocene based on high-resolution speleothem isotope records from northern Venezuela, Quaternary Science Reviews, 307, 108 056, https://doi.org/https://doi.org/10.1016/j.quascirev.2023.108056, 2023.

Medina-Elizalde, M., Burns, S. J., Lea, D. W., Asmerom, Y., von Gunten, L., Polyak, V., Vuille, M., and Karmalkar, A.: High resolution stalagmite climate record from the Yucatán Peninsula spanning the Maya terminal classic period, Earth and Planetary Science Letters, 298, 255–262, https://doi.org/10.1016/j.epsl.2010.08.016, 2010.

Met Office: Cartopy: a cartographic python library with a Matplotlib interface, Exeter, Devon, https://scitools.org.uk/cartopy, 2010 - 2015.

Moquet, J. S., Cruz, F. W., Novello, V. F., Stríkis, N. M., Deininger, M., Karmann, I., Santos, R. V., Millo, C., Apaestegui, J., Guyot, J. L., Siffedine, A., Vuille, M., Cheng, H., Edwards, R. L., and Santini, W.: Calibration of Speleothem $\delta 18O$ Records against Hydroclimate Instrumental Records in Central Brazil, Global and Planetary Change, 139, 151–164, https://doi.org/10.1016/j.gloplacha.2016.02.001, 2016.

Morales, M. S., Christie, D. A., Villalba, R., Argollo, J., Pacajes, J., Silva, J. S., Alvarez, C. A., Llancabure, J. C., and Soliz Gamboa, C. C.: Precipitation Changes in the South American Altiplano since 1300 AD Reconstructed by Tree-Rings, Climate of the Past, 8, 653–666, https://doi.org/10.5194/cp-8-653-2012, 2012.

Morales, M. S., Cook, E. R., Barichivich, J., Christie, D. A., Villalba, R., LeQuesne, C., Srur, A. M., Ferrero, M. E., González-Reyes, Á., Couvreux, F., et al.: Six hundred years of South American tree rings reveal an increase in severe hydroclimatic events since mid-20th century, Proceedings of the National Academy of Sciences, 117, 16 816–16 823, 2020.

Morales, M. S., Crispín-DelaCruz, D. B., Álvarez, C., Christie, D. A., Ferrero, M. E., Andreu-Hayles, L., Villalba, R., Guerra, A., Ticse-Otarola, G., Rodríguez-Ramírez, E. C., LLocclla-Martínez, R., Sanchez-Ferrer, J., and Requena-Rojas, E. J.: Drought Increase since the

1845   Mid-20th Century in the Northern South American Altiplano Revealed by a 389-Year Precipitation Record, Climate of the Past, 19, 457–476, https://doi.org/10.5194/cp-19-457-2023, 2023.

Nash, J. E. and Sutcliffe, J. V.: River Flow Forecasting through Conceptual Models Part I — A Discussion of Principles, Journal of Hydrology, 10, 282–290, https://doi.org/10.1016/0022-1694(70)90255-6, 1970.

Neukom, R. and Gergis, J.: Southern Hemisphere High-Resolution Palaeoclimate Records of the Last 2000 Years, The Holocene, 22, 501–
1850   524, https://doi.org/10.1177/0959683611427335, 2012.

Neukom, R., del Rosario Prieto, M., Moyano, R., Luterbacher, J., Pfister, C., Villalba, R., Jones, P. D., and Wanner, H.: An Extended Network of Documentary Data from South America and Its Potential for Quantitative Precipitation Reconstructions Back to the 16th Century, Geophysical Research Letters, 36, L12 703, https://doi.org/10.1029/2009GL038351, 2009.

Neukom, R., Luterbacher, J., Villalba, R., Küttel, M., Frank, D., Jones, P. D., Grosjean, M., Esper, J., Lopez, L., and Wanner,
1855   H.: Multi-Centennial Summer and Winter Precipitation Variability in Southern South America, Geophysical Research Letters, 37, https://doi.org/10.1029/2010GL043680, 2010.

Neukom, R., Luterbacher, J., Villalba, R., Küttel, M., Frank, D., Jones, P. D., Grosjean, M., Wanner, H., Aravena, J.-C., Black, D. E., et al.: Multiproxy summer and winter surface air temperature field reconstructions for southern South America covering the past centuries, Climate Dynamics, 37, 35–51, 2011.

1860   Neukom, R., Gergis, J., Karoly, D., Wanner, H., Curran, M., Elbert, J., González Rouco, J. F., Linsley, B., Moy, A., Mundo, I., Raible, C., Steig, E., van Ommen, T., Vance, T., Villalba, R., Zinke, J., and Frank, D.: Inter-Hemispheric Temperature Variability over the Last Millennium, Nature Climate Change, 4, https://doi.org/10.1038/nclimate2174, 2014.

Neukom, R., Steiger, N., Gómez-Navarro, J. J., Wang, J., and Werner, J. P.: No Evidence for Globally Coherent Warm and Cold Periods over the Preindustrial Common Era, Nature, 571, 550–554, https://doi.org/10.1038/s41586-019-1401-2, 2019.

1865   Novello, V. F., Cruz, F. W., Karmann, I., Burns, S. J., Stríkis, N. M., Vuille, M., Cheng, H., Lawrence Edwards, R., Santos, R. V., Frigo, E., and Barreto, E. A. S.: Multidecadal Climate Variability in Brazil's Nordeste during the Last 3000 Years Based on Speleothem Isotope Records, Geophysical Research Letters, 39, https://doi.org/10.1029/2012GL053936, 2012.

Novello, V. F., Vuille, M., Cruz, F. W., Stríkis, N. M., de Paula, M. S., Edwards, R. L., Cheng, H., Karmann, I., Jaqueto, P. F., Trindade, R. I. F., Hartmann, G. A., and Moquet, J. S.: Centennial-Scale Solar Forcing of the South American Monsoon System Recorded in Stalagmites,
1870   Scientific Reports, 6, 24 762, https://doi.org/10.1038/srep24762, 2016.

Novello, V. F., Cruz, F. W., Moquet, J. S., Vuille, M., de Paula, M. S., Nunes, D., Edwards, R. L., Cheng, H., Karmann, I., Utida, G., Stríkis, N. M., and Campos, J. L. P. S.: Two Millennia of South Atlantic Convergence Zone Variability Reconstructed From Isotopic Proxies, Geophysical Research Letters, 45, 5045–5051, https://doi.org/10.1029/2017GL076838, 2018.

Novello, V. F., William da Cruz, F., Vuille, M., Pereira Silveira Campos, J. L., Stríkis, N. M., Apaéstegui, J., Moquet, J. S., Azevedo, V.,
1875   Ampuero, A., Utida, G., Wang, X., Paula-Santos, G. M., Jaqueto, P., Ruiz Pessenda, L. C., Breecker, D. O., and Karmann, I.: Investigating δ13C Values in Stalagmites from Tropical South America for the Last Two Millennia, Quaternary Science Reviews, 255, 106 822, https://doi.org/10.1016/j.quascirev.2021.106822, 2021.

Okazaki, A., Miyoshi, T., Yoshimura, K., Greybush, S. J., and Zhang, F.: Revisiting Online and Offline Data Assimilation Comparison for Paleoclimate Reconstruction: An Idealized OSSE Study, Journal of Geophysical Research: Atmospheres, 126, e2020JD034 214,
1880   https://doi.org/10.1029/2020JD034214, 2021.

Oke, P. R., Schiller, A., Griffin, D. A., and Brassington, G. B.: Ensemble Data Assimilation for an Eddy-Resolving Ocean Model of the Australian Region, Quarterly Journal of the Royal Meteorological Society, 131, 3301–3311, https://doi.org/10.1256/qj.05.95, 2005.

Orrison, R., Vuille, M., Smerdon, J. E., Apaéstegui, J., Azevedo, V., Campos, J. L. P. S., Cruz, F. W., Della Libera, M. E., and Stríkis, N. M.: South American Summer Monsoon Variability over the Last Millennium in Paleoclimate Records and Isotope-Enabled Climate Models, Climate of the Past, 18, 2045–2062, https://doi.org/10.5194/cp-18-2045-2022, 2022.

Osman, M. B., Tierney, J. E., Zhu, J., Tardif, R., Hakim, G. J., King, J., and Poulsen, C. J.: Globally Resolved Surface Temperatures since the Last Glacial Maximum, Nature, 599, 239–244, https://doi.org/10.1038/s41586-021-03984-4, 2021.

PAGES 2k Consortium: [SI] Consistent Multidecadal Variability in Global Temperature Reconstructions and Simulations over the Common Era, Nature Geoscience, 12, 643–649, https://doi.org/10.1038/s41561-019-0400-0, 2019.

Parsons, L. A., Loope, G. R., Overpeck, J. T., Ault, T. R., Stouffer, R., and Cole, J. E.: Temperature and Precipitation Variance in CMIP5 Simulations and Paleoclimate Records of the Last Millennium, Journal of Climate, 30, 8885–8912, https://doi.org/10.1175/jcli-d-16-0863.1, 2017.

Parsons, L. A., LeRoy, S., Overpeck, J. T., Bush, M., Cárdenes-Sandí, G., and Saleska, S.: The Threat of Multi-Year Drought in Western Amazonia, Water Resources Research, 54, 5890–5904, https://doi.org/10.1029/2017wr021788, 2018.

Parsons, L. A., Amrhein, D. E., Sanchez, S. C., Tardif, R., Brennan, M. K., and Hakim, G. J.: Do Multi-Model Ensembles Improve Reconstruction Skill in Paleoclimate Data Assimilation?, Earth and Space Science, 8, e2020EA001 467, https://doi.org/10.1029/2020EA001467, 2021.

Pörtner, H.-O., Roberts, D. C., Poloczanska, E. S., Mintenbeck, K., Tignor, M., Alegría, A., Craig, M., Langsdorf, S., Löschke, S., Möller, V., et al.: IPCC, 2022: Summary for policymakers, 2022.

Prieto, M. d. R.: ENSO Signals in South America: Rains and Floods in the Paraná River Region during Colonial Times, Climatic Change, 83, 39–54, https://doi.org/10.1007/s10584-006-9188-1, 2007.

Prieto, M. d. R. and García Herrera, R.: Documentary Sources from South America: Potential for Climate Reconstruction, Palaeogeography, Palaeoclimatology, Palaeoecology, 281, 196–209, https://doi.org/10.1016/j.palaeo.2008.07.026, 2009.

Rohde, R. A. and Hausfather, Z.: The Berkeley Earth Land/Ocean Temperature Record, Earth System Science Data, 12, 3469–3479, https://doi.org/10.5194/essd-12-3469-2020, 2020.

Rojas, M., Arias, P. A., Flores-Aqueveque, V., Seth, A., and Vuille, M.: The South American Monsoon Variability over the Last Millennium in Climate Models, Climate of the Past, 12, 1681–1691, https://doi.org/10.5194/cp-12-1681-2016, 2016.

Saenger, C., Cohen, A. L., Oppo, D. W., Halley, R. B., and Carilli, J. E.: Surface-Temperature Trends and Variability in the Low-Latitude North Atlantic since 1552, Nature Geoscience, 2, 492–495, https://doi.org/10.1038/ngeo552, 2009.

Sanchez, S. C., Hakim, G. J., and Saenger, C. P.: Climate Model Teleconnection Patterns Govern the Niño-3.4 Response to Early Nineteenth-Century Volcanism in Coral-Based Data Assimilation Reconstructions, Journal of Climate, 34, 1863–1880, https://doi.org/10.1175/JCLI-D-20-0549.1, 2021.

Schneider, U., Fuchs, T., Meyer-Christoffer, A., and Rudolf, B.: Global precipitation analysis products of the GPCC, Global Precipitation Climatology Centre (GPCC), DWD, Internet Publikation, 112, 2008.

Schurer, A. P., Tett, S. F. B., and Hegerl, G. C.: Small influence of solar variability on climate over the past millennium, Nature Geoscience, 7, 104–108, https://doi.org/10.1038/ngeo2040, 2013.

Sekhon, N., Novello, V. F., Cruz, F. W., Wortham, B. E., Ribeiro, T. G., and Breecker, D. O.: Diurnal to seasonal ventilation in Brazilian caves, Global and Planetary Change, 197, 103 378, https://doi.org/10.1016/j.gloplacha.2020.103378, 2021.

Sigl, M., Winstrup, M., McConnell, J. R., Welten, K. C., Plunkett, G., Ludlow, F., Büntgen, U., Caffee, M., Chellman, N., Dahl-Jensen, D., et al.: Timing and climate forcing of volcanic eruptions for the past 2,500 years, Nature, 523, 543–549, 2015.

Sjolte, J., Adolphi, F., Vinther, B. M., Muscheler, R., Sturm, C., Werner, M., and Lohmann, G.: Seasonal Reconstructions Coupling Ice Core Data and an Isotope-Enabled Climate Model – Methodological Implications of Seasonality, Climate Modes and Selection of Proxy Data, Climate of the Past, 16, 1737–1758, https://doi.org/10.5194/cp-16-1737-2020, 2020.

Smerdon, J. E.: Climate Models as a Test Bed for Climate Reconstruction Methods: Pseudoproxy Experiments: Pseudoproxy Experiments, Wiley Interdisciplinary Reviews: Climate Change, 3, 63–77, https://doi.org/10.1002/wcc.149, 2012.

Stansell, N. D., Steinman, B. A., Abbott, M. B., Rubinov, M., and Roman-Lacayo, M.: Lacustrine Stable Isotope Record of Precipitation Changes in Nicaragua during the Little Ice Age and Medieval Climate Anomaly, Geology, 41, 151–154, https://doi.org/10.1130/G33736.1, 2013.

Steiger, N. and Hakim, G.: Multi-Timescale Data Assimilation for Atmosphere–Ocean State Estimates, Climate of the Past, 12, 1375–1388, https://doi.org/10.5194/cp-12-1375-2016, 2016.

Steiger, N. J., Hakim, G. J., Steig, E. J., Battisti, D. S., and Roe, G. H.: Assimilation of Time-Averaged Pseudoproxies for Climate Reconstruction, Journal of Climate, 27, 426–441, https://doi.org/10.1175/JCLI-D-12-00693.1, 2014.

Steiger, N. J., Smerdon, J. E., Cook, E. R., and Cook, B. I.: A Reconstruction of Global Hydroclimate and Dynamical Variables over the Common Era, Scientific Data, 5, 180 086, https://doi.org/10.1038/sdata.2018.86, 2018.

Stevenson, S., Otto-Bliesner, B. L., Brady, E. C., Nusbaumer, J., Tabor, C., Tomas, R., Noone, D. C., and Liu, Z.: Volcanic Eruption Signatures in the Isotope-Enabled Last Millennium Ensemble, Paleoceanography and Paleoclimatology, 34, 1534–1552, https://doi.org/10.1029/2019PA003625, 2019.

Swart, P. K., Dodge, R. E., and Hudson, H. J.: A 240-year stable oxygen and carbon isotopic record in a coral from South Florida: Implications for the prediction of precipitation in southern Florida, Palaios, pp. 362–375, 1996.

Tardif, R., Hakim, G. J., Perkins, W. A., Horlick, K. A., Erb, M. P., Emile-Geay, J., Anderson, D. M., Steig, E. J., and Noone, D.: Last Millennium Reanalysis with an Expanded Proxy Database and Seasonal Proxy Modeling, Climate of the Past, 15, 1251–1273, https://doi.org/10.5194/cp-15-1251-2019, 2019.

Thompson, L. G., Mosley-Thompson, E., Davis, M. E., Zagorodnov, V. S., Howat, I. M., Mikhalenko, V. N., and Lin, P.-N.: Annually Resolved Ice Core Records of Tropical Climate Variability over the Past ~1800 Years, Science, 340, 945–950, https://doi.org/10.1126/science.1234210, 2013.

Tierney, J. E., Abram, N. J., Anchukaitis, K. J., Evans, M. N., Giry, C., Kilbourne, K. H., Saenger, C. P., Wu, H. C., and Zinke, J.: Tropical sea surface temperatures for the past four centuries reconstructed from coral archives, Paleoceanography, 30, 226–252, https://doi.org/10.1002/2014pa002717, 2015.

Tierney, J. E., Zhu, J., King, J., Malevich, S. B., Hakim, G. J., and Poulsen, C. J.: Glacial Cooling and Climate Sensitivity Revisited, Nature, 584, 569–573, https://doi.org/10.1038/s41586-020-2617-x, 2020.

Tierney, J. E., Zhu, J., Li, M., Ridgwell, A., Hakim, G. J., Poulsen, C. J., Whiteford, R. D. M., Rae, J. W. B., and Kump, L. R.: Spatial Patterns of Climate Change across the Paleocene–Eocene Thermal Maximum, Proceedings of the National Academy of Sciences, 119, e2205326 119, https://doi.org/10.1073/pnas.2205326119, 2022.

Tindall, J. C., Valdes, P. J., and Sime, L. C.: Stable Water Isotopes in HadCM3: Isotopic Signature of El Niño–Southern Oscillation and the Tropical Amount Effect, Journal of Geophysical Research, 114, D04 111, https://doi.org/10.1029/2008JD010825, 2009.

Utida, G., Cruz, F. W., Vuille, M., Ampuero, A., Novello, V. F., Maksic, J., Sampaio, G., Cheng, H., Zhang, H., Dias de Andrade, F. R., and Edwards, R. L.: Spatiotemporal ITCZ Dynamics during the Last Three Millennia in Northeastern Brazil and Related Impacts in Modern Human History, Preprint, Proxy Use-Development-Validation/Terrestrial Archives/Holocene, https://doi.org/10.5194/cp-2023-2, 2023.

Valler, V., Brugnara, Y., Franke, J., and Brönnimann, S.: Assimilating Monthly Precipitation Data in a Paleoclimate Data Assimilation Framework, Climate of the Past, 16, 1309–1323, https://doi.org/10.5194/cp-16-1309-2020, 2020.

Valler, V., Franke, J., Brugnara, Y., Samakinwa, E., Hand, R., Lundstad, E., Burgdorf, A.-M., Lipfert, L., Friedman, A. R., and Brönnimann, S.: ModE-RA: a global monthly paleo-reanalysis of the modern era 1421 to 2008, Scientific Data, 11, https://doi.org/10.1038/s41597-023-02733-8, 2024.

Van Rossum, G. and De Boer, J.: Interactively testing remote servers using the Python programming language, CWI quarterly, 4, 283–303, 1991.

Vetra-Carvalho, S., van Leeuwen, P. J., Nerger, L., Barth, A., Altaf, M. U., Brasseur, P., Kirchgessner, P., and Beckers, J.-M.: State-of-the-Art Stochastic Data Assimilation Methods for High-Dimensional Non-Gaussian Problems, Tellus A: Dynamic Meteorology and Oceanography, 70, 1–43, https://doi.org/10.1080/16000870.2018.1445364, 2018.

Vicente-Serrano, S. M., Beguería, S., and López-Moreno, J. I.: A Multiscalar Drought Index Sensitive to Global Warming: The Standardized Precipitation Evapotranspiration Index, Journal of Climate, 23, 1696–1718, https://doi.org/10.1175/2009JCLI2909.1, 2010.

Virtanen, P., Gommers, R., Oliphant, T. E., Haberland, M., Reddy, T., Cournapeau, D., Burovski, E., Peterson, P., Weckesser, W., Bright, J., van der Walt, S. J., Brett, M., Wilson, J., Millman, K. J., Mayorov, N., Nelson, A. R. J., Jones, E., Kern, R., Larson, E., Carey, C. J., Polat, İ., Feng, Y., Moore, E. W., VanderPlas, J., Laxalde, D., Perktold, J., Cimrman, R., Henriksen, I., Quintero, E. A., Harris, C. R., Archibald, A. M., Ribeiro, A. H., Pedregosa, F., van Mulbregt, P., and SciPy 1.0 Contributors: SciPy 1.0: Fundamental Algorithms for Scientific Computing in Python, Nature Methods, 17, 261–272, https://doi.org/10.1038/s41592-019-0686-2, 2020.

von Gunten, L., Grosjean, M., Rein, B., Urrutia, R., and Appleby, P.: A quantitative high-resolution summer temperature reconstruction based on sedimentary pigments from Laguna Aculeo, central Chile, back to AD 850, The Holocene, 19, 873–881, https://doi.org/10.1177/0959683609336573, 2009.

Vuille, M. and Werner, M.: Stable isotopes in precipitation recording South American summer monsoon and ENSO variability: observations and model results, Climate Dynamics, 25, 401–413, https://doi.org/10.1007/s00382-005-0049-9, 2005.

Vuille, M., Bradley, R. S., Werner, M., Healy, R., and Keimig, F.: Modeling d18O in precipitation over the tropical Americas: 1. Interannual variability and climatic controls, Journal of Geophysical Research: Atmospheres, 108, https://doi.org/10.1029/2001jd002038, 2003.

Vuille, M., Burns, S. J., Taylor, B. L., Cruz, F. W., Bird, B. W., Abbott, M. B., Kanner, L. C., Cheng, H., and Novello, V. F.: A Review of the South American Monsoon History as Recorded in Stable Isotopic Proxies over the Past Two Millennia, Climate of the Past, 8, 1309–1321, https://doi.org/10.5194/cp-8-1309-2012, 2012.

Wang, J., Emile-Geay, J., Guillot, D., Smerdon, J. E., and Rajaratnam, B.: Evaluating Climate Field Reconstruction Techniques Using Improved Emulations of Real-World Conditions, Climate of the Past, 10, 1–19, https://doi.org/10.5194/cp-10-1-2014, 2014.

Wang, X., Edwards, R. L., Auler, A. S., Cheng, H., Kong, X., Wang, Y., Cruz, F. W., Dorale, J. A., and Chiang, H.-W.: Hydroclimate Changes across the Amazon Lowlands over the Past 45,000 Years, Nature, 541, 204–207, https://doi.org/10.1038/nature20787, 2017.

Ward, B. M., Wong, C. I., Novello, V. F., McGee, D., Santos, R. V., Silva, L. C., Cruz, F. W., Wang, X., Edwards, R. L., and Cheng, H.: Reconstruction of Holocene coupling between the South American Monsoon System and local moisture variability from speleothem δ18O and 87Sr/86Sr records, Quaternary Science Reviews, 210, 51–63, https://doi.org/10.1016/j.quascirev.2019.02.019, 2019.

Werner, M., Haese, B., Xu, X., Zhang, X., Butzin, M., and Lohmann, G.: Glacial–Interglacial Changes in $H_2{}^{18}O$, HDO and Deuterium Excess – Results from the Fully Coupled ECHAM5/MPI-OM Earth System Model, Geoscientific Model Development, 9, 647–670, https://doi.org/10.5194/gmd-9-647-2016, 2016.

Wes McKinney: Data Structures for Statistical Computing in Python, in: Proceedings of the 9th Python in Science Conference, edited by Stéfan van der Walt and Jarrod Millman, pp. 56 – 61, https://doi.org/10.25080/Majora-92bf1922-00a, 2010.

Wilks, D. S.: Forecast verification, in: International geophysics, vol. 100, pp. 301–394, Elsevier, 2011.

Winter, A., Miller, T., Kushnir, Y., Sinha, A., Timmermann, A., Jury, M. R., Gallup, C., Cheng, H., and Edwards, R. L.: Evidence for 800years of North Atlantic multi-decadal variability from a Puerto Rican speleothem, Earth and Planetary Science Letters, 308, 23–28, https://doi.org/10.1016/j.epsl.2011.05.028, 2011.

Wong, M. L., Wang, X., Latrubesse, E. M., He, S., and Bayer, M.: Variations in the South Atlantic Convergence Zone over the mid-to-late Holocene inferred from speleothem D18O in central Brazil, Quaternary Science Reviews, 270, 107178, https://doi.org/10.1016/j.quascirev.2021.107178, 2021.

Wortham, B. E., Wong, C. I., Silva, L. C. R., McGee, D., Montañez, I. P., Troy Rasbury, E., Cooper, K. M., Sharp, W. D., Glessner, J. J. G., and Santos, R. V.: Assessing Response of Local Moisture Conditions in Central Brazil to Variability in Regional Monsoon Intensity Using Speleothem 87Sr/86Sr Values, Earth and Planetary Science Letters, 463, 310–322, https://doi.org/10.1016/j.epsl.2017.01.034, 2017.

Yoshimura, K., Kanamitsu, M., Noone, D., and Oki, T.: Historical Isotope Simulation Using Reanalysis Atmospheric Data, Journal of Geophysical Research: Atmospheres, 113, https://doi.org/10.1029/2008JD010074, 2008.

Zhou, J. and Lau, K.: Does a monsoon climate exist over South America?, Journal of climate, 11, 1020–1040, 1998.